ABSTRACT

Title of Document: REGENERATION, FISSION AND THE EVOLUTION OF DEVELOPMENTAL NOVELTY IN NAID ANNELIDS

Eduardo E. Zattara, Doctor of Philosophy, 2012

Directed By: Associate Professor Alexandra E. Bely, Department of Biology

Regeneration of lost structures and asexual reproduction by fission are post-embryonic trajectories related at the evolutionary and developmental levels. Their phylogenetic distribution within Metazoa has led to the hypothesis that fission can evolve by co-opting regenerative abilities. Fission has evolved multiple times within Annelida, including independent origins at the base of the Pristininae and Naidinae lineages of naid worms. Naids are thus a great system to study the evolution of developmental trajectories of regeneration and fission and their mutual physiological interactions. I made a comparative study of morphogenesis during regeneration and fission in a representative species, *Pristina leidyi* Smith (Pristininae), to test the hypothesis that both trajectories are closely linked by common origin, yet have undergone functional divergence; results show that regeneration and fission share numerous, sometimes exclusive developmental processes, but also present a number of differences spread out along their trajectories. I also examined cell proliferation

and growth patterns in *P. leidyi* to characterize the resource allocation strategies it uses to integrate multiple developmental trajectories. I found evidence for a non-linear antero-posterior gradient in proliferation potential and clear interactions between regeneration and fission that strongly depend on fission stage and what body part is lost; similar interactions have been described for naidine annelids and turbellarian flatworms representing independent origins of fission, indicating convergence of fission-associated allocation strategies. I then extended the fission-regeneration comparative study in *P. leidyi* to additional annelids, describing and comparing regeneration and fission in another pristinine, seven naidine and one outgroup species, and found very similar regeneration trajectories among all of them, along with striking levels of convergence of paratomic fission trajectories. Despite similarities, the two paratomic clades presented a distinctive mode of central nervous system development. Finally, I developed novel protocols for dynamic studies of the cellular basis of regeneration, laying groundwork for future comparisons at that level. Altogether, these results strongly support that fission originated multiple times by co-option of regenerative abilities; furthermore, convergence of fission trajectories and resource allocation strategies suggests that similar developmental capabilities, functional constraints and ecophysiological contexts can channel evolutionary trajectories into parallel paths, both in close and distant lineages.

REGENERATION, FISSION AND THE EVOLUTION OF DEVELOPMENTAL NOVELTY IN NAID ANNELIDS.

By

Eduardo Enrique Zattara

Dissertation submitted to the Faculty of the Graduate School of the
University of Maryland, College Park, in partial fulfillment
of the requirements for the degree of
Doctor of Philosophy
2012

Advisory Committee:
Associate Professor Alexandra E. Bely, Chair
Associate Professor Eric S. Haag
Professor William R. Jeffery
Assistant Professor Lisa A. Taneyhill
Associate Professor Jeffrey W. Shultz

Preface

As seems to be the rule rather than the exception in Science, the process of wrapping up and writing down six years of research into a single doctoral dissertation yields an ambiguous feeling of closure and incompleteness. Closure, because observations and results finally crystallize in a set of hopefully interesting scientific stories; and incompleteness, because very often we reach one answer only to discover that a new, higher and harder question is up there waiting for further investigation, much like peaks during mountain hiking. But then, it is not the destination but the journey that really matter.

In this dissertation, a case is made for the influence of developmental capabilities on the evolution of novel developmental features, here exemplified by the hypothetical gain of asexual reproduction through co-option of pre-existing regenerative abilities. It might disappoint hardcore developmental biologists for its lack of evidence on molecular mechanisms, and also some evolutionary biologist who focus too much on the details of the process. But details of mechanism and process are higher peaks that cannot be reached without going up the foothills first; it is my hope that the material presented herein will furnish material to build the base camp from which new daring expeditions will be launched. After all, careful observation and phenomenological characterization are the very first steps of the scientific method, and without them many scientists would be proposing answers to fundamentally wrong questions.

As no graduate student is an island, I'd like here to acknowledge some of the many people that made completion of this dissertation possible. First and foremost, I am enormously grateful to Dr. Alexa Bely, not only for welcoming a fish biogeographer in her lab, but also for being such an awesome mentor and advisor, providing me the support, freedom to explore and encouragement to focus that were necessary for the completion of this dissertation. I also want to thank to the Bely Lab members present and past, and in particular to James Sikes, who helped me navigate the intricacies of the U.S. academic system and has been since the start a great colleague and friend. I have a particular place in my heart for the undergraduate researchers that I mentored during these years, for I found in mentoring there is way more learning than teaching: Katie Cuilla, Simran Kaushal, María Gabriela Balarezo, Kate Turlington, Thomas Chang and Andrew Li. Finally, I want to thank my wife Paula for her love, company and support throughout the last 6 years, and for her courage in leaving so many things behind to join me in this adventure.

Eduardo E. Zattara, July 2012

Dedication

To Julia and Enrique;
being the son of a librarian and a journalist
gave me the love for books and words,
and the freedom to pursue my own path
to my heart's content

To Paula;
for she co-opted me to be with her
and made of the last 6 years the best ones of my life;
I wish we could always follow parallel paths,
and converge while embracing our divergences

And to Prof. Felipe Valverde;
the philosopher-teacher who taught me that
as Dobzhansky once said,
"nothing in biology makes sense
except in the light of evolution"

Acknowledgements

General dissertation acknowledgments

Confocal imaging was done in full at the UMCP-CLFS-CBMG Imaging Core Facility. This research was supported by National Science Foundation grants IOB-0520389 and IOS-0920502 to A.E. Bely, and by scholarships from the University of Maryland Graduate School and the Behavior, Ecology, Evolution and Systematics Graduate Program to E.E.Z.

Chapter 2 acknowledgments
I thank members of the Bely lab for helpful discussions; J. Sikes, P. Casanovas, L. Shapiro and two anonymous reviewers for comments on the manuscript; and A. Beaven for support during CLSM imaging. This work was supported by National Science Foundation grant IOB-0520389 to Alexa E. Bely. This chapter has been published in its entirety in Evolution & Development 13(1): 80-95, and permission has been granted by Wiley-Blackwell (Oxford, UK) to include the materials herein.

Chapter 3 acknowledgments
Thanks to Katie Cuilla, Simran Kaushal and María G. Balarezo for help in scoring BrdU labeled cells; and P. Casanovas for her invaluable help at taming R scripts. The G3G4 anti-BrdU antibody developed by S.J.Kaufman, was obtained from the Developmental Studies Hybridoma Bank developed under the auspices of the NICHD and maintained by The University of Iowa, Department of Biology, Iowa City, IA 52242

Chapter 4 acknowledgments
I am grateful to Christopher Laumer for his tips on fixation of unruly invertebrates.

Chapter 5 acknowledgments
Thanks to Elaine Seaver, Neva Meyer John Henry and Bob Zeller for helpful tips and advice on pulse-chase experiments and iontophoretic injections. Discovery of TTX as a worm immobilizer was the result of collaborative work with Peter J. Smith and Michael Levin at the BioCurrents Research Center, Marine Biological Laboratory at Woods Hole.

Table of Contents

List of Figures

CHAPTER 1: Introduction

Background and general aim

The evolution of novelty is one of the major topics in evolutionary developmental biology (Raff, 2000; Haag and Lenski, 2011). Novel traits are proposed to evolve mainly by co-option of pre-existing ones, followed by adaptive fine-tuning to their new role (Raff, 1996). Numerous examples of novelty by co-option have been shown at the molecular, genetic and structure level (Keys et al., 1999; Jeffery et al., 2004; Schlosser and Wagner, 2004; Stone and Hall, 2004; Harris et al., 2005; Meulemans and Bronner-Fraser, 2005; Moczek, 2005; Shubin et al., 2009). Developmental trajectories, sequences of developmental processes resulting in a particular trait or structure, can also evolve anew. New trajectories can result in relatively small changes, like forming a new structure or appendage, to the complete restructuring of a body plan, as in intercalation of larval stages and metamorphosis in holometabolous insects and many marine organisms. Post-embryonic developmental trajectories like regeneration and agametic reproduction can also be deployed to restore lost body parts or reproduce asexually. Even though co-option of developmental trajectories has been proposed as a source for many key innovations, scenarios of evolution of novel developmental trajectories have not been formally tested yet.

The close developmental and evolutionary connection between regeneration and agametic asexual reproduction offers an interesting opportunity to study the evolution of developmental trajectories. Reparative regeneration, the ability to re-

form a lost structure, is widely spread across multicellular organisms; its origin is considered to date back to the origins of multicellularity (Vorontsova and Liosner, 1960; Sánchez Alvarado, 2000; Birnbaum and Alvarado, 2008; Brockes and Kumar, 2008). Agametic asexual reproduction, the ability of organisms to replicate without passing through a gametic/zygotic stage, is also broadly distributed among animals and plants (Birnbaum and Alvarado, 2008). Furthermore, when present, both trajectories tend to occur together (Vorontsova and Liosner, 1960; Hughes, 1989). Is there a relationship between them? The most widely held view is that regenerative capabilities are a pre-requisite for the evolution of agametic asexual reproduction (Morgan, 1901; Vorontsova and Liosner, 1960; Ghiselin, 1987); however, it has also been proposed that regeneration evolved from asexual reproduction (Sánchez Alvarado, 2000). The problem is further complicated by the fact that asexual reproduction has been treated as equivalent to regeneration by many workers (Bourne, 1891; Galloway, 1899; Dehorne, 1916; Berrill, 1952; Gibson and Paterson, 2003). Detailed comparative studies of complete developmental trajectories are necessary to understand their origin and pattern of divergence.

The general aim of this dissertation is to examine the developmental, physiological and evolutionary relationship between regeneration and agametic asexual reproduction. I propose as a general working hypothesis that asexual reproduction by fission evolved independently several times by co-option of regenerative abilities, and that each initial co-option event was followed by adaptive functional divergence between both trajectories. Under this scenario, I expect that developmental trajectories of regeneration and fission will show extensive similarities

resulting from their common origin, including autapomorphic features not found in other trajectories like embryogenesis; that despite these similarities, differences will be found due to adaptive divergence; that the physiological load that both trajectories impose on the organism will be balanced by novel resource allocation strategies; and that independently gained reproductive trajectories within related taxa will evidence extensive parallel evolution due to co-option of the same underlying regenerative abilities.

Regeneration and asexual reproduction in Metazoa: which came first?

Regeneration and asexual reproduction are commonly found together in Metazoa. This evident correlation has been echoed for more than a century, and causality and polarity have been proposed both ways, yet never formally tested (Morgan, 1901; Vorontsova and Liosner, 1960; Ghiselin, 1987; Hughes, 1989; Sánchez Alvarado, 2000). Most proponents of a "regeneration first" model argue that taxonomic distribution of regeneration is broader than that of asexual reproduction, and that the former is necessary for the latter (Vorontsova and Liosner, 1960; Schroeder and Hermans, 1975; Ghiselin, 1987); in contrast, supporters of an "agametic reproduction first" model assert that regeneration is an exaptation of the organisms' ability to reproduce asexually (Darwin, 1868; Vorontsova and Liosner, 1960; Sánchez Alvarado, 2000). What should we expect under each scenario? A very strong correlation between regenerative and asexual capability will result in species having either both or neither capability, making it difficult to test for causal polarity. However, if one trajectory acts as a pre-requisite for the other, then this should cause a looser correlation and allow telling the polarities apart. I explored these predictions

by assessing the co-occurrence of regenerative and agametic reproductive abilities at two taxonomic levels: across all animal phyla, and within a single phylum, the Annelida.

For the animal-wide analysis, I made a list of 30 recognized clades at the phylum or sub-phylum level, and searched the existing literature to determine their regenerative and asexual reproductive capabilities. Since homologizing regenerative abilities across taxa with wildly different body plans is difficult, I opted to code regenerative ability from a functional approach based on features easier to categorize and that could relate directly to asexual reproduction ability. I defined five regeneration categories: 1) Appendage regeneration, restoration of any structures not included in the main body axis; 2) Axial type I, restoration of terminal structures along the main body axis; 3) Axial type II, restoration of significant portions of the main body axis, but no possible amputation plane will result in two regeneration competent pieces; 4) Axial type III, as the previous, but at least one plane can separate the animal in two parts each capable of regenerating complete individuals; 5) Whole body regeneration, where a very small fraction of the original animal can regenerate a complete individual. These five categories are not mutually exclusive, instead being usually nested. However, phyla with no obvious appendages could not be assigned appendage regeneration. Asexual reproduction was assigned to four categories: 1) Architomic fission, in which the animal separates and each piece then develops missing structures; 2) Paratomic fission, in which new structures develop before the animal splits; 3) Budding, in which the daughter individual forms as a second main body axis; 4) Propagular budding, in which a small fragment of the

organism detaches and then reforms a complete individual. I also scored for the presence of parthenogenesis, a form of gametic asexual reproduction, since it has been proposed that it negatively correlates with agametic reproductive modes (Hughes, 1989). Each category was coded as present/absent for every phylum. A single example was considered enough to score as present for the phylum as a whole; thus, the resulting patterns highlight the maximum potential achieved by each phylum, rather than the average expectation.

The results show that distribution of regenerative abilities is broader than that of asexual reproduction (Fig.1.1A). Architomy and budding are the most frequent reproductive modes, and usually occur together. Paratomy is rarer, and always occurs along with architomy. Propagular budding is very infrequent, which may be due to it being an uncommon adaptation or just reflect a detection bias. Since regenerative abilities are nested, the maximum regeneration level can be plotted against the number of the number of reproductive modes, showing that phyla not reaching Type III axial regeneration do not present any agametic reproduction mode (Fig. 1.1B). This suggests that an animal must be able to be split in at least two regeneration competent pieces for its lineage to evolve any agametic reproductive mode; while this may sound trivial for architomy, there is no obvious reason why paratomy or budding should require type III regeneration. Parthenogenesis, a gametic reproductive strategy, has been considered as the alternative path to asexual reproduction for those groups without enough regenerative abilities, and thus predicted to be negatively correlated with the presence of agametic reproduction (Hughes, 1989), but such a trend is not found in this dataset.

This overview of regeneration and fission ability across phyla provides a good broad picture, but lacks enough resolution to reliably answer the polarity question. Furthermore, character scoring may be misleading; for example, it would just take one species with good regenerative ability and another capable of agametic reproduction to drive the correlation for the whole phylum and lead to a wrong conclusion. Thus it is desirable to examine each phylum more in-depth; while a fully detailed examination of all metazoan phyla is beyond the scope of this work, I tested the informative value of this approach by surveying in more detail a single phylum, the Annelida.

Distribution of regeneration and fission within Annelida supports regeneration as a pre-requisite for agametic reproduction

A Metazoan-wide overview of the distribution of regenerative and agametic reproductive capabilities suggests that the former is a pre-requisite for the later. However, given the shortcomings of such broad survey, I decided to test whether the above patterns hold and receive further support after a finer scale review. I chose the phylum Annelida because they present a broad range of regenerative and reproductive abilities (and because they are really cool creatures). In contrast with the above survey, I used species as the taxonomic unit for this intra-phylum analysis. I searched previous reviews and primary literature for references to the ability of each species to: 1) regenerate the posterior end of the body, including the annelid posterior growth zone, from a posterior wound surface; 2) regenerate one or more anterior segmental units from an anterior wound surface; 3) reproduce asexually by architomic or paratomic fission. In most cases, absence of regenerative abilities was scored only

when the sources specified an experimental confirmation; however, I also scored it in groups for which I found general "blanket" statements by two or more independent sources; a similar criterion was used for asexual reproduction. I found and scored data for a total 326 annelid species grouped in 35 clades, plus an outgroup formed by 9 nemertean species grouped in 2 clades.

The resulting dataset shows that regeneration and fission are highly variable across the Annelida (Fig. 1.2). Posterior regeneration is highly prevalent across the phylum, with only opheliids, echiurids, branchiobdellids and leeches showing total absence as a group. Distribution patterns of anterior regeneration are more variable. For example, most Sedentaria are capable of regenerating an anterior end, but groups basal to Clitellata (opheliids, echiurids and capitellids) are not; yet most aeolosomatids and oligochaetous clitellates do regenerate the anterior end. This suggests that anterior regeneration abilities can increase or decrease along lineages. Fission shows a slightly more clustered pattern, with most clades either showing presence or absence for most of its members; independent gains of this ability are evidenced by the presence of a few fissioning species within large clades where most other species do not fission. However, the large number of missing data highlight that the current tally of regenerative and agametic capabilities is very incomplete. The fact that even this sample of 326 out of about 15 000 species has so many missing data emphasizes the need to conduct more systematic surveys for the presence of these developmental trajectories.

What polarity scenario is better supported by this Annelida dataset? The clade-specific frequency of regeneration and fission can be calculated as the number

of species in which each trajectory is present divided by the total number of species scored for each clade in this dataset; then each clade can be plotted on a fission versus regeneration graph. If regeneration and fission are fully independent, clades would be scattered and without pattern; conversely, if they are so tightly linked that each species presents both trajectories or none, all points should fall along a unity line. But if presence of one trajectory is required for evolving the other, then the nested distribution is expected to cause all points to be restricted to either the upper diagonal (if fission is required for regeneration) or the lower diagonal (if regeneration is required for fission).

After calculating the frequency of anterior and posterior regeneration and fission for each of the 35 annelid and 2 nemertean clades, a plot of fission versus anterior regeneration frequencies shows that most clades fall within a triangular region to the lower right of the diagonal (Fig. 1.3). This is what would be expected under a scenario were anterior regenerative ability acts as a permissive pre-requisite. Since most annelids are capable of posterior regeneration, anterior regeneration is the limiting factor that determines whether a species can reach type III axial regeneration (see above). Out of 188 species without missing data, only 5 fission in the absence of anterior regeneration; all 5 belong to three naidine genera thought to have lost anterior regeneration secondarily after gain of fission in the clade (Bely, 1999; Bely and Sikes, 2010). Thus, they do not constitute an exception to the general observation that gains of fission are only seen when type III axial regeneration or better is present.

Despite the large amount of missing data, distribution of regeneration and fission among annelids supports the hypothesis that regeneration is a pre-requisite to

evolve agametic asexual reproduction. It also agrees with the analysis of the broader Metazoan-wide dataset, showing that scoring a phylum's maximum realized potential rather than the average capability is an informative approach. It would be worthwhile to apply this methodology for other phyla, both more diverse (like Cnidaria, Platyhelminthes) or restricted in developmental capabilities (Panarthropoda, Nematoda) to verify if these hypotheses holds beyond Annelida.

An overview of this work

The general aim of this dissertation is to provide novel insights into the developmental, physiological and evolutionary relationships between regeneration and agametic asexual reproduction in naid annelids. I used comparative analyses of developmental trajectories as my main approach, but also explored experimentally how these trajectories interact with each other within a physiological context. I also developed and tested novel techniques to study the dynamics of these developmental processes.

Chapter 2 sets to answer whether regeneration and paratomic fission are distinct developmental trajectories. Using the naid species *Pristina leidyi* as a model, I made a detailed description and comparative study of both developmental trajectories in this species. I found that while regeneration and fission share numerous common elements, including an autopomorphic feature not seen in other trajectorios, they also present significant differences distributed throughout the trajectories, indicating that divergence has occurred along their entire developmental course.

Chapter 3 explores the allocation strategies used by *Pristina leidyi* to balance resource investment between somatic growth, regeneration and reproduction by

fission. I used cell proliferation and size changes as a "common currency" to compare relative investment in each process, and to study how baseline allocation patterns change when more than one developmental trajectory occurs at the same time. I found that worms have a characteristic baseline antero-posterior distribution pattern of proliferation that is altered in level but not in shape with changes in nutritional level and fission; amputation however causes body-wide down-regulation of proliferation. I also show that contemporaneous regeneration and fission interact with each other, and that the results of that interaction depend on the stage of fission and whether the cut removed an anterior or a posterior end.

Chapter 4 steps out to compare developmental trajectories along two independent origins of fission in the two fissioning clades of Naididae, the subfamilies Pristininae and Naidinae. Using a similar approach to Chapter 2, I studied regeneration and fission in a second pristinine species, seven naidine species and one outgroup species representing a distant relative, and found evidence of extensive evolutionary convergence in fission trajectories between the two groups, suggesting strong developmental channeling due to co-option of regeneration in a similar organismal context. However, I also found that each clade has its own distinctive mode of building a new central nervous system, indicating that this feature was less constrained during the origin of fission.

Chapter 5 investigates the cellular basis of annelid regeneration in *Pristina leidyi* to test some long-standing hypotheses about cell proliferation and migration. I used thymidine analogue incorporation to perform pulse-chase experiments and carbocyanine dye iontophoretic injections to mark and trace groups of cells and

patches of tissue. I also developed a novel immobilization and mounting technique for long-term, high-resolution live 4D imaging that allowed me to record the full process of regeneration. I used this technique to characterize migrating cell populations and their behavior, which among other results yielded the first direct evidence for the migration of neoblasts, first proposed more than 120 years ago.

Chapter 1 Figures

Figure 1.1: Phylogenetic distribution of regenerative abilities and asexual reproductive strategies

A) Distribution of regenerative and asexual reproductive abilities across 30 metazoan phyla. The dendrogram represents phylogenetic relationships between phyla based on recent studies (Dunn et al., 2008; Srivastava et al., 2008; Paps et al., 2009; Philippe et al., 2011); the three main bilaterian clades are color coded red (Deuterostomia), blue (Ecdysozoa) and green (Lophotrochozoa). B) The number of asexual reproductive modes increases non-linearly with regeneration level. Bubble-pie plot showing number of reproductive modes in a phylum as a function of the regeneration level; the size of the circles is proportional to the number of phyla, and the internal divisions show the proportional contribution of each superclade. Note that no agametic reproduction occurs at regeneration level 3 (axial type II) or lower. (Coe, 1934; Vorontsova and Liosner, 1960; Whitfield and Evans, 1983; Hughes, 1989; Thiemann and Ruthmann, 1991; Hummon and Hummon, 1993; Runham, 1993; Shostak, 1993; Benazzi and Benazzi-Lentati, 1993; Fell, 1993; Gilbert, 1993; Alvariño, 1994; Mladenov and Burke, 1994; Nielsen, 1994; Petersen, 1994; Azariah, 1994; Chuang, 1994; Wallace et al., 1996; Åkesson et al., 2002; Neuhaus and Higgins, 2002; Martinelli and Spring, 2004; Read, 2008; Srivastava et al., 2008; Streit, 2008; Sköld et al., 2009; Manylov, 2010; Hanelt et al., 2012)

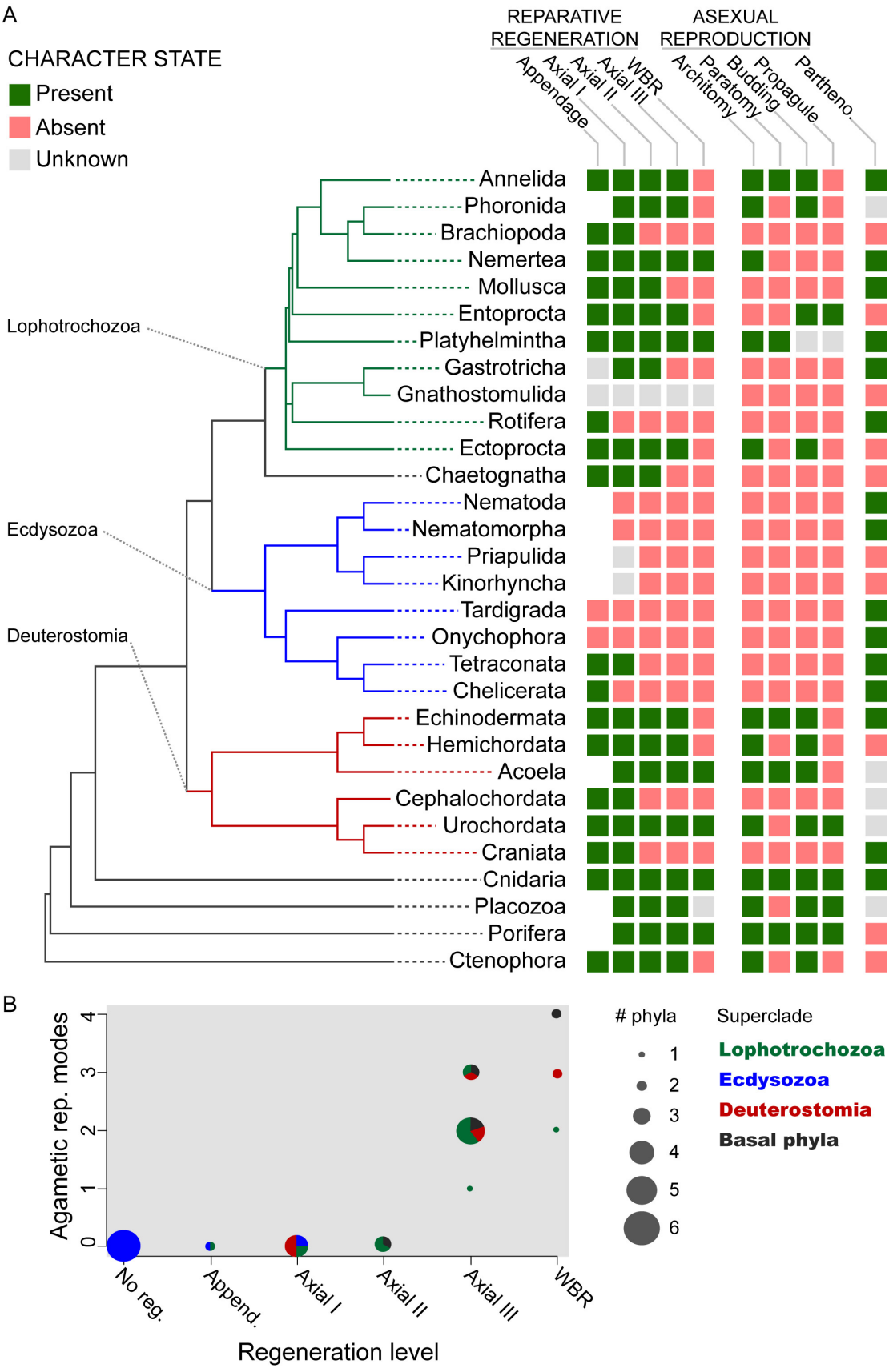
A
CHARACTER STATE
Present
Absent
Unknown
REPARATIVE REGENERATION
ASEXUAL REPRODUCTION
Appendage
Axial I
Axial II
Axial III
WBR
Architomy
Paratomy
Budding
Propagule
Partheno
Annelida
Phoronida
Brachiopoda
Nemertea
Mollusca
Entoprocta
Platyhelmintha
Gastrotricha
Gnathostomulida
Rotifera
Ectoprocta
Chaetognatha
Nematoda
Nematomorpha
Priapulida
Kinorhyncha
Tardigrada
Onychophora
Tetraconata
Chelicerata
Echinodermata
Hemichordata
Acoela
Cephalochordata
Urochordata
Craniata
Cnidaria
Placozoa
Porifera
Ctenophora
Lophotrochozoa
Ecdysozoa
Deuterostomia
B
Agametic rep. modes
0
1
2
3
4
No reg.
Append.
Axial I
Axial II
Axial III
WBR
Regeneration level
phyla
1
2
3
4
5
6
Superclade
Lophotrochozoa
Ecdysozoa
Deuterostomia
Basal phyla

Figure 1.2: Phylogenetic distribution of regeneration and fission in the phylum Annelida

Diagram showing presence (green) or absence (red) of posterior regeneration (left column, P), anterior regeneration (center column, A) and agametic reproduction by fission (right column, F); empty spaces represent unknowns. 326 annelid and 9 nemertean species (rows) are grouped within grey boxes representing clades at approximately the family level; colored bars at the right show traditional but not necessarily monophyletic higher order groups. Phylogenetic relationships between groups are shown by a dendrogram based on recent molecular studies (McHugh, 2000; Erséus, 2005; Zrzavy et al., 2009; Erséus et al., 2010; Struck et al., 2011). The table shows the frequency of each developmental trajectory within each group (number of species presenting the trajectory over total number of species scored for the group) and the number of species in each group. NA means no data are available for all species in the group. (Morgan, 1897; Michel, 1898; Galloway, 1899; Harper, 1904; Watson, 1906; Krecker, 1910; Allen, 1911; Dehorne, 1916; Hyman, 1916, 1938, 1940; Korschelt, 1919; Consoli, 1923; Gates, 1927, 1949; Okada, 1929; Berrill, 1931, 1952, 1978; Coe, 1934; Sayles, 1936; Van Cleave, 1937; Chu and Pai, 1944; O'Brien, 1946; Harms, 1948; Sperber, 1948; Moment, 1951; Stout, 1958; Bell, 1959; Clark and Bonney, 1960; Christensen, 1964, 1994; Herlant-Meewis, 1964; Rajulu and Krishnan, 1969; Rice, 1970; Brinkhurst and Jamieson, 1971; Bilello and Potswald, 1974; Lasserre, 1975; Schroeder and Hermans, 1975; Harman and Loden, 1978; Naidu and Naidu, 1979; Casellato, 1984; Clavier, 1984; Timm, 1984; Alonso-Bedate and Sequers, 1985; Nemec and Brinkhurst, 1987; Brusca and Brusca, 1990; Finogenova and Arkhipova, 1994; Bely, 1999; L.C. Armendariz, 1999; Bely, 2006; Myohara et al., 1999; Gibson and Paterson, 2003; Müller et al., 2003; Williams, 2004; Lindsay et al., 2007; Lindsay, 2010; Bely and Sikes, 2010; David and Williams, 2011; Glasby et al., 2012).

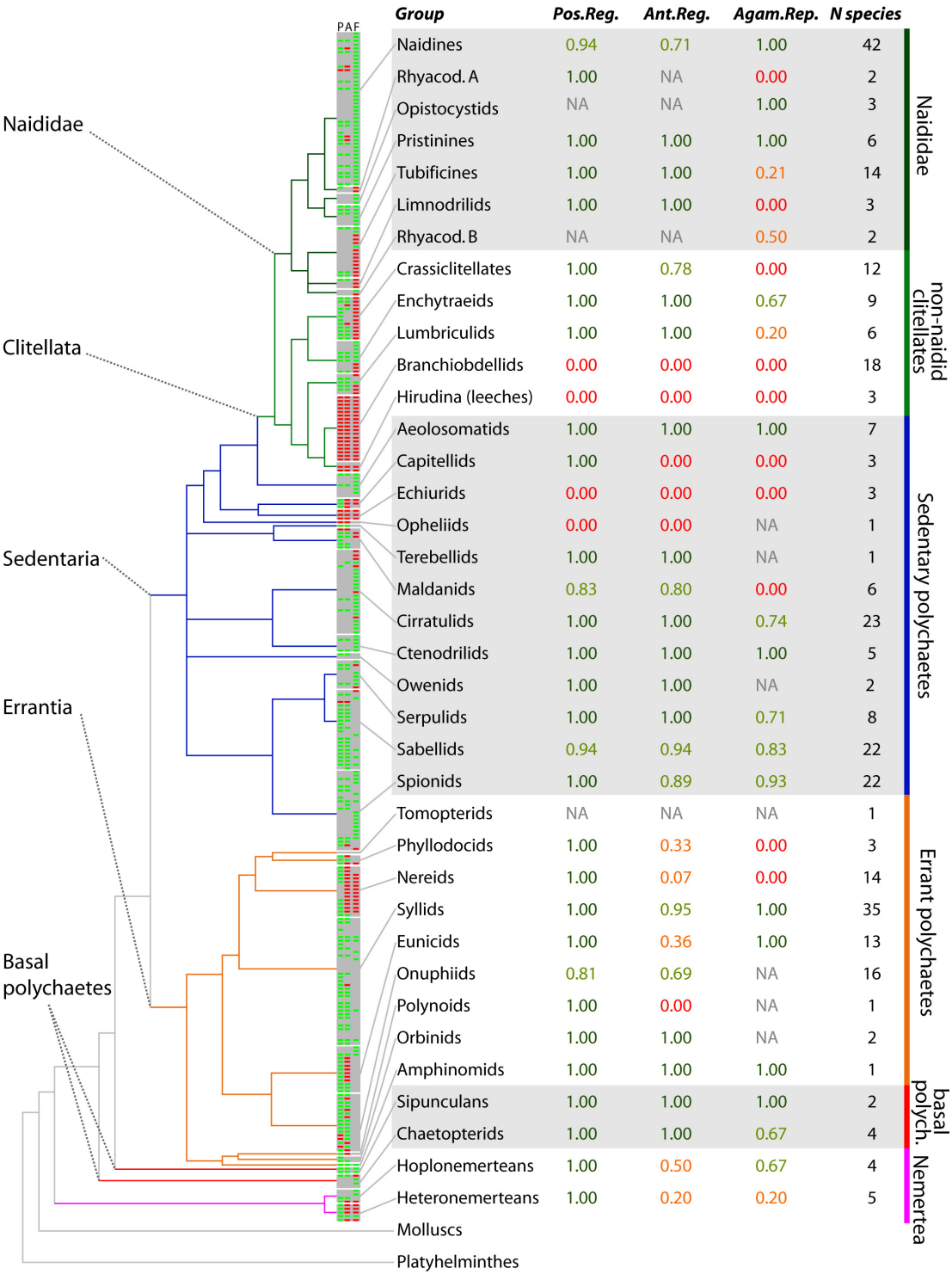
PAF
Group
Pos.Reg.
Ant.Reg.
Agam.Rep.
N species
Naidines 0.94 0.71 1.00 42
Rhyacod. A 1.00 NA 0.00 2
Opistocystids NA NA 1.00 3
Pristinines 1.00 1.00 1.00 6
Tubificines 1.00 1.00 0.21 14
Limnodrilids 1.00 1.00 0.00 3
Rhyacod. B NA NA 0.50 2
Crassiclitellates 1.00 0.78 0.00 12
Enchytraeids 1.00 1.00 0.67 9
Lumbriculids 1.00 1.00 0.20 6
Branchiobdellids 0.00 0.00 0.00 18
Hirudina (leeches) 0.00 0.00 0.00 3
Aeolosomatids 1.00 1.00 1.00 7
Capitellids 1.00 0.00 0.00 3
Echiurids 0.00 0.00 0.00 3
Opheliids 0.00 0.00 NA 1
Terebellids 1.00 1.00 NA 1
Maldanids 0.83 0.80 0.00 6
Cirratulids 1.00 1.00 0.74 23
Ctenodrilids 1.00 1.00 1.00 5
Owenids 1.00 1.00 NA 2
Serpulids 1.00 1.00 0.71 8
Sabellids 0.94 0.94 0.83 22
Spionids 1.00 0.89 0.93 22
Tomopterids NA NA NA 1
Phyllodocids 1.00 0.33 0.00 3
Nereids 1.00 0.07 0.00 14
Syllids 1.00 0.95 1.00 35
Eunicids 1.00 0.36 1.00 13
Onuphiids 0.81 0.69 NA 16
Polynoids 1.00 0.00 NA 1
Orbinids 1.00 1.00 NA 2
Amphinomids 1.00 1.00 1.00 1
Sipunculans 1.00 1.00 1.00 2
Chaetopterids 1.00 1.00 0.67 4
Hoplonemerteans 1.00 0.50 0.67 4
Heteronemerteans 1.00 0.20 0.20 5
Molluscs
Platyhelminthes
Naididae
Clitellata
Sedentaria
Errantia
Basal polychaetes
Naididae
non-naidid clitellates
Sedentary polychaetes
Errant polychaetes
basal polych.
Nemertea

Figure 1.2

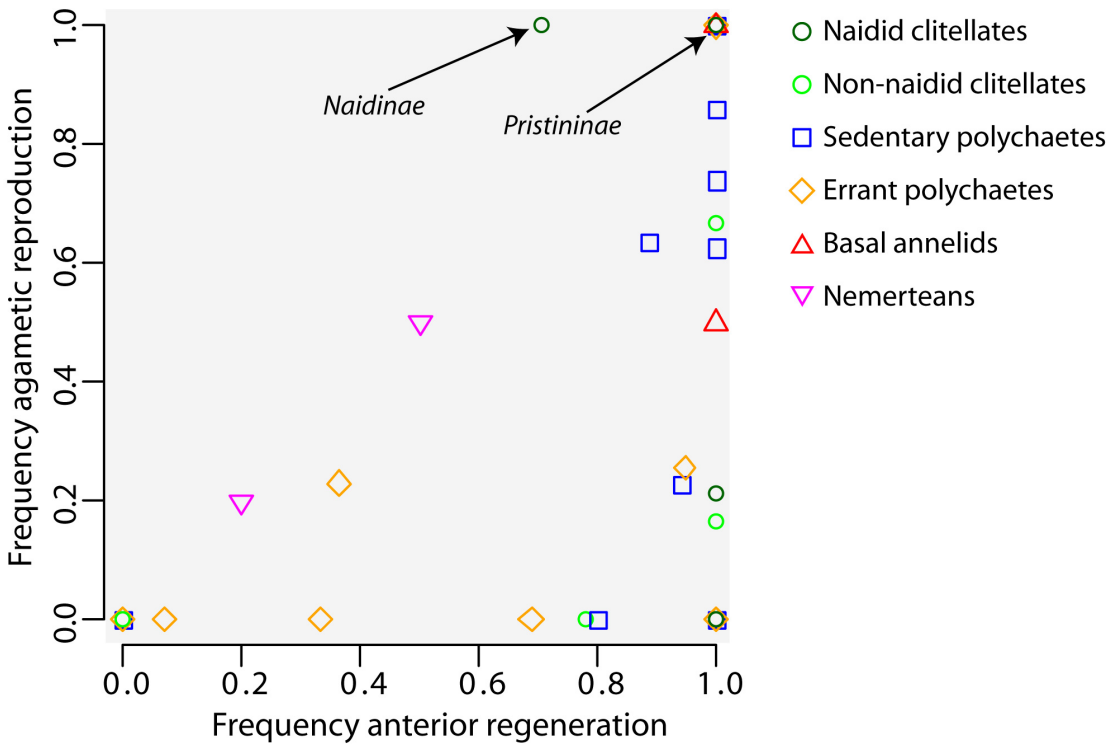

Figure 1.3: Presence of agametic reproduction is contingent on anterior regeneration in Annelida

Plot of frequency of agametic reproduction by fission within each group as a function of the frequency of anterior regeneration ability. The frequency was calculated as number of species presenting the trajectory over total number of species scored for the group. The only five fissioning species incapable of anterior regenerating are within the Naidinae group.

CHAPTER 2: Evolution of a novel developmental trajectory: fission is distinct from regeneration in the annelid *Pristina leidyi*

Abstract

Understanding how novelty arises has been a major focus of evolutionary developmental biology. While the origin of new genes, gene functions, and morphological features has been studied intensely, the origin of entire developmental trajectories, such as regeneration or agametic reproduction, remains poorly understood. Agametic reproduction by fission is a novel trajectory evolved numerous times among animal phyla, including Annelida, in which it is thought to arise by co-option of regeneration. To gain insight into how a novel trajectory may evolve, I investigated a relatively recent origin of fission. I performed a detailed comparison of morphogenesis during regeneration and fission in the annelid *Pristina leidyi* (Clitellata, Naididae), from the onset of these trajectories to the achievement of the final morphology. I found extensive similarities between fission and regeneration morphogenesis, and, of particular note, found evidence for a synapomorphy of fission and regeneration (apparently not shared with embryogenesis) in peripheral nervous system development, providing strong support for the hypothesis that fission is derived from regeneration. I also found important differences between fission and regeneration, during development of multiple organ systems. These are manifested by temporal shifts in developmental events and by the presence of elements unique to only one process. Differences are not obviously temporally clustered at the beginning,

middle, or end of development but rather occur throughout, indicating that divergence has occurred along the entire developmental course of these trajectories.

Introduction

The origin of novelties is a key aspect of biological diversification. Understanding how novel features evolve has consequently been a major focus of evolutionary developmental biology (Carroll et al., 2005). Gradual modification of pre-existing elements, sometimes referred to as "evolutionary tinkering," is a common process by which novelties arise (Jacob, 1977; Moczek, 2008; Zhou and Wang, 2008; Shubin et al., 2009). Molecular and developmental evolutionary studies have shown, for example, that new morphological structures can often be traced back to pre-existing morphological structures, that new cell types can arise from pre-existing cell types, and that new genes often arise through modification of pre-existing genes (Shubin et al., 1997; Keys et al., 1999; Jeffery et al., 2004; Schlosser and Wagner, 2004; Stone and Hall, 2004; Harris et al., 2005; Meulemans and Bronner-Fraser, 2005; Moczek, 2005). Although the process of co-option in the evolution of new morphologies, cell types, and genes is becoming well documented, other types of novelty, such as the origin of whole new developmental trajectories for building an organism, remain poorly studied.

Multiple developmental trajectories for generating the adult phenotype have arisen during animal evolution. Embryogenesis is an ancient, universal process among animals, but it is not the only way to build an adult. Regeneration, agametic reproduction (i.e., cloning by fission or budding), and large-scale tissue renewal (e.g., continuous whole-body renewal as occurs in Hydra and planarians) are alternative

processes by which this same endpoint, the adult body, can be built or rebuilt. Although they converge on a common endpoint, these trajectories have qualitatively different starting points. How do novel developmental trajectories evolve? Like other types of novelties, new trajectories most likely arise by a gradual modification of pre-existing trajectories.

To understand how new trajectories evolve, comparisons of developmental trajectories within a species are needed (Reitzel et al., 2007). Such comparisons reveal the source and pattern of developmental divergence between trajectories within a lineage, keeping the endpoint phenotype constant. Most intraspecific studies comparing development across trajectories (e.g., comparing embryogenesis and regeneration, or regeneration and agametic reproduction) report extensive similarities between them (Berrill, 1952; Vorontsova and Liosner, 1960; Technau and Bode, 1999; Bely and Wray, 2001; Carlson, 2007; Ghosh et al., 2008; Gurley et al., 2008; Burton and Finnerty, 2009; Lengfeld et al., 2009; Sikes and Bely, 2010), consistent with the idea that these trajectories are, at some level, evolutionarily related. Although much less common, a handful of detailed studies have also uncovered differences among trajectories. For example, a few genes have been shown to be differentially expressed between embryogenesis and regeneration in vertebrates (Akimenko et al., 1995; Gardiner et al., 1995; Carlson et al., 2001; Christen et al., 2003; Sugiura et al., 2004; Whitehead et al., 2005), and comparisons between regeneration and agametic reproduction in cnidarians, annelids, and platyhelminths have revealed differences in the extent and timing of tissue remodeling and in the expression of several genes (Hori and Kishida, 1998, 2001; Bely and Wray, 2001;

Martinez et al., 2005; Burton and Finnerty, 2009; Lengfeld et al., 2009). These findings indicate that trajectories converging on the same phenotype can be distinct. However, to better understand the process of trajectory divergence, studies are needed that investigate complete trajectories (from initiation to completion of final morphology) and, importantly, that focus on trajectories of recent origin to reveal an early stage in the process.

Agametic reproduction by fission, in which an individual physically divides its body to reproduce, has evolved numerous times among animals, including among annelids, echinoderms, nemerteans, cnidarians, and sponges (Ghiselin, 1987; Brusca and Brusca, 1990; Sköld et al., 2009). Some of these occurrences of fission clearly represent recent origins, and these are particularly useful for investigating early stages in the evolution of a new developmental trajectory. Several lines of evidence suggest that fission can be derived from regeneration (Morgan, 1901; Ghiselin, 1987), and this evidence is particularly clear within the phylum Annelida. Fission has evolved at least a dozen times within this group (Lasserre, 1975; Schroeder and Hermans, 1975), and origins have consistently occurred within regenerating clades but never within nonregenerating clades (even large ones such as the leeches). Furthermore, at a gross level, morphogenesis of new tissue is so similar between fission and regeneration that these processes have sometimes been described as being equivalent in annelids (Bourne, 1891; Galloway, 1899; Dehorne, 1916; Berrill, 1952; Gibson and Paterson, 2003).

To investigate the recent evolution of a new trajectory, I performed a detailed comparison of morphogenesis during fission and regeneration in the annelid *Pristina*

leidyi Smith (Annelida, Clitellata, Naididae, Pristininae). Although all species in the genus *Pristina* and some of their close relatives can reproduce by fission (Erséus et al., 2010), the majority of species within the Naididae (former Tubificidae), as well as the majority of the Clitellata, reproduce strictly sexually (Brinkhurst and Jamieson, 1971), indicating that fission in *P. leidyi* is of a relatively recent origin. Like most of its fissioning close relatives, *P. leidyi* reproduces by paratomic fission, a type of fission in which a new head and tail are intercalated in the middle of an individual's body, forming transiently linked chains of individuals which then split apart once development of new body regions is complete (Fig. 2.1B). *P. leidyi* can also regenerate both anteriorly and posteriorly (Fig. 2.1A), capabilities which are likely ancestral for the phylum (Bely, 2006) and are thought to be the trajectories co-opted during the evolution of fission. A previous study in this species found largely similar, though not identical, gene expression patterns for the body-patterning gene orthodenticle across fission and regeneration (Bely and Wray, 2001). For this study, I investigated morphogenesis throughout fission and regeneration, from the onset of each process to the achievement of the final morphology, and focus especially on cell proliferation, muscle development, gut development, presence of nephridia, and central and peripheral nervous system development. I also establish staging schemes for both regeneration and paratomic fission to facilitate their study and comparisons between processes.

Materials and Methods

Animal material

P. leidyi specimens were originally obtained from Carolina Biological Supply (sold as *Stylaria*). Animals were cultured in artificial spring water (1% artificial seawater), fed dried spirulina powder, and otherwise maintained as described previously (Bely and Wray, 2001). Fissioning worms were collected from actively growing cultures. To elicit regeneration, worms without fission zones were anesthetized in 0.05 mM nicotine in spring water and amputated with a scalpel. Anterior regeneration was elicited by amputating seven anterior segments, cutting posterior to the stomach and anterior to the chaetae (bristles) of segment 7 (Fig. 2.S1A). Posterior regeneration was elicited by amputating the tail, cutting posterior to the chaetae of segment 14 (Fig. 2.S1A). Regenerating animals were collected within the first hour after amputation and every day thereafter through day 5. Unlabeled specimens were examined live (in spring water) or fixed in 75% glycerol:25% phosphate-buffered saline (PBS) using differential interference contrast microscopy. For fixations, worms were relaxed 10 min in cold (4°C) relaxant solution (10 mM $MgCl_2$/5 mM NaCl/1 mM KCl/8% ethanol), fixed 30 min in 4% formaldehyde in 0.75 × PBS, and rinsed in 1 × PBS. At least 15 individuals were examined for each analysis and timepoint.

Bromodeoxyuridine (BrdU) analysis

Cell proliferation was assessed using BrdU incorporation to detect cells in, or recently in, S-phase, using a protocol modified from Seaver *et al*. (2005). Worms

were incubated in 0.2 mg/ml BrdU (Sigma, St. Louis, MO, USA) in culture water for 6 h, relaxed and fixed as described above, incubated in 6 m HCl for 30 min at 37°C, washed with PBS, permeabilized with 0.1% Triton-X in PBS (PBTx), blocked 1 h in 10% normal goat serum (NGS) in PBTx, and incubated 15–20 h at 4°C in mouse anti-BrdU monoclonal antibody (clone BU33, Sigma B2531) diluted 1:100 in blocking solution. Specimens were then washed in PBTx and incubated 3–5 h at room temperature in horseradish peroxidase-conjugated goat anti-mouse IgG(H+L) antibodies (Jackson ImmunoResearch, West Grove, PA, USA). Specimens were pre-incubated for 10 min in 500 µl in diaminobenzidine and 0.064% NiCl in PBTx, and 1 µl of 0.3% hydrogen peroxide was then added to develop the stain for 2–4 min. Samples were washed with PBTx and PBS, transferred through a graded glycerol series (33%, 50%, and 75% glycerol in PBS) and mounted in glycerol (75% in PBS).

Phalloidin staining

Muscle F-actin was labeled with phalloidin. Fixed specimens were permeabilized in PBTx, blocked 10 min in 10% NGS in PBTx, incubated 8–16 h in 66 nm Alexa-Fluor-488-conjugated phalloidin (Invitrogen, Carlsbad, CA, USA) in blocking solution at 4°C, washed three times in PBS, transferred through a graded glycerol series, and mounted in Fluoromount-G (Southern Biotech, Birmingham, AL, USA). AF488-phalloidin strongly labeled the muscle fibers of the body wall, gut, and chaetal bundles.

α-tubulin, serotonin and nuclear labeling

Fixed specimens were permeabilized in PBTx, blocked 1 h in 10% NGS in PBTx, and incubated 15–20 h at 4°C with mouse anti-acetylated-α-tubulin monoclonal antibody (Sigma) and rabbit anti-serotonin polyclonal antibodies (Sigma), both diluted 1:100 in blocking solution. Specimens were then washed in PBTx and incubated for 3–5 h at RT in FITC-conjugated goat anti-mouse IgG(H+L) antibodies (Jackson ImmunoResearch) and Alexa-Fluor-546-conjugated goat anti-rabbit IgG antibodies (Invitrogen), both diluted 1:200 in blocking solution. After washing with PBTx and PBS, specimens were transferred through a graded glycerol series and mounted in Fluoromount-G. The acetylated-α-tubulin antibody labeled cilia in the gut and nephridia, external sensory hairs, and nerves of the peripheral nervous system and cerebral ganglion. The ventral nerve cord was also weakly labeled. Anti-serotonin antibodies labeled nerves and cell bodies in the ventral nerve cord and cerebral ganglion, the circumenteric connectives (nerves connecting the ventral nerve cord to the cerebral ganglion), and nerves innervating the prostomium and pharynx. Nuclei were labeled using either 0.2 mg/ml DAPI or 0.1 μm TO-PRO-3 (Invitrogen).

Microscopy and imaging

Samples were imaged using a Zeiss Axioplan2 microscope equipped with a Zeiss AxioCam HRc camera (Zeiss, Oberkochen, Germany) interfaced through Openlab (Improvision, Conventry, UK) or Zeiss LSM 510 and Leica SP5-X confocal laser scanning microscopes (Leica, Wetzlar, Germany) (CLSM). Postacquisition image processing (level corrections, color merging, and Z-stack projections) was

performed using ImageJ (Bethesda, MD, USA). Two dimensional deconvolution of non-CLSM images and image montages were carried out using Adobe Creative Suite CS3.

Results

General anatomy

The general anatomy of *P. leidyi* is diagrammed in Fig. 2.S1. Individuals are typically 0.15–0.20 mm in diameter, 2–4 mm in length, and comprised of approximately 15–35 segments. An asegmental cap of tissue is present at either end of the worm, the posterior cap being the pygidium, and the anterior cap being the prostomium (elongated into a proboscis in this species). A proliferative region just anterior to the pygidium, the posterior growth zone, produces new segments during normal growth. Fission zones are typically formed between segments 15 and 18.

Segments have a muscular body wall, composed of a single-layered epidermis underlain by longitudinal and circular muscles, and a spacious coelomic cavity subdivided by septa into segmentally iterated pouches. In each segment, four bundles of chaetae protrude from the body wall, a left/right pair of ventrolateral bundles and a left/right pair of dorsolateral bundles. The digestive tract is comprised of an anteroventral mouth and buccal cavity, which are unciliated, followed by a protrusible pharynx, esophagus, stomach (in segment 7), and hindgut, all of which are ciliated. In segments posterior to segment 7, nephridia (ciliated excretory structures) are typically present laterally, beneath the body wall, on one or both sides of the segment. A dorsal cerebral ganglion lies above the foregut in segment 1 and a

ganglionated ventral nerve cord runs along the length of the body, with one ganglion per segment. A nerve loop connects the cerebral ganglion and ventral nerve cord: a left/right pair of circumenteric connectives extends anterodorsally from the ventral nerve cord ganglion of segment 1, loops around the foregut, and connects in the cerebral ganglion, forming the cerebral commissure connecting the left and right halves of the brain. Three subepidermal peripheral nerve rings[1] (nr1, nr2, and nr3, from anterior to posterior) occur in all segments posterior to segment 6. Ventrally each nerve ring connects to the ventral nerve cord, and fine extensions from these rings connect to epidermal sensory hair tufts. A main dorsal blood vessel and a main ventral blood vessel each run along the length of the animal, being connected to each other directly at the termini and by smaller transverse vessels along the length of the body.

Regeneration: general morphogenesis and staging series

Unstained fixed and live regenerating material was investigated to provide a general description of morphogenesis and to establish a staging series for anterior and posterior regeneration. I divide anterior regeneration (AR) and posterior regeneration (PR) each into six stages (AR and PR Stages 1–6; Fig. 2.1, A and C). During anterior regeneration, four anterior segments are produced (if four or more segments were removed), while during posterior regeneration the number of segments produced is variable. The duration of regeneration is highly variable, being sensitive to both physiological and environmental conditions. Typical worms at room temperature

[1] A comparative study of peripheral nerve rings across Clitellata has shown that 4 rings (I-IV, numbered according to their position relative to each ventral nerve ganglion) seem to be the ancestral state for the group, and that in *P. leidyi*, ring III is much reduced (Zattara and Bely, *in preparation*). Because *P. leidyi* have septate ganglia, nr1, nr2 and nr3 correspond to rings IV, I and II respectively.

complete anterior regeneration in approximately 5 days and posterior regeneration in approximately 3–4 days. Thus, each of the stages I define lasts roughly 12–24 h.

AR/PR Stage 1, wound healing

After amputation, the wound is closed by contraction of circular muscles and a wound plug comprised of aggregated cells and acellular material forms at the wound site. The severed edges of the body-wall epidermis seal together, forming a wound epithelium over the wound, and the severed edges of the gut seal, forming a blind tube.

AR/PR Stage 2, blastema formation

The blind end of the gut attaches to the wound epithelium, and, during posterior regeneration, the anus reopens. Epidermis at the wound site thickens and a hyaline mass of cells, the blastema, forms there. During anterior regeneration, blastemal cell masses accumulate just below the wound epithelium and surrounding the gut, while during posterior regeneration, paired cell masses form ventrolaterally, later spreading dorsally. Dorsal and ventral blood vessels are reconnected by this stage, restoring blood circulation at the wound site.

AR/PR Stage 3, blastema patterning

The blastema grows and becomes visibly segmented, forming bilateral groups of cell packets. During anterior regeneration, four (sometimes five) paired packets form and divide into ventral, ventrolateral, and lateral portions; epidermis at the distal tip thickens, forming the presumptive prostomium. During posterior regeneration, a variable number of paired packets divide into ventral, ventrolateral, and dorsolateral portions; epidermis at the posterior tip thickens and acquires the rounded morphology of the pygidium.

AR/PR Stage 4, early differentiation

The blastemal packets begin differentiating, with ventral nerve cord ganglia, ventral chaetal sacs, and dorsal chaetal sacs developing from the ventral, ventrolateral, and lateral/dorsolateral blastemal portions, respectively. Septa form between developing segments. During anterior regeneration, the prostomium adopts a conical shape and develops sensory hairs, the prospective mouth forms as an invagination of the prostomium's ventral margin, the cerebral ganglion primordium forms dorsally just behind the prostomium, and the foregut begins forming the dorsal pharynx. During posterior regeneration, the pygidium develops sensory hairs.

AR/PR Stage 5, late differentiation

Ventral nerve cord ganglia and chaetal sacs complete differentiation, and chaetal sacs begin to secrete chaetae that emerge from the body wall. Segment development follows an anterior to posterior gradient that is only slight in anterior regeneration but marked in posterior regeneration. During anterior regeneration, the prostomium elongates and the mouth and pharyngeal sac differentiate. During posterior regeneration, the posterior growth zone forms between the pygidium and the newly formed segments and begins adding new segments, such that regeneration grades into normal posterior growth.

AR/PR Stage 6, growth

Chaetae from all new head segments have emerged. The new head or tail grows in size until it is indistinguishable from that of a normal, uncut animal. During anterior regeneration, because only four anterior segments regenerate when seven segments are removed (as was done for my studies), the remaining original segments experience an anterior shift in axial position. Original segments undergo a

morphallactic change (taking on new, more anterior segment identities) which becomes evident during this stage. The original gut behind the amputation plane is remodeled to become consistent with new segment identities, and this is most noticeable as the gut in original segment 9 thickens and is remodeled into a stomach, characteristic of segment 7.

Fission: general morphogenesis and staging series

Unstained fixed and live fissioning material was investigated to provide a general description of morphogenesis during fission and to establish a fission staging series. I divide fission into five stages (Fission Stages A–E; Fig. 2.1, B and D), which are roughly comparable to anterior and posterior regeneration Stages 2–6. Within the fission zone, and topologically separated by a fission plane, six new head segments (two more than those made during regeneration) and a variable number of new posterior segments are produced. Progression through fission stages is dependent on physiological and environmental conditions and is extremely variable. Typical worms at room temperature complete fission in 2–6 days.

Fission Stage A, fission-zone formation

A narrow circumferential ring of epidermis thickens, below which rounded cells accumulate. This thickening occurs approximately one third of a segment behind the anterior septum of the fissioning segment (anterior to the chaetal bundles). The rounded cells form blastema-like cell masses that I refer to as "fission masses," with one mass immediately anterior to the fission plane (forming the new posterior end) and one immediately posterior to the fission plane (forming the new anterior end).

Fission Stage B, fission-zone patterning

The fission plane becomes evident externally as a constriction between the anterior (presumptive tail) and posterior (presumptive head) cell masses of the fission zone. A dorsal arc of epidermis immediately behind the fission plane thickens, forming the presumptive prostomium. The primordia of the cerebral ganglion lobes become evident as a bilateral pair of dorsal cell masses immediately behind the fission plane. The anterior and posterior fission masses grow, obliterating most of the coelomic space, and become segmented, forming iterated bilateral pairs of cell packets each divided into ventral, ventrolateral, and lateral portions.

Fission Stage C, fission-zone early differentiation

Immediately posterior to the fission plane, the prostomium protrudes dorsally, while immediately anterior to the fission plane, the epidermis thickens forming the pygidium. Both prostomium and pygidium develop sensory hairs. Cell packets within the fission masses differentiate into ventral nerve cord ganglia, ventral chaetal sacs, and dorsal chaetal sacs. Septa form between developing segments and the gut inside the developing head begins to narrow.

Fission Stage D, fission-zone late differentiation

Segmental organs complete differentiation and chaetal sacs begin to secrete chaetae that protrude from the body wall. The anterior to posterior differentiation gradient is subtle in the developing head but marked in the developing tail. In the head, the prostomium elongates and a pharyngeal sac differentiates dorsal to the narrowed gut, behind the brain.

Fission Stage E, growth

Ventral and dorsal chaetae of all six new head segments have emerged, and the new head and tail grow in size. In living worms, the gut and blood vessels remain continuous and functional across the fission plane at this stage, and it appears that vascular and gut connections persist until individuals physically separate. The original segments behind the new head experience a segment identity shift that is evident during this stage. The most obvious manifestation of this shift is the thickening and dilation of the gut in the segment immediately behind the fission zone, as this region of the gut forms a new stomach. The two daughter worms may split apart at any point during this stage.

Cell proliferation

BrdU incorporation assays reveal extensive cell proliferation in new body regions forming by both regeneration and fission (Fig. 2.2), and spatial and temporal proliferation patterns are largely similar between the two processes. In both, abundant BrdU-labeled cells are seen in the epidermis, gut and inside the blastema and fission masses, with the most extensive labeling in the epidermis. During regeneration, cell proliferation is initiated at the end of Stage 1, in the epidermis covering and adjacent to the wound site, and remains high in the epidermis throughout Stages 2–4 (Fig. 2.2, A–D). During Stages 5 and 6, proliferation is concentrated at the base of the prostomium and in the posterior growth zone (Fig. 2.2, E and F). When a segment initiates a fission zone (Stage A), cell proliferation first occurs within the ventrolateral epidermis (Fig. 2.2G) and this proliferative region expands into a ring surrounding most of the segment, except at the dorsal midline. Cell proliferation

within the fission zone is extensive through Stage C (Fig. 2.2H), and then, over Stages D and E, is concentrated at the base of the prostomium and within the posterior growth zone (Fig. 2.2I).

Body wall muscle development

Phalloidin staining reveals important differences in the development of the body wall musculature during regeneration and fission. At amputation, the longitudinal muscle fibers are severed at the wound site (Fig. 2.3, A and B), and the broken ends of these fibers then gradually extend over the blastema, reaching its tip and then elongating as the blastema continues to grow (Fig. 2.3, C–F). In contrast, during fission, longitudinal muscle fibers are not broken at fission zone initiation and maintain their integrity across the fission zone throughout most of the duration of fission (Fig. 2.3, G–K). Longitudinal muscle fibers lengthen as the fission zone grows, and gradually break late during fission, during Stages D and E (Fig. 2.3K). Some fibers are modified and rerouted to form the prostomial and mouth musculature during intermediate stages (Fig. 2.3J). Even in late Stage E fission zones, however, a few muscle fibers remain continuous across the fission plane (Fig. 2.3K).

After amputation, the circular muscle fibers at the wound margin contract immediately, helping to seal the wound. These fibers are subsequently removed or displaced, since by the beginning of Stage 2 the wound epithelium covering the stump has no underlying muscle (Fig. 2.3, A and B). As the blastema develops, there is no evidence that original circular muscle fibers are incorporated into the new head. Instead, all circular muscles appear to form anew during Stages 3–5, appearing first as very fine fibers (Fig. 2.3C). When a fission zone is initiated, the original circular

muscles of the segment are gradually pushed apart except for three bands of fibers that remain at the fission plane (Fig. 2.3, G, H, and J). These bands are detectable throughout much of fission, and at least the outer bands are evident even at late stages, associated with the tip of the new tail and the tip of the new head (Fig. 2.3K). New circular muscle fibers form within the developing head and tail, as during regeneration (Fig. 2.3J).

Pharyngeal retractor muscles form in a similar way in both regeneration and fission: individual spindle-shaped muscle cells appear in the coelomic space between the dorsal body wall and the pharynx, stretching between these two surfaces (Fig. 2.3, L and M).

Gut development

Several aspects of foregut development differ between regeneration and fission (Fig. 2.4). During anterior regeneration, the foregut forms anew from central blastemal cells that generate the new buccal cavity, pharynx, and esophagus, and the mouth is formed when the anterior-most region of the developing foregut fuses with the anteroventral epidermis, around Stage 4 or 5. Cells lining the new pharynx and esophagus (but not the mouth or buccal cavity) become ciliated as these regions differentiate, around Stage 5 (Fig. 2.4K). By contrast, during fission, the original gut in the fission zone never closes up, but instead lengthens as the fission zone grows and is gradually remodeled into the different regions of the foregut during Stages C–E (Fig. 2.4, G–I). The stretch of gut in the fission zone remains ciliated throughout the fission process, and only the region transforming into the buccal cavity loses its

ciliation around the time the individuals physically separate (Fig. 2.4, G–I and L). The mouth becomes open to the exterior upon physical separation.

Development of the new posterior gut is much more similar between fission and regeneration. During both processes, the original gut lengthens as the blastema and fission masses grow, and is gradually remodeled to take on axially appropriate morphologies. The stretch of gut being converted to hindgut remains ciliated during both processes (Fig. 2.4, A, C, E, and J). The anus forms by fusion of the original gut to the posterior epidermis during regeneration (Stage 2), while during fission it opens when the daughter worms physically separate (Stage E).

Anterior development by either regeneration or fission also involves gut remodeling in the original segments behind the blastema or fission zone, as these segments take on new axial identities. Gut remodeling is evidenced by changes in gut ciliation, diameter, and coiling, and is more dynamic during anterior regeneration than during fission. During anterior regeneration (following the removal of seven segments, as performed for this study), the original gut within the one to three segments closest to the wound site narrows, straightens, and completely loses its ciliation, developing a sharp boundary between the ciliated and unciliated gut regions (Fig. 2.4, D and O, arrow). Ciliation within this stretch of original gut is lost beginning at Stage 2 and is not regained until Stage 5, when the regions of the new regenerated foregut also become ciliated (Fig. 2.4K). Thus, it appears that in a stretch of gut closest to the regenerating head endodermal cells lose one of their key differentiated characteristics following anterior amputation, and that reacquisition of this feature is temporally correlated with the differentiation of the new foregut within

the regenerating head. In contrast, during fission no gut ciliation loss is evident posterior to the new head of the fission zone (Fig. 2.4, G–I and L), suggesting no or less dedifferentiation than occurs during regeneration.

During head development by both regeneration and fission, a new stomach is remodeled from the original gut (Fig. 2.4, K and L). During anterior regeneration, a stretch of gut two segments posterior to the developing head (comprised of four new head segments) dilates and its walls thicken to form the new stomach beginning at Stage 6 (Fig. 2.4, Q and R). During fission, a stomach forms by a similar process beginning at Stage E, although this occurs immediately posterior to the developing head (comprised of six new head segments).

Degradation of nephridia

During both regeneration and fission, nephridia in certain original segments degrade. Following either anterior or posterior amputation, nephridia in the terminal (injured) segment are typically lost during regeneration Stage 1. In addition, during anterior regeneration (following amputation of seven anterior segments, as performed here), the two original segments immediately behind the four regenerating head segments (i.e., original segments 8 and 9) lose their nephridia as they take on segmental identities not normally associated with nephridia (i.e., segments 6 and 7) (Fig. 2.4, B and D). The highly coiled tubule of the nephridium disintegrates rapidly (during Stage 1), while the anteriorly directed nephridial funnel, which is embedded in the segmental septum, often remains longer (Fig. 2.4, M–O).

During fission, nephridia in the fission-zone forming segment become stretched across the growing fission zone and eventually degrade (Fig. 2.4, G, H, and

P). This original segment is split apart by the fission process, the anterior and posterior parts being inherited by the anterior and posterior worms, respectively. Although the anterior part is then reconstituted into a complete midbody segment, I found no evidence that nephridia redevelop within this segment (although more posterior segments formed from scratch do develop nephridia). The posterior part of this original segment is reconstituted into segment 7 of the posterior worm, which is normally devoid of nephridia. No additional nephridial degradation occurs during fission.

Nervous system development

During both regeneration and fission, peripheral nerve rings near the developing tissues produce temporary α-tubulin-positive nerves that extend horizontally over the developing cell masses. The source, density, and developmental timing of these nerves differ between the two processes, however. During regeneration, nerves extend from the closest 1 to 2 peripheral nerve rings adjacent to the blastema (Fig. 2.5, B and C). In contrast, during fission, they extend toward the fission plane only from the two nerve rings that bound the fission zone, nerve ring nr1 (which forms posteriorly projecting nerves) and nerve ring nr2 (which forms anteriorly projecting nerves) (Fig. 2.5, A1–A3 and D). Thus, during fission, nerve ring nr3 never produces horizontal nerves, while nerves from this ring are common during both anterior and posterior regeneration. Furthermore, during regeneration, horizontal nerves are most evident during Stages 3–5 and are long and numerous (Fig. 2.5, B, C, E, and F), while during fission, such nerves are evident earlier, during Stages A–C, and are sparse and much shorter (Fig. 2.5, D and G). Eventually, the tips

of these horizontal nerves contact the epidermal surface and connect to developing sensory hair tufts. These tufts become innervated by new nerve rings when the horizontal nerves disappear at late stages of regeneration and fission.

Central nervous system development in the new head involves the formation of three separate neural elements: the bilobed cerebral ganglion; the ventral nerve cord ganglia; and the nerve loop that forms the tracts of the ventral nerve cord (ventrally), the circumenteric connectives (laterally), and the cerebral commissure (dorsally). During both regeneration and fission, the cerebral ganglion and ventral nerve cord ganglia develop from dorsal and ventral cell packets, respectively, within the blastema or fission mass, while the new nerve tracts stem from outgrowths of the remaining ventral nerve cord. How these neural elements develop appears similar across the two contexts, but the configuration of nerve tracts, as revealed by serotonin labeling, differs between them. During early regeneration (Stages 2–3) new serotonin-positive nerves grow forward from the severed end of the old ventral nerve cord, split into left and right tracts, and connect dorsally to complete the nerve loop (Fig. 2.5, H and I). During fission, however, the ventral nerve cord is unsevered and the nerve tracts from the original ventral nerve cord remain intact across the fission zone. During late Stage B to mid Stage C, new nerves grow anterodorsally from the ganglion immediately behind the fission zone (Fig. 2.5, L and M) (i.e., the ganglion of the original fission-zone forming segment). As during regeneration, these nerve tracts split into left and right tracts and then meet dorsally to complete the nerve loop. Thus, the new ventral nerve cord represents a simple extension of the original severed

nerve cord during regeneration, but represents a dorsal branch of the intact, original nerve cord during fission (Fig. 2.5, S and T).

Central nervous system development in the new tail is largely comparable to that in the new head. During both posterior regeneration and fission, the ventral nerve cord ganglia form anew from ventral cell packets within the blastema or fission mass, while new nerve tracts of the new tail form from nerve extensions from the old cord. During regeneration, serotonin-positive nerve tracts grow posteriorly from the severed end of the ventral nerve cord (Fig. 2.5R), but during fission the new nerve tracts extend posterodorsally from the ganglion immediately in front of the fission zone (Fig. 2.5T).

Serotonin labeling reveals subtle but consistent differences between regeneration and fission in the relative timing of events associated with ventral nerve cord development. During anterior regeneration, serotonin-positive tracts of the new nerve cord begin growing forward during Stage 2, before the appearance of serotonin-positive cell bodies in the ganglia, which appear during Stages 4–5 (Fig. 2.5, H–J and N). In contrast, during fission, the serotonin-positive cell bodies appear first, beginning late in Stage B, and the nerve tracts emerge later, during stage C (Fig. 2.5, K–M, and O). Thus, nerve tract formation and ganglion differentiation appear to occur in a different order during fission and regeneration. In addition, serotonin labeling clearly reveals that only four ventral nerve ganglia form during anterior regeneration, while six ganglia form during anterior development of fission (Fig. 2.5, P and Q).

Cerebral ganglion development also reveals timing differences between regeneration and fission. When fully developed, the cerebral ganglion consists of left and right hemi-ganglia connected by a transverse commissure, and each hemi-ganglion consists of a forelobe and hindlobe (Fig. 2.6A). All four lobes harbor a small α-tubulin-positive center, the hind lobes each possess one serotonin-positive cell, and the commissure is serotonin-positive. During regeneration, the serotonergic commissure appears first (Fig. 2.6, B and B′), before the appearance of the α-tubulin-positive centers of the cerebral lobes (Fig. 2.6C), while during fission, the α-tubulin-positive centers appear first (Fig. 2.6, D and D′), and the serotonergic commissure appears secondarily (Fig. 2.6E). The serotonin-positive cells appear later in development in both contexts. In addition to this temporal difference in internal development of the cerebral ganglion, when the ganglion primordia appear during development also differs. The primordia are first evident as a bilateral pair of dorsal cell masses (which appear to arise by internalization of dorsal epidermal cells) as early as late Stage A during fission but not until Stage 2.3 during regeneration. It is possible that, because blastemal cells are so tightly packed at early stages of regeneration, the ganglion primordia are present earlier but not easily detected.

Discussion

Our understanding of how new developmental trajectories evolve has been limited by the paucity of studies focusing on novel but recently evolved trajectories. Here, I investigated the recent evolution of fission from regeneration in the naidid annelid *P. leidyi*, providing a glimpse at an early step in the evolution of a novel developmental trajectory. The detailed trajectory-wide comparison of morphogenesis

during these two processes demonstrates that a core set of conserved morphogenetic processes is still shared between fission and regeneration, but that many differences occurring all along the course of these trajectories have accumulated between them. I conclude that fission and regeneration, although still extremely similar, must be recognized as developmentally distinct and that evolutionary divergence has proceeded along the entire developmental course of these trajectories.

Homology of fission and regeneration

The phylogenetic distribution of fission and regeneration suggests that fission evolves by recruitment of regeneration in annelids and other bilaterian groups (Lasserre, 1975; Schroeder and Hermans, 1975; Ghiselin, 1987). A core prediction of this hypothesis is that morphogenetic processes of fission and regeneration should be very similar if not identical. In support of this, I found that *P. leidyi* regeneration and paratomic fission do indeed proceed through a core set of very similar morphogenetic steps (Fig. 2.7, green elements), despite having such distinct starting points. In certain cases the unique spatial context of each process imposes differences in exactly where structures develop (e.g., the prostomium develops from the anterodorsal tip during regeneration but must develop from dorsal epithelium during fission; the mouth develops at the anteroventral tip of the blastema during regeneration but from the transverse epidermal ring encircling the fission plane during fission), but even in such cases the relative spatial relationships between developing structures is preserved.

The strongest developmental evidence for fission evolving specifically from regeneration would be the identification of features shared between fission and regeneration but absent from other developmental trajectories. Such developmental

synapomorphies of fission and regeneration have thus far remained elusive. Here, I identified a strong candidate for such a feature within the peripheral nervous system. During *P. leidyi* regeneration, numerous horizontal nerves extend from nearby original peripheral nerve rings and grow out over the developing blastema. Such nerve projections have been described during regeneration in several other species of oligochaete annelids (Yoshida-Noro et al., 2000; Müller, 2004; Myohara, 2004), but they have not been reported during embryogenesis or normal growth in oligochaetes or in any developmental context in polychaete annelids. They have thus been interpreted as being a regeneration-specific feature of oligochaetes (Müller, 2004). My finding that this unusual configuration of temporary peripheral nerves also occurs during fission represents strong developmental evidence that fission evolved specifically from regeneration, rather than from embryogenesis or normal growth.

Divergence of fission and regeneration

I have found numerous differences between morphogenesis during fission and regeneration in *P. leidyi*, countering the widespread assumption that agametic reproduction is a simple redeployment of regeneration. Differences are apparent in the development of all major organ systems and divergence between these trajectories is manifested as both differences in the relative timing of developmental events between fission and regeneration (Fig. 2.7, yellow elements) as well as the presence of events that are exclusive to one process or the other (Fig. 2.7, red elements). Thus, although fission and regeneration have a common origin and still unfold via an

extremely similar set of events, the two trajectories have diverged and must be considered distinct from one another.

A recurring difference between regeneration and fission in *P. leidyi* is that physical breaks in longitudinally organized organs are greatly delayed during fission (Fig. 2.7). The gut, ventral nerve cord, body wall musculature, and blood vessels are all severed simultaneously by a transverse amputation, yet during fission these organ systems show no evidence of breaks until late developmental stages. Fission by paratomy (in which new structures are formed before physical separation, as in *P. leidyi*) probably does not evolve all at once from a non-fissioning ancestor but more likely evolves from an intermediate stage of architomic fission, or "simple fission" (in which physical separation occurs before the formation of new structures). I speculate that delays in the severing of longitudinally organized organ systems (relative to when fission is initiated) were selectively favored during the evolution from simple to paratomic fission in order to prolong organ functioning as long as possible, allowing the fissioning worm to function as a single individual, even as it becomes two.

The extreme delay in the severing of the ventral nerve cord during fission (relative to regeneration) suggests a fundamental difference in how the two processes are initiated. The severed nerve cord plays a key role in regeneration initiation in annelids (Berrill, 1952; Herlant-Meewis, 1964) and thus a reasonable hypothesis for fission initiation would be that it is triggered by a neuronal discontinuity. This appears not to be the case. The ventral nerve cord remains continuous across the fission zone throughout fission development in *P. leidyi*, as it does in other paratomically fissioning naidids (Galloway, 1899; Dehorne, 1916). Furthermore, in

another fissioning naidid, *Dero digitata*, electrophysiological studies demonstrate that axonal conduction is maintained across the fission zone, albeit at a slightly decreased velocity (Drewes and Fourtner, 1991). Severing the ventral nerve cord in a nonfissioning *P. leidyi* by clipping the ventral portion of a normal segment also does not in and of itself trigger a new outgrowth or fission (E. E. Z., unpublished data). Therefore, although finer resolution studies of neuroanatomy and neurophysiology are needed to evaluate whether more subtle physical or functional discontinuities in the nerve cord could be associated with fission initiation, available data suggest that a trigger other than a neuronal discontinuity initiates fission.

Another consistent, but more subtle, temporal shift between regeneration and fission occurs during the development of new neural elements in *P. leidyi*. Differentiation of cerebral and ventral nerve cord ganglia (as judged by their expression of α-tubulin- and serotonin-positive components) precedes the formation of detectable nerve tracts in these regions during fission, but occurs after nerve tract formation during regeneration. Interestingly, an intraspecific comparison of embryogenesis and regeneration in the oligochaete *Enchytraeus japonensis* has revealed a similar timing shift between ganglion and nerve tract formation: ventral and cerebral ganglia form after nerve tracts during regeneration, as in *P. leidyi* regeneration, but ganglia form before nerve tracts during embryogenesis (Myohara, 2004). Thus, in oligochaetes, and possibly in annelids more generally, ganglion formation and nerve tract formation appear to be independent developmental events, either of which can occur first and still produce the same endpoint phenotype.

One of the most striking features I have found to be exclusive to fission is the formation of forked, dual ventral nerve cords in the fission masses. While the original nerve cord remains intact across the fission zone, the nerve cord ganglia that flank the fission zone sprout dorsal branches that migrate into the developing head and tail of the fission zone. How neural functions are integrated in this configuration warrants further study. The posterior head is behaviorally completely quiescent even through late stages of fission, but it exhibits normal behavior immediately upon either physical separation by fission or following removal of the anterior individual's head (E. E. Zattara and A. E. Bely, personal observation), suggesting that the anterior-most head normally represses the dorsal forks of the dual nervous system during fission. In *Lumbriculus variegatus*, a relatively distantly related oligochaete that does not undergo paratomic fission (and thus does not normally exist in a multiheaded form), laterally protruding ectopic heads can be induced at the midbody (Martinez et al., 2008). These ectopic, midbody heads are normally behaviorally quiescent but, as in *P. leidyi*, are immediately derepressed upon amputation of the anterior most head. Thus, the dominance of the anterior most head may be a ground state for oligochaetes, and the evolution of paratomic fission may not have required new mechanisms to keep posterior heads quiescent during the fission process.

Although gut morphallaxis, or tissue remodeling, occurs during both fission and regeneration as original segments behind a developing head take on new axial identities, my findings suggest that the mechanisms by which this is achieved differ in the two contexts in *P. leidyi*. The gut in this species is typically ciliated throughout (except for the buccal cavity) but, following amputation, a stretch of original gut

closest to the wound site completely loses its ciliation for several days, even though that same region will ultimately regain ciliation. Similarly, in another oligochaete (*E. japonensis*), transcription of several gene markers associated with specific gut regions are downregulated shortly after amputation, even in regions of the gut that will eventually re-express the very same markers (Takeo et al., 2008). These findings suggest that during annelid regeneration, gut morphallaxis may involve some level of cell dedifferentiation, although the possibility that some cell turnover occurs cannot be excluded. In contrast, during *P. leidyi* fission, gut ciliation is retained throughout the process, both within the fission zone and adjacent to it, even as the gut is reshaped into axially appropriate structures (e.g., foregut, pharynx, stomach). Retention of gut ciliation has likely been favored to retain gut functionality during fission. Gut morphallaxis may therefore proceed by dedifferentiation and redifferentiation during regeneration, but by transdifferentiation during fission. Comparisons of cell-type specific gene expression in the gut during regeneration and fission could be used to further test this hypothesis.

A framework for the evolution of novel developmental trajectories

I propose that novel developmental trajectories evolve by a form of duplication and divergence, analogous to the mechanism by which new morphological traits and new genes commonly evolve. In this case, the "unit" is a whole developmental trajectory, and the "duplication" event occurs as soon as a new biological function is gained for the original trajectory. The effective duplication occurs because once a second biological function evolves for an existing trajectory,

evolutionary forces can potentially act separately on these two functions, opening up the possibility for divergence of the morphogenetic processes underlying them. The speed and extent of trajectory divergence will depend on several factors, but major determinants are expected to be the ease with which pleiotropy between the two trajectories can be broken down and the strength of selection for trajectory-specific developmental adaptations.

With respect to paratomic fission, a likely scenario for its evolution is as follows. A species capable of anterior/posterior regeneration (i.e., the original trajectory) evolves the ability to endogenously trigger self-fragmentation, leading to regeneration of the fragments and thus a reproductive event. The acquisition of the ability to self-fragment represents the duplication phase of the process, because the biological function of fission is clearly distinct from that of regeneration: regeneration is a mechanism for recovery from injury, while fission provides a mechanism for reproduction, often particularly useful for rapid use of ephemeral resources (Hughes, 1989). Subsequent to the acquisition of this new capability, the morphogenetic processes underlying regeneration and fission may remain identical for some time (just as two copies of a duplicated gene may remain identical for some time), but will likely diverge through the accumulation of changes (adaptive or neutral) to one or both processes. Accumulation of changes that delay physical separation (relative to the timing of development of new structures) can then modify "simple" fission into "paratomic" fission. I speculate that divergence between regeneration and fission will proceed primarily through the accumulation of changes to fission (because it is the

more recently evolved trajectory, with a novel function), though comparative studies and rigorous outgroup analysis are needed to test this directly.

What is the pattern of divergence between recently duplicated trajectories? Virtually nothing is yet known about this important question. With respect to regeneration and paratomic fission, the starting conditions differ markedly (regeneration begins with an externally induced, traumatic injury, while paratomic fission is initiated endogenously in an uninjured animal) yet the processes converge on a common adult morphology. It might be expected, then, that regeneration and fission differ in their initial steps but then rapidly or gradually converge onto a shared path (Fig. 2.8 A and B). I do not find evidence for this model of divergence. Instead, paratomic fission and regeneration show differences throughout the trajectories (Fig. 2.8C), not simply at the beginning (or middle or end) of the processes, suggesting that the two trajectories are being evenly "pulled apart." The question of whether this pattern of trajectory divergence is characteristic of other recently evolved trajectories, such as other origins of paratomic fission, or origins of budding, awaits further study.

Chapter 2 Figures

Figure 2.S1: Body morphology of *Pristina leidyi*

A) Diagram of a whole, non-fissioning worm (lateral view). From anterior to posterior, the body is composed of an asegmental prostomium, six cephalic (head) segments, a variable number of trunk segments, a posterior growth zone (from which new segments are added by normal growth), and an asegmental pygidium. The amputation planes (Ant: anterior amputation; Post: posterior amputation) used in this study are shown as dashed red lines. B) Diagram of slightly more than one segment (including the septa, chaetae, and nerve-ring 3 on either side) (oblique view). The body wall epidermis secretes a thin external cuticle and is underlaid by body wall muscles, with an outer layer of circular and oblique muscles and an inner layer of longitudinal muscle grouped into bands. In each segment one dorsal and one ventral pair of chaetal sacs secrete chaetae, which worms use for locomotion. Within the body wall, peritoneal epithelia form bilaterally paired, fluid filled coelomic sacs that make up most of the volume of the animal. Sacs from consecutive segments are separated by septa. The gut, a dorsal blood vessel, a ventral blood vessel, and the ventral nerve cord all run lengthwise along the animal, traversing the septa. Single or paired nephridia (excretory organs) collect coelomic fluid using a ciliated funnel (nephrostoma), filter it through coiled tubules and excrete it through a pore located behind the ventral chaetae. The ganglionated ventral nerve cord branches off three peripheral nerve rings (nr1, nr2 and nr3) in every trunk segment. C) Detail of the anterior end of the worm, showing the cephalic elements of the central nervous system: a cerebral ganglion connected to the ventral nerve cord's anterior-most ganglion by a pair of circumenteric connective nerves, and prostomial and pharyngeal nerves branching off the connectives. The anterior-most region of the foregut is composed of a mouth and a pharynx. The pharynx can be protruded through the mouth during feeding and is retracted by pharyngeal retractor muscles. Figure color coding: body wall and muscles (gray); gut (light green); nervous system (purple); chaetal sacs (yellow-green); blood vessels (pink); nephridia (in B) (black); posterior growth zone (blue).

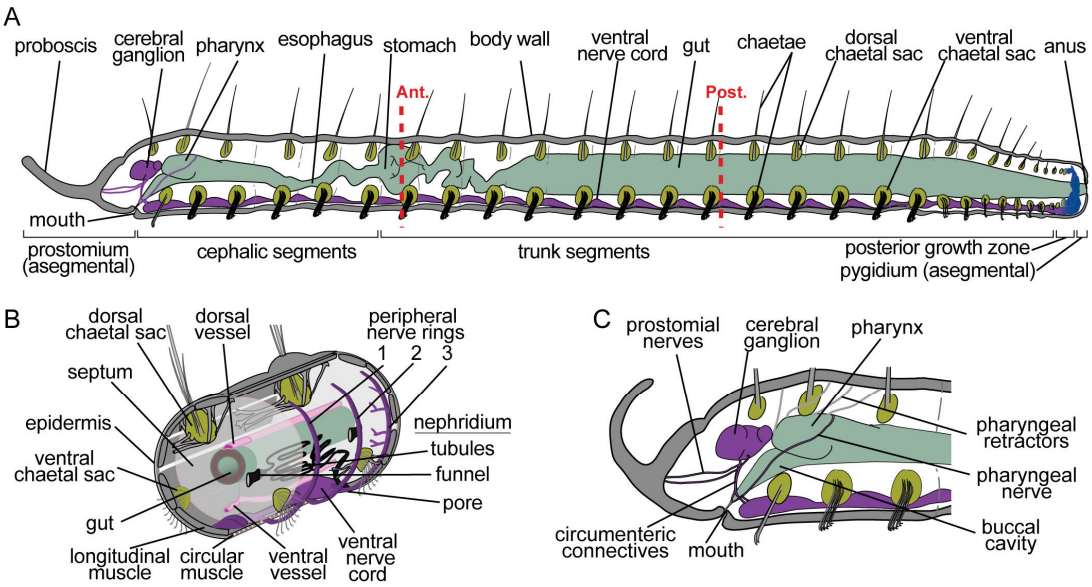
A
proboscis
cerebral ganglion
pharynx
esophagus
stomach
body wall
ventral nerve cord
gut
chaetae
dorsal chaetal sac
ventral chaetal sac
anus
Ant.
Post.
mouth
prostomium (asegmental)
cephalic segments
trunk segments
posterior growth zone
pygidium (asegmental)
B
dorsal chaetal sac
dorsal vessel
peripheral nerve rings
1 2 3
septum
epidermis
ventral chaetal sac
nephridium
tubules
funnel
pore
gut
longitudinal muscle
circular muscle
ventral vessel
ventral nerve cord
C
prostomial nerves
cerebral ganglion
pharynx
pharyngeal retractors
pharyngeal nerve
buccal cavity
circumenteric connectives
mouth

Figure 1.S1

Figure 2.1: Stages of regeneration and paratomic fission in *Pristina leidyi*

A) Following transverse amputation, an anteriorly amputated worm regenerates a new head and a posteriorly amputated worm regenerates a new tail. (B) Favorable conditions, including feeding, trigger asexual reproduction by paratomic fission, during which a new head and tail are intercalated in the middle of the body. (C,D) Stages of anterior and posterior regeneration (C) and paratomic fission (D). See text for stage definitions and description. Here and in subsequent figures (unless otherwise noted) views are lateral, anterior is to the left, the fission plane is marked by finely dashed lines, and new tissues are marked by colored bars as follows: posterior tissue formed by regeneration (dark blue), anterior tissue formed by regeneration (light blue), posterior tissue formed by fission (dark green), anterior tissue formed by fission (light green). In (A) and (B), dark gray shading marks newly forming tissue (blastema in A; fission zone in B; posterior growth zone in A and B) and light gray shading marks gut outline. an, anus; bl, blastema; cg, cerebral ganglion; dch, dorsal chaetae; fm, fission mass; mo, mouth; pb, proboscis; pgz, posterior growth zone; ph, pharynx; pr, prostomium; py, pygidium; st, stomach; vch, ventral chaeta; vg, ventral ganglion; we, wound epithelium; wnd, wound site.

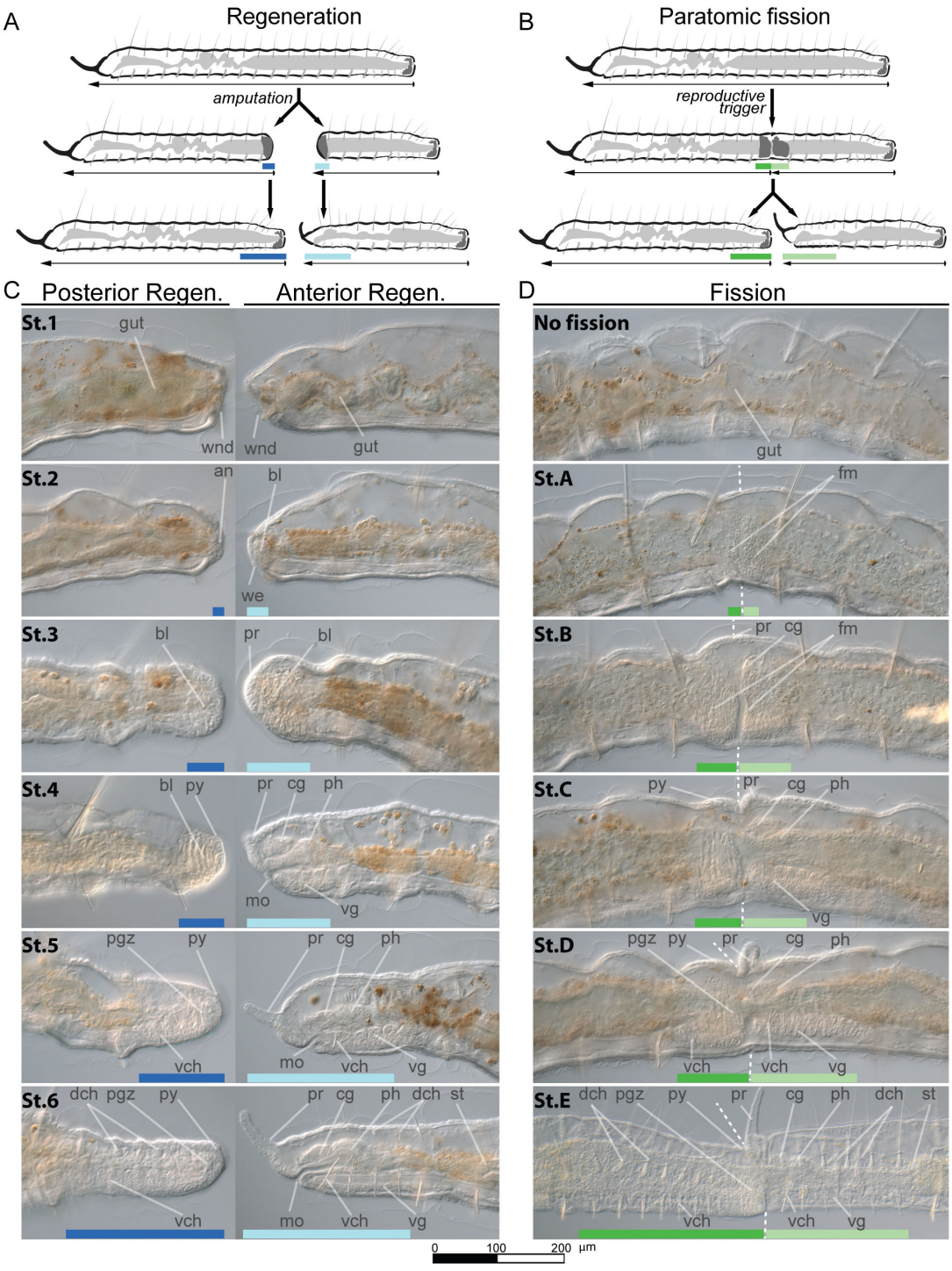
A
Regeneration
amputation
B
Paratomic fission
reproductive trigger
C
Posterior Regen.
Anterior Regen.
D
Fission
St.1
gut
wnd
wnd
gut
No fission
gut
St.2
an
bl
we
St.A
fm
St.3
bl
pr
bl
St.B
pr cg
fm
St.4
bl py
pr cg ph
mo
vg
St.C
py
pr
cg ph
vg
St.5
pgz
py
pr cg ph
vch
mo
vch
vg
St.D
pgz py
pr
cg ph
vch
vch
vg
St.6
dch pgz
py
pr cg ph dch st
vch
mo
vch
vg
St.E
dch pgz
py
pr
cg ph
dch st
vch
vch
vg
0
100
200 µm

Figure 2.1

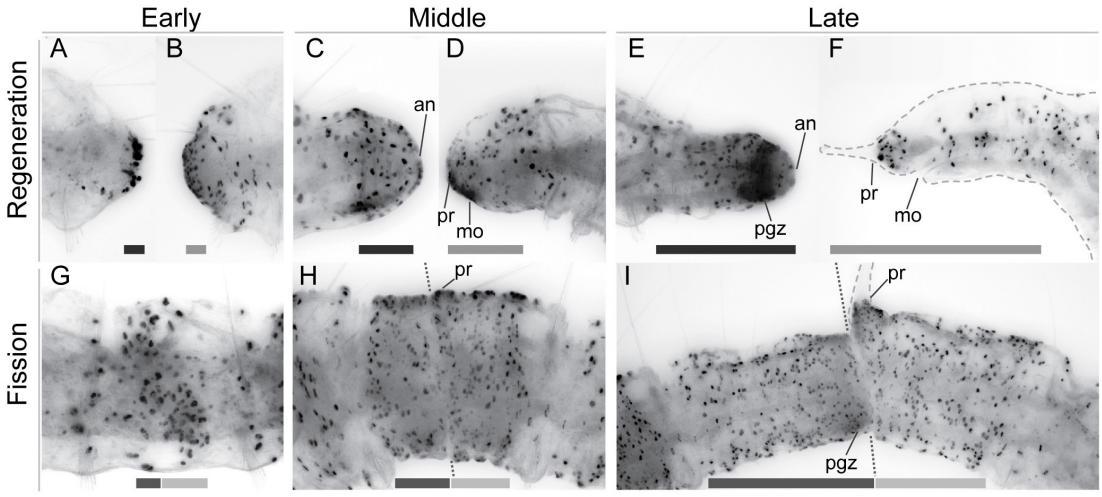

Figure 2.2: Cell proliferation during regeneration and fission

Amputated or fissioning worms were labeled at early (A–B,G), middle (C–D,H) or late (E–F, I) stages of development. Images shown are minimal intensity projections of a brightfield Z-series ranging from lateral to midline focal planes. New tissue formed by regeneration or fission is marked by bars, with dark bars marking new tail tissue and light bars marking new head tissue. In areas of low image contrast in F and I, coarsely dashed gray lines mark specimen's body contour. Stages shown are: A) Stage PR-2; B) Stage AR-2; C) Stage PR-3; D) Stage AR-3; E) Stage PR-5; F) Stage AR-5; G) Stage A; H) Stage B; I) Stage D. an, anus; mo, mouth; pgz, posterior growth zone; pr, prostomium.

Figure 2.3: Body wall muscle development during regeneration and fission

A–K) Phalloidin-labeling of longitudinal and circular body wall muscles during regeneration (A–F) and fission (G–K). Regeneration stages shown are: A) Stage PR-2; B) Stage AR-2; C) Stage PR-3; D) Stage AR-3; E) Stage PR-6; F) Stage AR-6. Fission stages shown are: G) Stage A; H) early Stage C; I) Stage E. J) and K) are magnified views of (H) and (I), respectively. Specimens are imaged by confocal (A–H, Z-projected confocal stacks) or wide-field microscopy (I,K). Newly formed tissue is marked by dark (tail) or light (head) bars. The main bands of longitudinal muscles are labeled in (C, D, and H) for comparison. Note that at mid-stage fission (J), most longitudinal muscle fibers are continuous across the fission zone (filled arrowheads) while a few muscle fibers have been rerouted toward the developing prostomium (arrows). At late-stage fission (K), many longitudinal muscles are broken near the fission plane (open arrowheads), but a few are still continuous across the fission zone (filled arrowheads). Note that during fission, three bands of original circular muscles remain at the fission zone (J). (L,M) Differential interference contrast imaging of pharyngeal retractor muscles forming from individual myocytes (arrowheads) during regeneration (L: Stage AR-5) and fission (M: Stage D). br, brain; db, dorsal longitudinal muscle band; cb, circular muscle band; ldb, laterodorsal longitudinal muscle band; lvb, lateroventral longitudinal muscle bands; ph, pharynx; pr, prostomium; vb, ventral longitudinal muscle band.

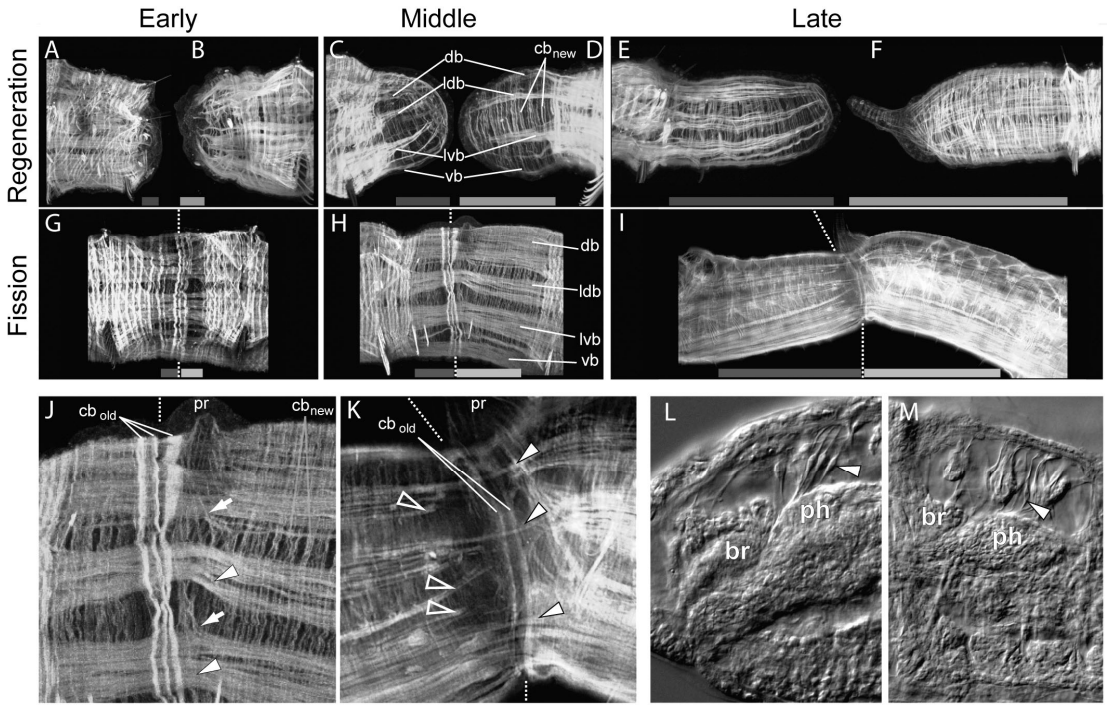
Early
Middle
Late
Regeneration
Fission
A
B
C
D
E
F
G
H
I
J
K
L
M
db
ldb
lvb
vb
cb new
cb old
pr
ph
br

Figure 2.3

Figure 2.4: Changes in the gut and nephridia during regeneration and fission

A–L) Regenerating and fissioning specimens at early (A,B,G), late early (C,D,H), mid (E,F,I), and late (J,K,L) stages of development, immunolabeled with acetyl-α-tubulin (green) and a DNA counterstain (blue). Specimens are imaged by confocal (A–F, H–K, Z-projected stacks) or wide-field microscopy (G,L). Regeneration stages shown are: A) Stage PR-1; B) Stage AR-1; C) Stage PR-2; D) State AR-2; E) Stage PR-4; F) Stage AR-4; J) Stage PR-5; K) Stage AR-5. Fission stages shown are: G) Stage A; H) Stage B; I) Stage C; L) late Stage E. Nephridia are marked by filled arrowheads in (B,G,H), and (I); lingering nephridial funnels are marked by open arrowheads in (D) and (H). Arrow in (D) marks boundary between original gut that has lost cilia (left of arrow) and original gut that has retained cilia (right of arrow). Note absence of gut ciliation within and adjacent to regenerating head in (D) and (F), in contrast to retention of gut ciliation within and adjacent to fission zone in (G–I). M–P) Higher magnification views of nephridium and gut ciliation changes during anterior regeneration (M–O) and fission (P). Specimens in (M), (O), and (P) are the same as those in (B), (D), and (G), respectively. Stages shown are: (M) early Stage AR-1; (N) late Stage AR-1; (O) Stage AR-2; (P) Stage A. The dashed line indicates the outline of the gut. Normal nephridium morphology is shown in (M). Remaining components of disintegrating nephridium are labeled in (N) and (O). Note fine tubule region stretched across the fission zone in (P). In (O), original gut ciliation has been lost anterior to the arrow. (Q–R) Remodeling of midgut into stomach following anterior amputation of seven segments (Q, Stage AR-4; R, late Stage AR-6). The gut in original segment 9 (labeled gut 9) dilates and takes on the characteristic morphology of the stomach located in segment 7 (labeled gut 9→7). Note that dorsal and ventral chaetae bundles are birefringent and appear as fluorescent needle-shaped structures projecting from the body wall in this and other figures. an, anus; bc, buccal cavity; es, esophagus; mo, mouth; nf, nephridial funnel; npr, nephropore; ntb, nephrotubules; ph, pharynx; st, stomach.

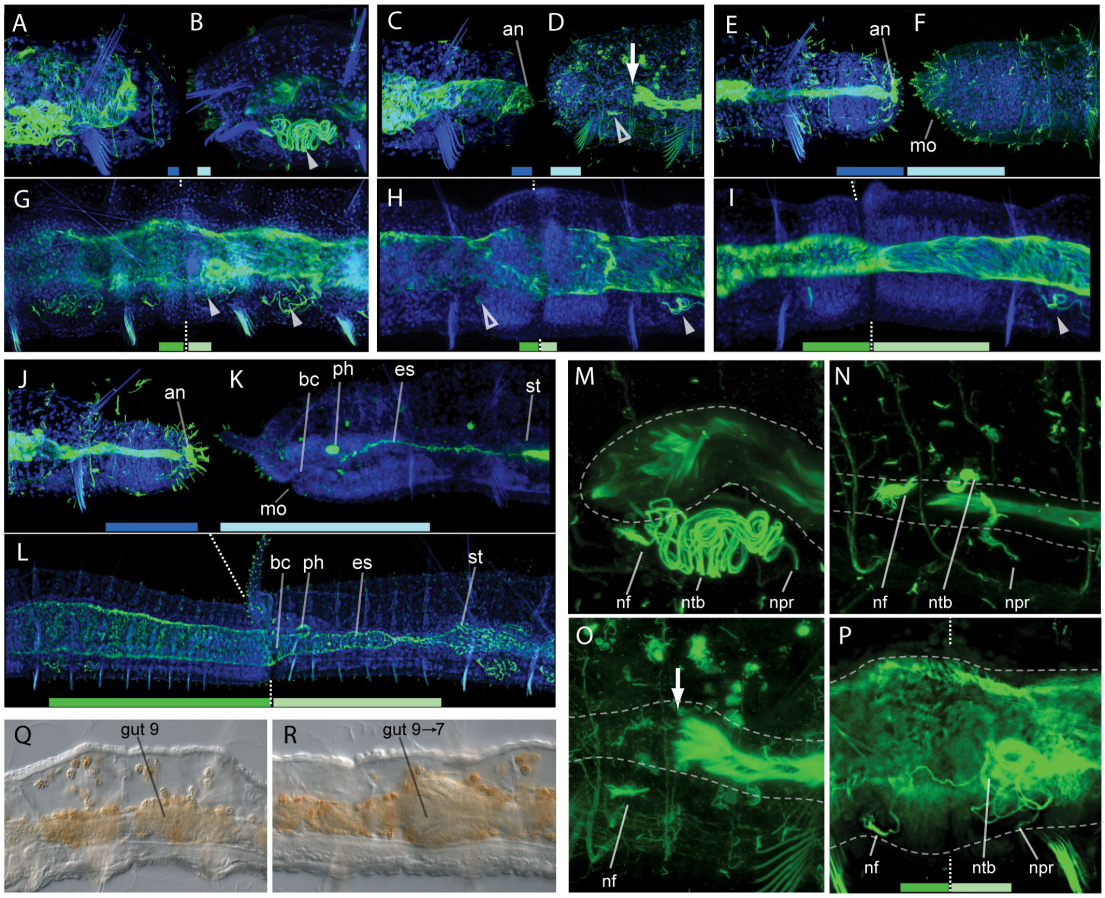
A
B
C
an
D
E
an
F
mo
G
H
I
J
an
K
bc
ph
es
st
mo
L
bc
ph
es
st
M
nf
ntb
npr
N
nf
ntb
npr
O
nf
P
nf
ntb
npr
Q
gut 9
R
gut 9→7

Figure 2.4

Figure 2.5: Peripheral and central nervous system development during regeneration and fission

A–G) Acetyl-α-tubulin labeling (green) reveals fine horizontal nerve fibers (arrowheads, marking tips of fibers) arising from circumferential peripheral nerve rings (labeled "nr#") and extending over the developing cell masses during regeneration and fission. Images are Z-projected confocal stacks of (A) fission Stage A; (B) regeneration Stage PR-3; (C) regeneration Stage AR-3; (D) fission Stage B; (E) regeneration Stage PR-4; (F) regeneration Stage AR-4; (G) fission late Stage C. Panels A1–A3 show α-tubulin labeling (green) (A1), nuclear labeling (blue) (A3) and the merged image (A2) for a segment with a recently initiated fission zone, showing that the dense cell masses of the fission zone are bounded by nerve rings nr1 and nr2. During regeneration, horizontal nerve fibers originate from the nearest nerve rings (including nr3, see C), while during fission only nr1 and nr2 form these fibers, projecting toward the fission plane. At mid to late stages of regeneration the new prostomium and pygidium develop dense tufts of sensory hairs (E,F, and G). For clarity, in (A–G) the strong signal from gut cilia was removed manually from some image slices before generating Z-stack projections to optimize visualization of faint peripheral nervous system signal. H–T) Serotonin labeling (yellow) of cell bodies and nerve tracts of the central nervous system. Filled arrowheads show new nerve tracts growing from the old ventral nerve cord (VNC); empty arrowheads indicate the VNC ganglion of the new segment 1. Images are Z-projected confocal stacks of regeneration Stage AR-2 (H), Stage AR-3 (I), and late Stage AR-5 (J), and fission early Stage B (K), early Stage C (L), and early Stage D (M). (N,O) Details of (I) and (L). Note that during regeneration (N) the serotonin-positive nerve tract loop (filled arrowheads) appears first, growing forward from the cut ends of the old VNC (arrows) (note absence of labeled new cell bodies at this stage), while during fission (O), new serotonin-positive cell bodies of the VNC ganglia appear first (open arrowhead and labeled cells to right), as the new nerve tracts (filled arrowhead marks leading tip) are just beginning to emerge as a branch of the old VNC (arrows). (P,Q) Labeling of the new ventral nerve cord of the head (nuclei labeled in blue) indicates that during regeneration (P: Stage AR-5) only four new segmental ganglia form, while during fission (Q: Stage D) six new ganglia form. In P, the ganglion from the adjacent original segment (labeled "old") abuts the regenerated ganglia. A full-sized chaeta from this same original segment (labeled

"ch") is also evident just behind the regenerated ganglia. (R,T) Final configuration of the serotonergic central nervous system showing that during regeneration (R, Stage PR-6; S, Stage AR-6) there is only a single, new VNC within the new head and tail, while during fission (T, late Stage D) both the old and new VNCs are present. cec, circumenteric connective; cg, cerebral ganglion; nr, nerve ring; pr, prostomium; py, pygidium.

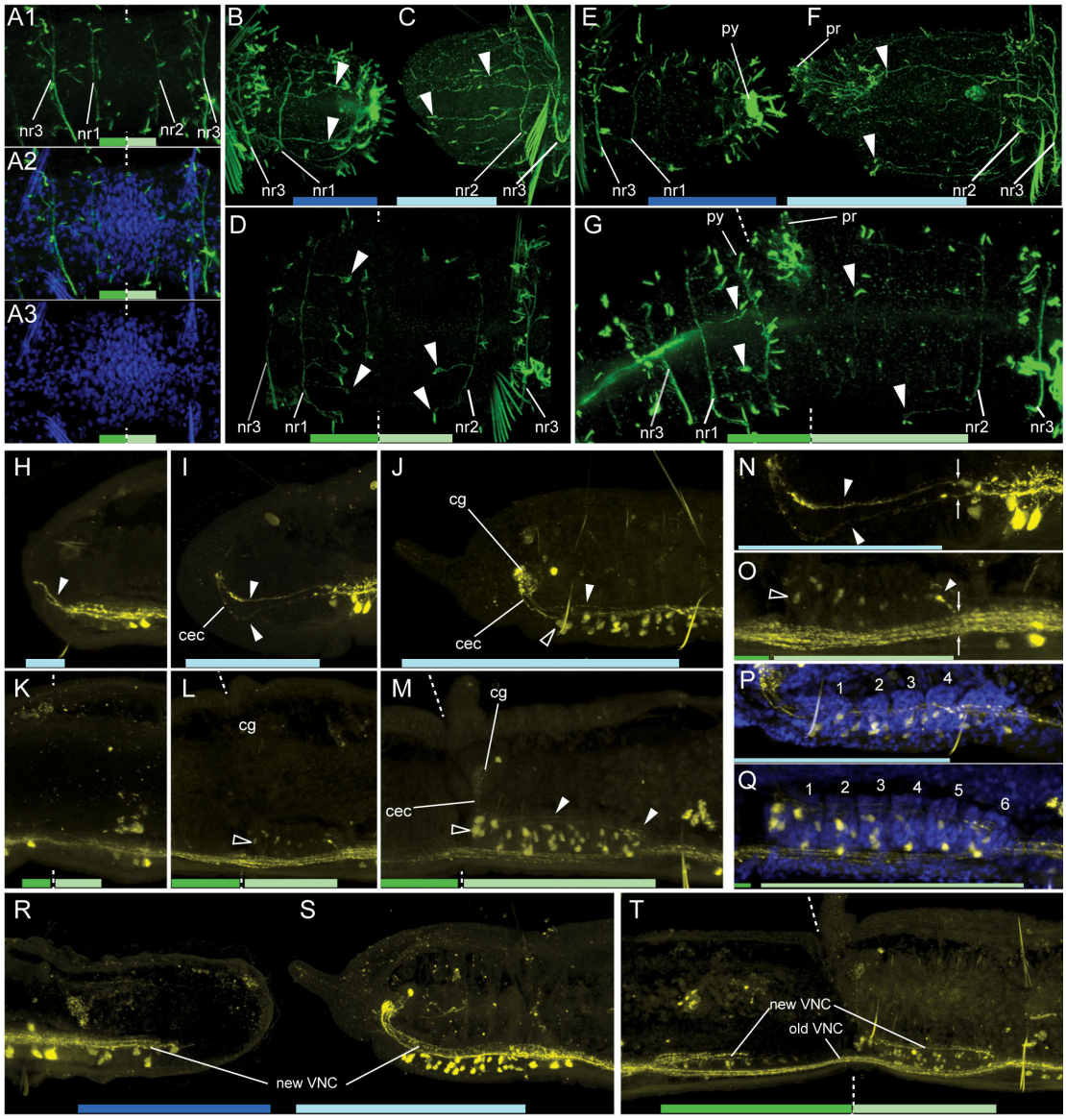

Figure 2.5

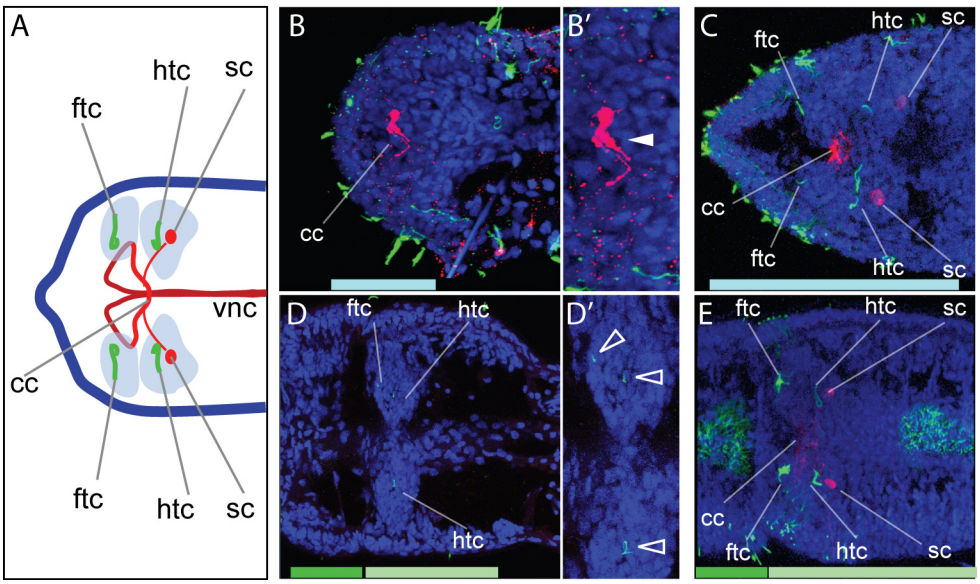

Figure 2.6: Brain development during regeneration and fission

A) Morphology of the fully developed brain (dorsal view), indicating the four brain lobes (gray shading), the acetyl-α-tubulin immunoreactive center in each lobe (green), the single serotonergic cell in each hindlobe (red dots), and the serotonergic nerve loop connected to the serotonergic nerve tracts of the ventral nerve cord (red lines). The dorsal section of the nerve loop is the cerebral transverse commissure. B–E) Confocal optical sections (dorsal views; anterior to left) of anteriorly regenerating (B,C) and fissioning (D,E) specimens simultaneously labeled for acetyl-α-tubulin (green) and serotonin (red), with nuclei labeled with TO-PRO-3 (blue). B′ and D′ are higher magnification views of images of B and D, respectively. At anterior regeneration Stage AR-3 (B,B′) the serotonergic cerebral commissure is present (B′, filled arrowhead) but tubulin-positive centers are absent. At fission Stage B (D,D′) tubulin-positive centers are present (D′, open arrowheads mark three detectable centers) but the cerebral commissure is absent. At later stages of regeneration (C: Stage AR-4) and fission (E: Stage C), the serotonergic commissure and tubulin-positive centers are both present, as are the serotonergic cerebral cells. Diffuse tubulin label along the midline in (E) is from the cilia of the gut, which is deflected ventrally (out of the focal plane shown) beneath the developing brain. cc, cerebral transverse commissure; ftc, forelobe tubulin-reactive center; htc, hindlobe tubulin-reactive center; sc, serotonergic cells; vnc, ventral nerve cord.

Figure 2.7: Summary of major morphogenetic events

Summary of major morphogenetic events and their relative timing during regeneration and fission, focusing specifically on the development of the new head. This comparison reveals many events that are shared and occur at similar times (green), as well as shared events that occur at different times (yellow) and events that occur during only one of the two processes (red). (Red stars are used to highlight specific unique elements of events otherwise coded as yellow or green.) Horizontal position of developmental events is drawn relative to the approximate timing of that event within that stage, not across the whole trajectory (i.e., horizontal position does not reflect an absolute timescale, but a relative time scale within each stage). Alignment of regeneration and fission stages to each other is based on major landmark events used to define stages; note that Stage 1 has no counterpart during fission.

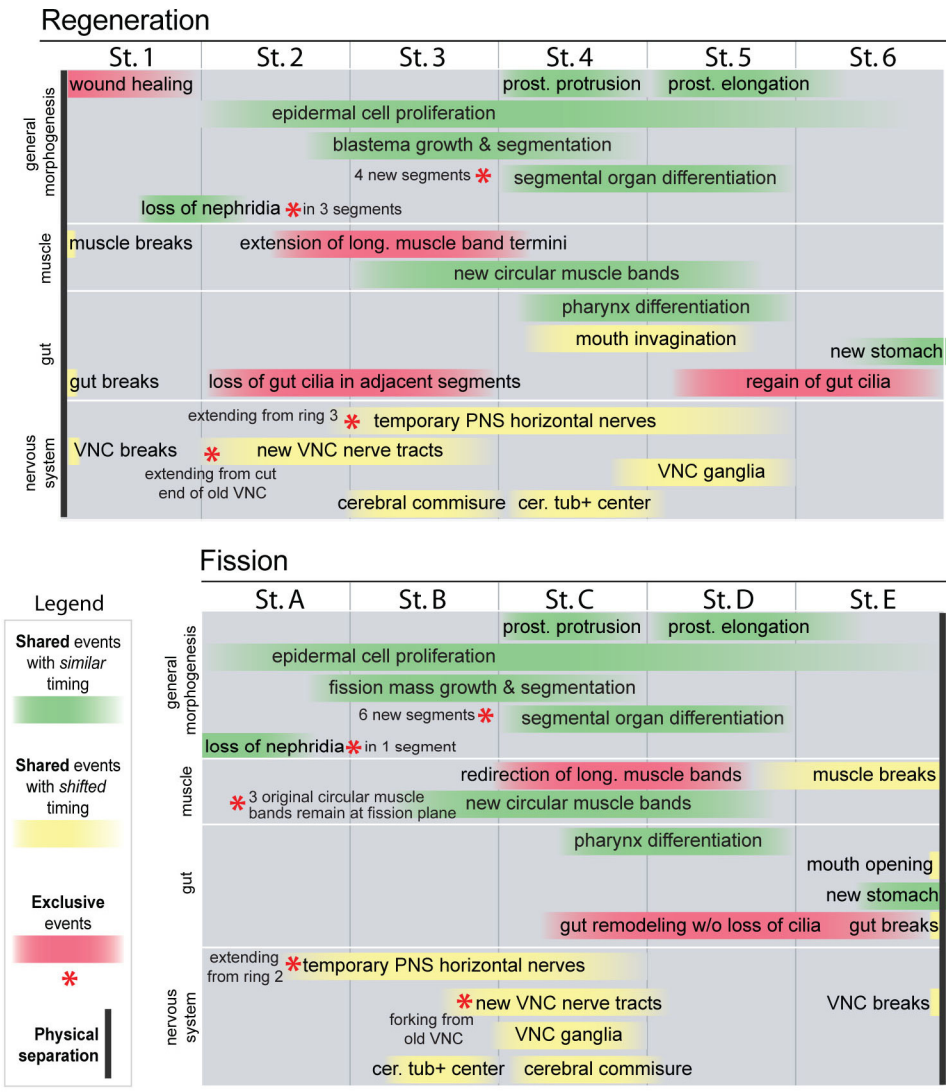
Regeneration
St. 1
St. 2
St. 3
St. 4
St. 5
St. 6
general morphogenesis
muscle
gut
nervous system
wound healing
prost. protrusion
prost. elongation
epidermal cell proliferation
blastema growth & segmentation
4 new segments
segmental organ differentiation
loss of nephridia
in 3 segments
muscle breaks
extension of long. muscle band termini
new circular muscle bands
pharynx differentiation
mouth invagination
new stomach
gut breaks
loss of gut cilia in adjacent segments
regain of gut cilia
extending from ring 3
temporary PNS horizontal nerves
VNC breaks
new VNC nerve tracts
extending from cut end of old VNC
VNC ganglia
cerebral commisure
cer. tub+ center
Fission
St. A
St. B
St. C
St. D
St. E
prost. protrusion
prost. elongation
epidermal cell proliferation
fission mass growth & segmentation
6 new segments
segmental organ differentiation
loss of nephridia
in 1 segment
redirection of long. muscle bands
muscle breaks
3 original circular muscle bands remain at fission plane
new circular muscle bands
pharynx differentiation
mouth opening
new stomach
gut remodeling w/o loss of cilia
gut breaks
extending from ring 2
temporary PNS horizontal nerves
new VNC nerve tracts
VNC breaks
forking from old VNC
VNC ganglia
cer. tub+ center
cerebral commisure
Legend
Shared events with similar timing
Shared events with shifted timing
Exclusive events
Physical separation

Figure 2.7

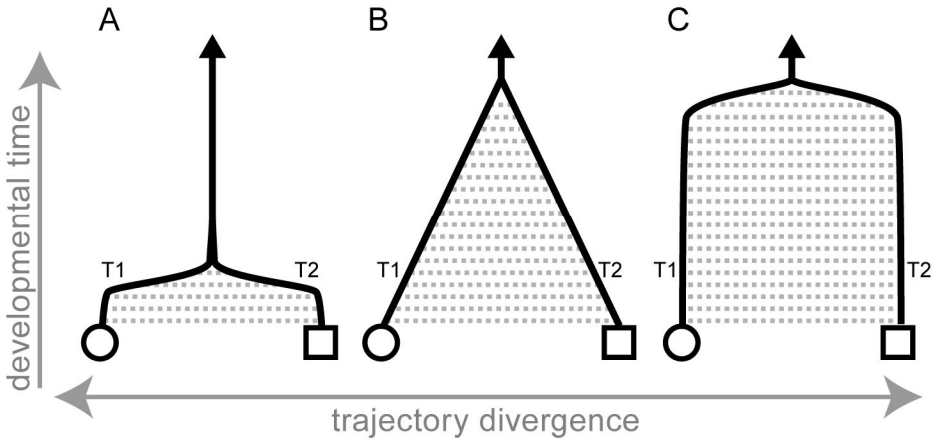

Figure 2.8: Alternative models of developmental trajectory divergence

Two developmental trajectories, T1 and T2, initiating from different starting points (circle, square) may arrive at the same endpoint morphology (filled triangle) by an early convergence (A, in which trajectory differences occur primarily at early stages), by a gradual convergence (B, in which the number of differences gradually diminishes from early to late stages), or by a late convergence (C, in which differences occur throughout development). My analysis of trajectory divergence between regeneration and fission in *Pristina leidyi* supports the model depicted in C.

CHAPTER 3: Interactions and resource allocation between growth, regeneration and asexual reproduction in the annelid *Pristina leidyi*

Abstract

Animals have repeatedly evolved new post-embryonic developmental trajectories, like regeneration or asexual reproduction by fission. How are such novelties integrated into the animal's resource allocation strategies? Naid annelids are worms with a body plan particularly convenient to study resource allocation patterns: they grow continuously by posterior segment addition, can regenerate lost body ends, and reproduce asexually by paratomic fission. Cell proliferation and size change are two processes common to somatic growth, regeneration and fission that can be readily quantified in order to test allocation models. Using thymidine analogue incorporation to label S-phase cells, I analyzed local and body-wide cell proliferation and growth patterns in the pristinine naid *Pristina leidyi* to investigate baseline growth patterns and how are they influenced by resource availability, changes in allocation patterns upon amputation and regeneration, and resource competition by simultaneous regeneration and fission. Body-wide patterns revealed that *Pristina* presents three growth regions: a posterior zone, a mid-body area where fission zones are eventually localized, and a previously undescribed anterior zone in the prostomium. Body-wide counts of BrdU-positive cells indicate that the underlying distribution of proliferation is independent of nutritional status but changes drastically upon amputation, which causes an immediate shutdown persisting over several days. Results from amputation of fissioning worms fell in three categories: 1) stalling or

regression of fission and normal regeneration, observed for cuts anterior and posterior to early fission zones; 2) mostly normal fission development and tail regeneration, observed for cuts behind mid to late fission zones; 3) strong shift in fission developmental trajectory and slow or null regeneration, observed for cuts anterior to mid to late fission zones. This shows that though qualitative patterns of cell proliferation are independent of resource availability, regeneration can significantly shift resource allocation; and that competitive interactions between somatic growth, regeneration and fission are stronger in anterior than in posterior amputees, suggesting that removal of the head, but not the tail, causes the worm to become a closed developmental system. Similar results were reported for naidine annelids and catenulid flatworms, suggesting that similar developmental and physiological contexts can drive convergent evolution of resource allocation strategies.

Introduction

Animals have repeatedly evolved new post-embryonic developmental trajectories, like regeneration or asexual reproduction by fission. Intercalation of such novel trajectories into the life history of an organism requires modifying pre-existing resource allocation strategies to accommodate new needs and constraints; in turn, allocation strategies and trade-offs can affect developmental and evolutionary trajectories (Fry, 2006; Simmons and Emlen, 2006; Parzer and Moczek, 2008). How are such novelties integrated into resource budgets? While life-history evolution studies have traditionally focused on resource allocation between somatic growth and sexual reproduction (Tuomi et al., 1983; Stearns, 1989; Heino and Kaitala, 1999; Zera and Harshman, 2001), reparative regeneration and asexual reproduction by fission use

up a sizable fraction of resources originally allotted to body growth; thus, if resources are insufficient to sustain both processes, trade-offs would be expected (Zera and Harshman, 2001). Since the phylogenetic origin of fission can be traced in many lineages (*see Chapter 1*), studying how resources are allocated to normal growth, regeneration and fission in those groups can offer new insights into how life histories evolve.

Tissue growth is common to somatic size increase, regeneration and fission. It represents a direct expression of resource investment by organisms, resulting from cell proliferation levels exceeding homeostatic tissue turnover. Active cell proliferation requires materials and energy, and is thus a significant resource sink for the organism. Proliferation control achieved through competition for limited factors has been proposed as a mechanism to control development of fly imaginal discs (Klingenberg and Nijhout, 1998), beetle horns (Parzer and Moczek, 2008) and vertebrate immune systems (De Boer and Perelson, 1995). Cell proliferation can thus be used as a proxy to quantify resource investment during somatic growth, regeneration and fission.

Annelid worms can add new tissues at different positions along the body. Most annelids grow by posterior tissue addition, whereby new tissues are added from a sub-terminal posterior growth zone, as well as exhibit cell turnover throughout existing segments. In annelids capable of regeneration, new tissues can also be added terminally (both anteriorly and posteriorly) following tissue loss. Those annelids that have evolved asexual reproduction by paratomic fission can also add new tissues in the midbody through a process of intercalation. In this reproductive mode, posterior

and anterior ends comprising segmental and non-segmental tissues are produced within a single segment, separated by a fission plane (Fig. 3.1A). Growth patterns seen during fission are closely related to those occurring during regeneration (Zattara and Bely, 2011), which in turn are likely to be based on somatic growth by terminal addition. These parallels make cell proliferation a good "common currency" with which to compare investment in each of these three processes.

Naid annelids (Annelida:Clitellata: Naididae) are a group of freshwater segmented worms with a body plan particularly convenient for studying resource allocation patterns. Besides growing by terminal segment addition, many are also capable of regenerating amputated ends: after transection, the wound is quickly healed and a regeneration blastema forms by cell proliferation, growing and differentiating into a replacement end similar to the lost one (Fig. 3.1A). Paratomic fission has evolved several times within the family and is present in all members of subfamilies Pristininae and Naidinae (*see Chapters 1 and 4*; see also Erseus et al. 2002, Envall et al. 2006, Bely and Wray 2004, Zattara and Bely 2011). *Pristina leidyi* Smith, a species belonging to Pristininae, is particularly suitable for looking at resource investment strategies, because its body-wide patterns of cell proliferation can be easily quantified by thymidine analogue incorporation and whole-mount immunodetection (Zattara and Bely, 2011). Early work on paratomic annelids and flatworms has shown that regeneration and fission can interfere with each other (Galloway, 1899; Child, 1903; Harper, 1904; Consoli, 1923; van Cleave, 1929). However, these studies were based on qualitative descriptions of developmental outcomes; no quantification of investment or formal testing of resource competition

has been reported in this group. Thus, studying cell proliferation dynamics in *Pristina leidyi* should not only yield insights into resource allocation strategies in this species, but also into the overarching principles underlying convergent evolution of life histories.

In this study, I measured cell proliferation and growth in size in developing regions and along the whole body in *Pristina leidyi* to answer three questions: a) how do baseline patterns of resource investment and growth change with feeding regime?; b) how are these growth patterns altered by amputation and regeneration?; c) what are the patterns of resource investment when fission and regeneration occur simultaneously? My working hypothesis is that in *P. leidyi* resource availability depends on nutritional status, and when resources are limited, competition between developmental trajectories results in a shift in resource allocation. While strong trade-offs are expected to cause negative correlations of investment or growth between competing trajectories, the strength of this interaction can be modulated by variation in resource availability or physiological context (Tuomi et al., 1983; Reznick, 1985; Stearns, 1989; Heino and Kaitala, 1999; Zera and Harshman, 2001).

Materials and Methods

Animal collection, culturing and general experimental conditioning

I used specimens of *Pristina leidyi* Smith derived from samples collected at an artificial pond at the University of Maryland (35°59’48”N, 76°56’25”W) in August 2009. Worms were cultured in artificial spring water (0.35 g/L InstantOcean aquarium mix) in glass bowls, and fed dried powdered *Spirulina*. To homogenize

physiological and nutritional status across individuals, healthy-looking worms with no visible fission zones were selected from stock cultures and placed in new cultures with no food for at least a week. Except where indicated, worms were then fed *ad-libitum* the day before the start of an experiment and transferred back to no-food conditions for the duration of the experiment.

Pulse-chase experiment to determine growth patterns and proximal fates

Worms fed as described above were incubated in 0.8mM BrdU for 2 hs, and either fixed immediately after the incubation (pulse) or moved into fresh spring water, and fixed after 24 or 48 hs (chases).

Effects of feeding level and amputation on baseline growth patterns

Ninety worms between 21 and 33 segments long (70% having 27±2 segments) were fed as described above. Thirty worms were left as-is, while the remaining 60 were fed a second time the day after the first feeding. One hour after this second feeding, 30 of the latter worms were amputated bisected, cutting at half the total segment number; anterior and posterior pieces were kept separately. From the resulting four sets of 30 worms (LF, “low food”, fed only once; HF, “high food”, fed twice; AR, “anterior regeneration”, anterior amputees; PR, “posterior regeneration”, posterior amputees), samples of 10 individuals were incubated for 3 hs in 0.8mM BrdU at 1, 24 and 48 hs, and subsequently fixed. After immunodetection, each worm was imaged at multiple focal planes, the Z-stack was flattened into a minimal intensity projection using ImageJ (Bethesda, MD, USA) and the resulting image was exported as a spatially calibrated raster. Using the ArcGIS geographic information

system (ESRI, Redlands, CA), each segment was delineated as a polygon, and positive cells were labeled as points. The segment corresponding to each point was then recorded into a database using a spatial query.

Experiments on post-amputation proliferation shutdown

Two experiments explored immediate and long term effects of amputation on proliferation and growth. In the first, 30 worms 26-28 segments long without visible fission zones were selected: 10 were set aside as a control group, and the rest were cut into anterior and posterior pieces right in front of bristles of segment 13. Ten pairs of anterior and posterior amputees were incubated in BrdU from 5 min to 35 min after amputation and 10 pairs were incubated in BrdU from 90 to 120 min after amputation. Worms were fixed immediately after BrdU incubation. After immunodetection, I scored the number of BrdU+ cells at region A (anterior prostomium) and P (posterior growth zone and pygidium) regions, and at segments 8, 11, 13, 15 and 18 (Fig. 3.3A). In the second experiment, I repeated exactly the procedure described in the previous paragraph, except that I had only three treatments (HF, AR, PR), and that worms were sampled at 24, 48 and 78 hs after amputation. BrdU+ cells per segment were scored body-wide, and analized comparing regenerating AR and PR worms to non-amputated HF worms.

Experiments on interaction of regeneration and fission

Worms used to measure the interaction of regeneration and fission were conditioned as described above, except that they were kept more than one day in *ad-libitum* food conditions. As worms initiated fission, I selected specimens at early and

mid stages of fission, and cut them ahead or behind the fission zone either 5 or 2 segments away (Fig. 3.4A); non-amputated worms were kept as controls. The proportion of worms at each stage was similar between controls and each amputation treatment.

In the first set of experiments, 10 worms for each amputation treatment and 13 control worms were live imaged immediately after amputation and every 24 hs thereafter until they had split into separate worms or the experiment had concluded. Worms were kept at individual containers throughout. The areas of the fission zone's anterior and posterior portions and of the regenerate were measured at the midsagital focal plane.

In the second set of experiments, a total of 140 worms were similarly treated, but pooled and kept at batches rather than individually; 24 hs after amputation they were incubated in 0.8mM BrdU for 3hs, fixed, immunoassayed and imaged using CLSM (see below). BrdU+ cells at the wound site were counted from Z-stacks; since at fission zones cells were often too closely packed for accurate counting, I instead created sum projections, measured total signal intensity for the anterior (developing tail) and posterior (developing head) portions of each fission zone, and divided it by mid-sagital cross-section area to calculate average signal intensity. Because there is no consistent way of standardizing intensity measurements to allow direct comparisons across images, I used only the signal intensity ratio between anterior and posterior portions of each fission zone within an individual image as a measure of cell proliferation intensity of the developing tail relative to the developing head.

Worm amputation, mounting for live imaging and fixation

To make amputations, worms were anesthetized with 50μM nicotine in spring water and cut with a scalpel at the desired location. For live imaging, specimens were anesthetized, mounted under a coverslip supported by clay beads, and imaged under a compound microscope using DIC optics. After imaging, they were un-mounted and nicotine was washed off with spring water. Worms destined for immunoassays were relaxed 10 minutes in cold 100 mM $MgCl_2$, 5 mM NaCl, 1 mM KCl, 8% ethanol solution, fixed with 4% formaldehyde in 0.75x PBS for 40 minutes, washed with PBS and stored at 4ºC until imaging.

BrdU detection immunoassay

To label cells in S-phase, worms were incubated in 0.8 mM 5-bromo-2′-deoxyuridine (BrdU, B5002; Sigma, St. Louis, MO) for 0.5, 2 or 3 hs. Fixed specimens were incubated in 6M HCl at 37°C for 1:45hs, washed with PBS, then PBTx (0.1% Triton-X in PBS) several times, blocked in 10% Normal Goat Serum in PBTx for 3hs and incubated overnight at 4°C in anti-BrdU mouse monoclonal primary antibodies (G3G4; DSHB, Iowa City, IA) diluted 1:25 in blocking solution. Then they were washed several times with PBTx over 3 hs, incubated 5 hs at room temperature in HRP-conjugated goat anti-mouse IgG secondary antibodies (115-036-003; Jackson Immunoresearch, West Grove, PA) diluted 1:200 in blocking solution, washed overnight with PBTx and developed by equilibration for 10 min in 0.1 mg/mL diaminobenzidine (DAB, B5905; Sigma) and 0.064% NiCl in PBTx, followed by addition of 1-3μL of 0.3% hydrogen peroxide and incubation for 5-10min. After development, the samples were washed with PBTx and PBS, transferred

through a graded glycerol series (25%, 50% and 75% in PBS) and mounted in 75% glycerol in PBS. For fluorescence detection, the following changes were made: anti-phosphorylated histone H3 (06-570, Millipore, Darmstadt, Germany) diluted 1:200 was added to the primary antibody incubation; the secondary antibody was replaced with FITC-conjugated goat anti-mouse IgG (115-096-003; Jackson Immunoresearch) diluted 1:200 in blocking solution with 0.1mg/mL 4, 6-diamidino-2-phenylindole HCl (DAPI; D9542 Sigma); and samples were mounted in 25 mM *n*-propyl-gallate (02370; Sigma) in 75% glycerol/25% PBS.

Microscopy and imaging

Live and stained samples were examined under a Zeiss Axioplan2 microscope equipped with a Zeiss AxioCam HRc camera (Zeiss, Oberkochen, Germany) interfaced through Openlab (Improvision, Conventry, UK) or Zeiss Axiovision (Zeiss, Oberkochen, Germany). Fluorescently labeled samples were imaged under epifluorescence using the above setup, or using confocal laser scanning microscopy (CLSM) with either a Leica SP5X (Leica, Wetzlar, Germany) or a Zeiss LSM710 (Zeiss, Oberkochen, Germany). Z-stacks with 1.0µm steps were acquired using the manufacturer's software and examined using ImageJ (Bethesda, MD, USA) (Abramoff et al., 2004) and/or Zen LE 2009 (Zeiss, Oberkochen, Germany).

Statistical analyses, plotting and figure montage

I used the R statistical computing environment (R Development Core Team, 2011) to analyze and plot all quantitative data, and compute statistical tests. Data from feeding /amputation experiments were used to calculate curves of relative

density of BrdU+ cells along the antero-posterior (AP) axis, using R's `density` function on segmental counts pooled by treatment/time. Because worms varied in total segment count, for each segment *s* a relative position s_r along the AP axis was calculated as s/s_t, with s_t being the total number of segments of that individual. The prostomium was coded as $s=s_r=0$; the posterior growth zone (PGZ) and pygidium were counted as a single unit and coded as $s=99$ and $s_r=1$. Wounded segments were coded as $s_r=0.5$. The algorithm used by `density` first approximates the empirical data distribution over a regular grid, then uses a fast Fourier transform to convolve this approximation with a discretized version of a Gaussian smoothing kernel and finally approximates linearly to evaluate density at every point in the plot; curves reflect the probability of finding a labeled cell at any given position; the Y-axis is dimensionless (R Development Core Team, 2011). Montages of plots and microscopy imagery were done using Adobe Creative Suite CS3.

Results

Growing worms have higher cell proliferation at three distinct regions

To observe qualitative patterns of cell proliferation, fed, actively growing worms were incubated in BrdU for 2 hs to label S-phase cells. Worms show BrdU+ cells along most of their body, but three regions show particularly high concentrations of labeled cells (Fig. 3.1B): the anterior non-segmental prostomium (A), the terminal posterior area (P), and one or a few mid-body segments about two-thirds of the body length (M). The A region is limited to a band antero-dorsal to the mouth; however, labeled cells are absent from the proboscis, a trunk-like extension of the prostomial

cap. At the P region, proliferation is concentrated in latero-ventral bands; the highest density of labeled cells is located immediately anterior to the terminal pygidium. The middle M region is the most variable: proliferation ranges from slightly higher densities of the peppered pattern seen throughout most of the body, to the presence of clear bilateral bands showing high density of labeled cells. In the latter case, they usually coincide with morphologically visible paired masses of mesenchymal cells, a hallmark of a fission zone. Outside of these three regions, most labeled cells are in the epidermis and gut, but many can be found in other ecto- and mesodermal tissues. Epidermal proliferation often shows a segmentally iterated pattern where a number of BrdU+ cells are found arranged along transverse lines, one or two per segment.

Growth patterns differ between A, P and M regions

To gain insight into the tissue growth dynamics and proximal fate of proliferating cells in the three growth regions, I performed a BrdU pulse-chase assay, with a 2hs pulse and 24 or 48 hs chases. After the pulse, worms presented the same pattern of proliferation described above (Fig. 3.1B). At the A region, peppered labeled cells are only present up to the base of the proboscis, but no labeling is seen distal to this point (Fig. 3.1C). After 24 hs, a slightly larger number of smaller labeled cells are concentrated closer to the proboscis (Fig. 3.1D); after 48 hs, smaller cells are present in most of the prostomium, and are clearly seen past the base of the proboscis (Fig.3.1E). In other words, an anterior shift of the distal limit of labeling is detected over time. At the P region, formation of new segments is evident over the 48 hs of the chase (Fig.3.1I-K). The area of greatest concentration of labeled cells is initially narrow, falling just anterior to the pygidium, and progressively widens (along the A-P

dimension) with increasing chase times. New tissues formed during this period are mostly comprised of cells labeled during the pulse, although BrdU+ signal ranges from strong to very weak, likely due to variation in the number of divisions each cell underwent since the label was incorporated. After 48 hs, the ventrolateral area corresponding to the original location of the most concentrated labeling is mostly devoid of labeled cells, as expected for a region still proliferating to make new segments. At the middle M region, labeling progressively widens along the A-P axis with increasing chase times, with relatively sharp and consistent borders to the labeling at the boundary between the fission zone and the original tissue (Fig.3.1F-H).

The distribution of cell proliferation is independent of feeding level but changes drastically during regeneration

To characterize body-wide patterns of distribution of cell proliferation in worms under low food (LF) and high food (HF) availability, and in posterior (PR) and anterior (AR) amputees, I incubated 10 worms from each group in BrdU for 3hs at 1-4, 21-24 and 45-48 hs after treatment, and scored BrdU+ cells at each segment along the entire worm (Fig. 3.2A).

The average total number of BrdU+ cells was not significantly different between LF and HF at 4 hs; at 24 hs, this number decreased substantially both for HF and LF; after 48 hs, counts in HF worms rebounded, while LF worms showed significantly fewer labeled cells (Fig. 3.2B; Wilcoxon rank sum test W=6, p = 3.2E-4, n=10). Although the actual number of BrdU+ cells along the body differed considerably among individuals, most specimens showed a relatively consistent spatial pattern of labeling (Fig. 3.2C).

Curves of relative density of BrdU+ cells along the antero-posterior axis (Fig.3.2D) reveal that the probability AP distribution of cell labeling is qualitatively similar across feeding levels and time points for uncut worms, but changes drastically upon amputation. Both LF and HF treatments, from 4 to 48 hs, showed three regions with consistent higher density of proliferating cells. Two are located at the tips of the animal, corresponding with regions A and P described above, while the third, located around two-thirds of an animal's length, approximates region M. The same pattern was observed in an additional set of worms taken from a separate, starved batch culture kept unfed throughout the experiment (data not shown).

While overall relative density distributions were qualitatively similar across feeding levels, absolute counts of BrdU+ cells at regions A (prostomium, coded as $s=0$; Fig. 3.2A), M (averaged across 5 segments, s=17±2, comprising all or most of the high-proliferation peak; Fig. 3.2A) and P (pygidium and posterior growth zone, coded as s = 99; Fig. 3.2A) showed different patterns (Fig. 3.2E). The LF treatment initially showed more proliferation at the M and P regions than at A, but counts fell down over time, while proliferation at the A region remained approximately constant throughout. The HF treatment, on the other hand, initially showed an even distribution of proliferation across the A, M and P regions, with counts at the P region increasing on the following day, and the counts at the M region increasing to comparable levels on the day after.

In contrast to feeding, amputation caused an rapid decrease in cell counts throughout the body (Fig. 3.2B; Wilcoxon rank sum test comparing HF counts vs. doubled AR and PR counts: W=11.5, p = 1.1E-4, n=10; counts at regenerates were

multiplied by 2 since each amputated piece had about half the segments). This body-wide reduction of labeled cells persisted through the 48 hs timepoint, although trend for a slight increase in the PR counts was evident across the 24 and 48 timepoints. The curve of relative density of BrdU+ cells 4hs after amputation shows a qualitatively similar shape to those of non-amputated worms; however, after 24 hs a clear change became evident as proliferation became concentrated exclusively near the amputated region and shut down elsewhere in the body (Fig. 3.2D).

Body-wide shutdown of proliferation occurs immediately after amputation and persists over several days

To quantify how quickly and how broadly the cell proliferation shutdown occurs after amputation, I cut worms without fission zones at segment 13, and incubated in BrdU either from 5-35 min after cutting or from 90-120 min. After immunodetection, I scored the number of BrdU+ cells at regions A (prostomium) and P (pygidium and PGZ), and at segments 8, 11, 13, 15 and 18 (Fig. 3.3A). Amputation caused a statistically significant reduction at both time points for all positions, except for anteriorly amputated pieces at 5-35 min within segment 13 where the cut was placed (Fig. 3.3A; Wilcoxon rank sum tests, $p < 0.05$, $n \geq 10$). Thus, the proliferation shutdown effect is detectable body-wide within the first half hour after amputation.

To quantify the extent and duration of this change in cell proliferation patterns, I amputated worms at about half of their length and incubated a subset (n=10) in BrdU for 3 hs at 24, 48 and 72 hours post-amputation (hpa). I then scored after immunodetection the number of labeled cells within each segment. In both anterior and posterior regenerates, most of the proliferating cells are found at the

amputated segment, or adjacent to it (Fig 3.3B). Body-wide counts on posterior amputees rise slightly from 24 to 72 hs, but most of the proliferation is still concentrated at the regenerating end. Qualitative observations made on longer time series show that proliferation patterns return to normal only after the regenerative process is complete, around 4-5 days after amputation (data not shown).

The effect of regeneration on fission development depends on the location of the cut relative to the fission zone

Since I found that amputation causes a body-wide shutdown in cell proliferation, I asked how this would affect a fission zone's development. In an extreme scenario where cell proliferation within a fission zone is exclusively regulated by the same mechanisms controlling normal turnover and growth, then amputation should cause a slowdown or complete stalling of the fission zone's development. In the opposite case where regulation of proliferation during fission is completely independent of normal growth, fission zone should not be affected by amputation. Results located in-between these two extremes would suggest a more complex interaction of shared and exclusive controls.

To test the effect of eliciting regeneration in a fissioning animal, worms with fission zones at early and mid stages were amputated 5 or 2 segments away, either ahead or behind the fission zone (Fig.3.4A); non-amputated worms were kept as controls. Each worm was imaged and the fission zone's anterior (developing tail) and posterior (developing head) portions were measured immediately after amputation and at 24 hs and 48 hs after amputation. I also scored regeneration progress and whether individuals had split into daughter parts.

On average, more amputated fissioning worms (40%; *n*=40) had split apart after 48 hs than uncut controls (0%; *n*=13). The probability of splitting depended on the location of the cut (Fig. 3.4B; *n*=10): worms amputated ahead of the fission zone were more likely to split than those amputated behind, and within each side, cutting closer to the fission zone caused more frequent and faster splitting. On the other hand, animals amputated ahead of the fission zone were less likely to show a sustained anterior regenerating response at the wound site than those amputated behind it (Fig. 3.4C; *n*=10); worms amputated behind the fission zone usually presented a consistent posterior regenerate that developed at the same rate independently of the distance between the cut and the fission zone (Fig. 3.4D; *n*=10), while worms amputated ahead of the fission zone had a small anterior regeneration or did not regenerate at all (Fig. 3.4D; *n*=10).

Amputation can alter the developmental trajectory of fission

In the experiment just described, the relative size of the developing tail and head within a fission zone were similar between controls and most animals amputated behind the fission zone, but some of the latter and all animals cut ahead of the fission zone showed a marked difference (Fig. 3.4E-F). For each worm, I plotted the sizes of the two portions of a fission zone before and after a period of 24hs as vectors in a developing head vs. tail size space; all animals contributed change vectors spanning 0-24 hpa, and those that had not split by then contributed additional 24hs vectors (up to 72hs).

Control worms represent a “baseline” trajectory of fission (Fig. 3.4E, black arrows) that is variable but in most cases is pointing within 0-90°, meaning that both

head and tail are growing; all exceptions had small modules and thus could have resulted from measurement variance in worms that had little or no growth. Worms amputated behind the fission zone (Fig. 3.4E, FZ+2 and FZ+5 orange arrows; *n*=20) usually showed the same directional trend. However, a number of worms with early stage fission zones showed instead change vectors in the 180-270° range (Fig. 3.4E, inset), indicating that both head and tail underwent de-growth; in 2 out of 40 cases, the fission zone that had been present at the start of the experiment was completely absent at 48hpa. Resorption was not observed in worms amputated ahead of the fission zone in this experiment, but was scored for this location in a replicate experiment with a larger sample size (see below). Full fission zone resorption was uncommon: among two replicates of this experiment, it was found in only 3% (6/186) of the cases, and always in cuts close to very early fission zones (FZ-5: 0/47; FZ-2: 3/47; FZ+2: 3/46; FZ+5: 0/46). However, very early fission zones are harder to see even under a dissecting microscope and less likely to be detected; thus, a low frequency of resorption cases may reflect a detectability bias in sample selection rather than (or along with) a rare outcome.

In contrast, all worms amputated ahead of the fission zone (Fig. 3.4E, FZ-2 and FZ-5 purple arrows; *n*=20) showed a striking directional change towards the 90-180° range, indicating that the head grew while the tail was reduced. Comparing growth of each portion of the fission zone, measured as the ratio of areal difference after a 24hs period to the original area, between anterior amputees (FZ-*n*) and controls (ctrl) reveals highly significant acceleration of head development ($\bar{x}_{FZ-n}$ = 1.30, n = 24; $\bar{x}_{ctrl}$ = 0.61, n = 27; Wilcoxon rank sum test p = 5.8 E-9) and regression

of the developing tail ($\bar{x}_{FZ-n}$ = -0.34, n = 21; $\bar{x}_{ctrl}$ = 0.39, n = 27; Wilcoxon rank sum test p = 5.8 E-9). Head acceleration and tail regression in amputees compensate each other: amputees and controls show no significant differences in growth of the fission zone as a whole ($\bar{x}_{FZ-n}$ = 0.64, n = 21; $\bar{x}_{ctrl}$ = 0.52, n = 27; Wilcoxon rank sum test p = 0.12). Compensation is also indicated by lack of significant differences in an ANOVA of the module of change vectors between anterior amputees and controls (F=0.707; d.f.=2; p = 0.50). There was no significant difference between FZ-2 and FZ-5 at any of the above mentioned variables.

Under a scenario where regeneration competes with fission for resources, I expect a negative correlation between fission zone and regenerate growth rates. Since worms amputated ahead of the fission zone usually failed to regenerate, I used worms amputated behind the fission zone to test this prediction and found no significant correlation between fission zone and regenerate growth over the 24 hs periods scored in this experiment; there was in fact a positive, though non-significant, trend (Spearman's rank correlation ρ: 0.15, p=0.36, n=37). A stratified analysis separating treatments as well as fission zone regions (developing head and developing tail) also revealed no evidence for a negative correlation between fission and regeneration growth rates. In FZ-5 worms there was a marginally significant positive correlation between the growth rates of the fission zone's tail and the regenerating tail (Spearman's rank correlation ρ: 0.46, p=0.047, n=19).

Cell proliferation levels at wound site and fission zone are slightly correlated

To determine whether the above interactions between fission and regeneration are evident at the cell proliferation level, I repeated the above amputation scheme,

and incubated worms 3 hs in BrdU at 24 hs after amputation. Counts of BrdU+ cells at the wound site showed that cell proliferation was low in worms cut ahead of the fission zone, and high in worms cut behind the fission zone (Fig. 3.4G). There were highly significant differences among treatments (ANOVA F=60.84, $p<2.2E\text{-}16$, n=137); differences were due to location (ahead vs. behind; Tukey's HSD $p<1E\text{-}7$ for all pairwise comparisons across locations) rather than distance to the fission zone (2 vs. 5 segments; Tukey's HSD p=0.688 for FZ-5:FZ-2, p=0.248 for FZ+5:FZ+2). After amputating ahead of the fission zone, I found no significant correlation between BrdU+ counts at the wound site and the log ratio of BrdU signal intensity of the anterior and posterior fission zone portions (Fig. 3.4H; n=67). In contrast, I found a significant positive correlation among those variables after amputating behind the fission zone (Fig. 3.4I; Pearson's r = 0.328, p = 0.007, n = 66); in other words, a stronger proliferative response at the cut end correlates with stronger proliferation of the developing tail relative to the developing head at the fission zone.

Discussion

Cell proliferation and size change are two processes common to somatic growth, regeneration and fission that can be readily quantified in order to characterize resource allocation strategies. I analyzed body-wide and localized cell proliferation and growth patterns in the naid annelid *Pristina leidyi* to investigate three different questions: a) how do baseline patterns of resource investment and growth change with feeding regime?; b) how are these growth patterns altered by amputation and regeneration?; c) what are the patterns of resource investment when fission and regeneration occur simultaneously?

Growth occurs by intercalation of tissue at distinct regions

Growth by tissue addition at a posterior subterminal zone has been proposed as an ancestral trait of bilaterians (Jacobs et al., 2005; Rosa et al., 2005). Most annelids have a posterior growth zone where segments are added , but cell proliferation patterns have been described in only a few species (Brusca and Brusca, 1990; Nielsen, 2005; Rosa et al., 2005; Seaver et al., 2005). I found that in the clitellate annelid *Pristina leidyi*, body-wide patterns of cell proliferation show that growth is concentrated in three regions: two narrower subterminal regions at each end of the antero-posterior (AP) axis, and a broader region located roughly at two-thirds of the body length. Pulse-chase experiments show that most tissues formed in the P region become incorporated in an antero-posterior sequence into newly formed segments; thus, cell proliferation at region P can be associated with terminal segment addition driven by a posterior growth zone.

In contrast, the A region shows a different pattern: most cell proliferation is found at the base of the prostomium and peristomium. While the presence of a posterior growth zone from which new segments are formed is well known in annelids, this is the first study to indicate that the prostomium abuts and is made by an anterior growth zone. Since no permanent addition of tissue occurs at that position, where do new cells go? Pulse-chase experiments suggest that at least a fraction is actually incorporated into the proboscis, the trunk-like extension protruding from the tip of the prostomium in this species. The proboscis, however, does not increase significantly in size in adult worms; this implies that some mechanism must be responsible for removing cells in order to maintain organ size. Preliminary data from

whole-mount TUNEL assays hint at increased apoptosis towards the distal end of the proboscis (E.E.Z., unpublished data). This suggests a "conveyor belt" model of cell turnover where intercalary growth at the A region is offset by apoptosis at the proboscis. This model may also apply to the posterior non-segmental cap, or pygidium, with new cells made at the posterior edge of the posterior growth zone being incorporated into the pygidium, while old terminal cells are sloughed off by apoptosis. Under the "conveyor belt" model, size and shape of the terminal caps are expected to be dependant on a steady equilibrium point between tissue addition and attrition; changes in that point could underlie the many phylogenetically independent origins of extensions of the prostomium (into a proboscis) or the pygidium (into branchial pavilions and other posterior structures) that have occurred in this phylum. The naid non-segmental caps and their growth zones could provide a novel and simple system in which to study dynamic control of organ size in a post-embryonic context.

Qualitative patterns of cell proliferation are independent of resource availability

Differential resource investment along the body depends on specific allocation strategies for a given context; when resources are limited, allocation trade-offs result from competition between different developmental processes (Heino and Kaitala, 1999; Zera and Harshman, 2001). Conversely, increases in resource availability should decrease competition and cause a shift in allocation patterns. Do patterns of cell proliferation in *Pristina leidyi* change with nutritional level? While low and high food treatments showed clear differences in absolute counts, antero-posterior distribution of proliferation presented similar peaks in regions A, M and P. Thus,

resource availability changes the levels but not the shape of an underlying AP distribution of investment; in other words, variations in resource acquisition just depress or exaggerate a pre-existing allocation pattern.

That internal factors controlling growth are independent of nutritional status had been previously proposed for naids by Hughes (1989), based on work on *Pristina longiseta* (Van Cleave, 1937) and *Allonais paraguayensis* (Hyman, 1938), but this study is the first to formally characterize this concept. In the appendicularian tunicate *Oikopleura dioica*, somatic growth was found to be non-responsive to food levels beyond that needed for survival; resource surplus was instead invested in reproductive structure development (Troedsson et al., 2002). A similar pattern was seen in *Pristina leidyi*: worms at both feeding levels retained the same distribution patterns of proliferation, but those with higher resource availability initiated fission zones at the peak of the M region. The existence of intrinsic AP gradients in developmental potential has also been shown for the naid *Stylaria lacustris*, and linked to variations in regeneration and fission rates (Chu and Pai, 1944). Such an intrinsic non-linear AP gradient in proliferative response could explain the patterns observed in *Pristina*, and also be a significant factor determining AP distribution of regenerative potential and placement of fission zones.

Worms shift resource allocation patterns after amputation

Loss of an important body structure can have significant negative effects on an individual's survival and fitness, and these can be lessened or negated by regenerating it; however, regeneration requires allocation of resources otherwise

destined for other developmental processes, like growth or reproduction (Maginnis, 2006). How do *Pristina*'s allocation patterns respond to tissue loss and regeneration? I found that amputation causes rapid (within 30 minutes) body-wide down-regulation of cell proliferation, although it does not initially change the overall distribution of cell proliferation. Temporal resolution of the proliferation shutdown is limited by kinetics of BrdU incorporation, as incubations shorter than 15 minutes yield no signal (E.E.Z., unpublished data), and even 30 minute incubations may be insufficient for uniform label uptake by S-phase cells, causing measurement bias. Observations on worms doubly immunoassayed for BrdU and phosphorylated histone H3 (a mitotic marker) suggest that removal of the head, but not the tail, can reduce uptake of thymidine analogues and lead to an underestimation of the number of S-phase cells (E.E.Z., unpublished data); however, this bias is not present in posteriorly amputated worms, which in my experiments also show a clear shutdown effect.

What mechanism may be behind this long-range effect of amputation? Direct competition for a nutrient or growth factor (Klingenberg and Nijhout, 1998) is unlikely, since regeneration-associated proliferation at the wound site only becomes significantly higher many hours after amputation (*Chapter 5*). Other alternatives are either a diffusing or blood-borne signaling molecule, nervous system-mediated communication or a combination of both: hormonal modulation of regeneration has been shown in nereid polychaetes (Clark and Clark, 1959; Clark and Bonney, 1960; Fischer and Dorresteijn, 2004), and a role of the nervous system in regeneration has long been suggested in annelid literature (Goldfarb, 1909; Berrill, 1952; Herlant-Meewis, 1964). In any case, the fact that cell proliferation decreases body-wide

without a simultaneous increase at the cut segment supports an active mechanism rather than a passive result of increased resource competition.

A persistent high ratio of regenerate/body proliferation indicates a shift in resource allocation during regeneration. Body-wide downregulation of cell proliferation persists over several days; meanwhile, most proliferative activity occurs almost exclusively at the regenerating tip of the worm. Return to basal body-wide patterns coincides with reduction of that activity at the final stages of regeneration (Zattara and Bely, 2011). Results suggest that inhibition of body-wide proliferation is stronger and longer lasting during anterior, rather than posterior regeneration. This asymmetry may be due to anterior amputees lacking a mouth and thus being unable to gain additional resources until regeneration is complete, but underestimation of proliferation due to BrdU incorporation bias cannot be ruled out as an alternate explanation. Even then, body-wide low levels of cell proliferation during regeneration demonstrate that worms shift their resource allocation pattern after amputation.

Does this shift in allocation support a resource competition model between growth and regeneration? The intuitive interpretation is that animals prioritize re-building of lost structures over somatic growth; however, it is unclear whether this shift represents an actual trade-off strategy. This is further complicated during posterior regeneration: with the exception of the pygidium, tissues formed during this process are the same ones made during normal posterior growth, so it is difficult to separate regenerative from somatic growth investment. Trade-offs between regeneration and somatic growth have been postulated as having a pivotal role in evolutionary loss of regenerative ability by generating an adaptive “cost” offsetting

its benefits (Maginnis, 2006; Bely, 2010). Yet, many studies failed to find such costs (reviewed by Maginnis, 2006); at least for some studies, experimental subjects were fed *ad-libitum*, which can diminish or obviate trade-offs (Zera and Harshman, 2001). Since *Pristina leidyi* individuals can be starved for several weeks and still be able to regenerate (E.E.Z., personal observations), masking of trade-offs by high resource availability could be formally tested by measuring body-wide proliferation response to amputation over several feeding levels: after a longer starvation period, stronger shutdown and tighter negative correlation between somatic and regenerative growth are expected.

Amputation experiments on reproducing worms reveal context-dependant interactions between regeneration and fission

While both terminal segment addition and regeneration can be viewed as investments in somatic growth, resource allocation to development within a fission zone is an instance of reproductive investment. Considerable effort has been devoted to study allocation trade-offs between somatic growth and sexual reproduction (Tuomi et al., 1983; Stearns, 1989; Heino and Kaitala, 1999; Zera and Harshman, 2001), but reports on interactions between regeneration and asexual reproduction are scarcer, coming mostly from work done or inspired by Charles M. Child during the first half of last century in phylogenetically disparate groups like cnidaria, flatworms and annelids (Child, 1903, 1906; Harper, 1904; Hyman, 1916; Child and Hyman, 1919; Consoli, 1923; van Cleave, 1929; Van Cleave, 1937). Early studies found clear evidence for interactions between regeneration and paratomic fission both in catenulid flatworms (Child, 1903, 1906; van Cleave, 1929) and naid annelids

(Galloway, 1899; Harper, 1904; Consoli, 1923), which at the time where interpreted in the context of Child's theory of physiological dominance due to metabolic gradients (Child, 1915). While Child's underlying model has been mostly abandoned (Blackstone, 2009), his findings, still awaiting a mechanistic explanation, highlight the importance of accounting for physiological context in understanding the role of resource allocation trade-offs in post-embryonic development.

In *Pristina,* amputation and regeneration have a clear body-wide effect on cell proliferation. Given that fission zones show high levels of proliferation, what happens when a fissioning worm is amputated? My results show that the answer depends both on the developmental stage of the fission zone, and the location of the cut relative to it. After amputating a fissioning *Pristina,* the outcome usually falls in one of three categories: 1) fission stalling or regression and normal regeneration, observed for cuts anterior and posterior to early fission zones; 2) mostly normal fission development and tail regeneration, observed for cuts posterior to mid to late fission zones; 3) strong shift in fission developmental trajectory, including acceleration of fission head development, and slow or null regeneration, observed for cuts anterior to mid to late fission zones. This range of outcomes is similar to the one reported for the naids *Dero vaga* (Galloway, 1899)*, Stylaria lacustris* (Harper, 1904) and *Nais elinguis* (Consoli, 1923), and for the catenulid flatworms *Stenostomum grande* and *S. leucops* (Child, 1903; van Cleave, 1929). That a comparable fission-regeneration interaction has been found across three independent origins of paratomic fission (Pristininae, Naidinae and catenulids, *see Chapters 1 and 4*) suggests it may best be explained by a model of

competitive resource allocation and investment trade-offs rather than by underlying homologies or phylogenetic relationships.

Interactions between early fission, nutritional status and regeneration suggest competition for resources. Amputation of *Pristina* worms with early fission zones results in developmental stalling or regression of fission, and a strong regenerative response. Interestingly, starvation can cause similar effects on early fission zones (F. Smith, pers. comm. in Harper, 1904, and my observations). Thus, it would seem that fission is particularly labile at earlier stages; this flexibility makes fission zones double as reproductive and reserve tissue, which could be advantageous for species living in environments where resource availability is patchy or unpredictable. Stalling or regression of early fission zones after initiation of a resource intensive process elsewhere (such as regeneration), or due to a generalized decrease in resource availability, supports a resource competition model. Nonetheless, larger sample sizes and replication over different nutritional levels would be needed to formally test for the presence of allocation trade-offs between early fission and regeneration.

Cell proliferation patterns reveal weak but consistent interaction between posterior regeneration and fission. Cuts made behind the fission zone generally resulted in normal regeneration and did not have a significant impact on fission developmental trajectory. A strong trade-off strategy of resource allocation should cause a negative correlation between growth rates of fission zones and posterior regenerates. This expectation is not met by the data; instead, a slight trend in the opposite direction was found. A possible explanation is individual variation in proliferative response, so that some worms grow faster than others; even in the

presence of resource trade-offs, competing traits may show positive correlations if inter-individual variation is high enough (van Noordwijk and de Jong, 1986). On the other hand, stronger regenerative responses did correlate positively with higher tail/head proliferation ratios within the fission zone. While it is not possible to determine from the data if this correlation stems from proliferation decrease at the posterior portion of the fission zone or increase at the anterior portion, it is clear that posterior regeneration has a weak but recognizable influence on fission, either by competing for resources with the new head, or else by changing the investment allocation between fission zone portions.

In contrast, removal of the head reveals a strong regeneration-fission interaction and a clear shift in resource allocation within the fission zone. Amputation in front of a fission zone causes a drastic change in the fission trajectory, irrespective of the distance between the zone and the cut segment. In worms cut at all but very early stages of fission, removal of segments anterior to the zone results in regression of the developing tail, acceleration of new head development, earlier splitting and slow or null regeneration. Similar qualitative results had been reported in the naid *Stylaria lacustris* (Harper, 1904), the naid *Nais elinguis* (Consoli, 1923) and the platyhelminth *Stenostomum* spp. (Child, 1903; van Cleave, 1929), but this is the first time this phenomenon is quantified and statistically tested. The striking asymmetry between the results of amputations ahead and behind a fission plane make evident that anterior and posterior regeneration have quite different physiological effects in annelids.

Anterior amputations change fission trajectories, either by causing stalling or regression of early fission zones, or provoking a shift in resource allocation within later fission zones. Mutual exclusion of regeneration and fission investment is seen at all anterior cuts: either fission stalls or regresses while regeneration proceeds or fission proceeds and regeneration is prevented. In the latter case, there is no overall acceleration of fission zone growth in amputated animals: results show that total areal change is no different from that of the uncut controls. Furthermore, there is a very clear shift in resource investment between the two fission zone portions, so that the new head's development does accelerates, but at the expense of the new tail, whose growth not only slows down but regresses. Upon anterior amputation, the developing head seems capable of monopolizing resource allocation and also of capturing resources previously allocated to the new tail. This allows faster completion of paratomic development and physical separation into a posterior complete worm and an anterior fragment; that fragment usually dies in FZ-2 cuts, but that in FZ-5 cuts it may survive for several days and initiate anterior regeneration. Time-lapse imaging of FZ-2 worms suggests that the posterior individual can not only capture resource from the anterior fission zone portion, but from adjacent segments (E.E.Z., pers. obs.). Thus, amputation ahead of a fission zone not only reveals evidence of competitive interactions between regeneration and fission, but also results in a clear shift in resource allocation within the zone, suggesting that during fission the developing head and tail also compete for resources.

Anterior amputation switches worms from an open to a closed developmental system

Amputation of a worm can have strikingly different consequences depending on the location of the cut and the presence and stage of a fission zone. In all cases, anterior amputations cause a stronger body-wide effect than posterior ones, either by depressing cell proliferation elsewhere, or by shifting the resource allocation balance within the fission zone. Anterior amputations also reveal a stronger statistical signal for competitive interactions. What could explain this asymmetry? The more obvious reason is that anterior cuts remove the original head of the animal, a specialized region of the worm containing structures not found at the posterior end, including the worm's mouth. Removal of the mouth blocks acquisition of new resources. In contrast, worms can still potentially feed after posterior amputation; furthermore, opening of the new mouth in anterior regenerates takes much longer than opening of a new anus in posterior regenerates (Zattara and Bely, 2011). Thus, anterior amputation causes a stronger inhibition of resource acquisition than posterior amputation.

Since increased resource availability can mask or even change the expected direction of putative competitive interactions, trade-offs are expected to be stronger and easier to detect in closed system than in open systems (van Noordwijk and de Jong, 1986; Nijhout and Emlen, 1998; Zera and Harshman, 2001; Tomkins et al., 2005). Consistent with this expectation, in *Pristina leidyi*, competitive interactions between somatic growth, regeneration and fission are stronger in anterior than in posterior amputees, suggesting that removal of the head, but not the tail, causes the worm to become a closed developmental system. Interestingly, this switch in

modality does not necessarily result from actual changes in resource availability: in my experiments, all individuals were kept in food-free conditions after treatment, so that differences between anterior and posterior amputees cannot result from asymmetric resource acquisition. Thus, changes in resource allocation strategies derived from switching from an open to a closed system must be hardwired to the post-amputation response rather than contingent on actual interruption of resource acquisition.

Concluding remarks: parallel adjustment to parallel novelties

In the naid subfamily Pristininae, paratomic fission is thought to have evolved by co-option of regenerative processes (*see Chapter 2*), which are themselves tightly related to normal growth processes (Sánchez Alvarado, 2000; Brockes and Kumar, 2008). These processes are likely to share common regulation tools capable of modulating competitive interactions in a way that optimizes fitness. Such interactions can be readily quantified in naids by measuring two common components of these processes, growth and cell proliferation. Manipulating resource availability and switching between open and closed developmental states is relatively straightforward in *Pristina ledyi*, making it a powerful system to test predictions for the role of trade-offs and other resource allocation strategies in life history evolution.

The gain of a novel developmental trajectory must be accompanied by a modification of resource allocation strategies to accommodate new resource demands. Evolution of new sets of allocation rules and trade-offs must have independently occurred every time a novel trajectory was acquired by a lineage. Yet the resulting strategies are strikingly similar across lineages: the pattern of resource allocation

described here for *Pristina* (Pristininae) is akin to those described for three species of Naidinae (Galloway, 1899; Harper, 1904; Consoli, 1923), a lineage likely to have evolved fission independently (see *Chapter 4*). Pristininae and Naidinae are relatively close phylogenetically and share numerous morphological and ecological characteristics, so parallel evolution of strategies to integrate fission is not that unexpected. However, the outcome of interactions between regeneration and fission are the same as those described for catenulid flatworms (Child, 1903; van Cleave, 1929), which have a very different body plan. The fact that clear parallels in resource allocation strategies have evolved across independent gains of fission in distantly related groups supports the idea that a combination of analogous yet functionally equivalent developmental capabilities and similar ecological and physiological constraints can be a driver for convergent evolution of post-embryonic development.

Chapter 3 Figures

Figure 3.1: Morphology, regeneration, paratomic fission and growth zones in *Pristina leidyi*.

Anterior to the left in all panels. A) Schematic drawing of adult worms, illustrating post-amputation regeneration and asexual reproduction by paratomic fission. Blue bars show the regenerated tissues; green bars show the two portions of a fission zone. B) Body-wide pattern of cell proliferation in a recently fed worm; three regions showing higher local density of labeled cells can be seen: an anterior growth zone A, a middle fission zone M and a posterior growth zone P. C-E) Pulse-chase labeling of proliferating cells at the A region: after a 2 hs BrdU incubation (C, pulse), labeled cells can be seen 24hs (D) and 48hs (E) later spreading around the prostomium and moving up past the base of the proboscis (arrowheads). F-H) Pulse-chase labeling of proliferating cells at the M region: abundant cells labeled during early fission (F) are incorporated into most of the developing tail and head of the fission zone (G,H); green bars as in A. I-K) Pulse-chase labeling of proliferating cells at the P region: a subterminal ring of labeled cells (I) forms new segments (J) and is eventually displaced forward by newly forming cells at the posterior growth zone (K, red arrowhead); pink bars denote newly formed segments.

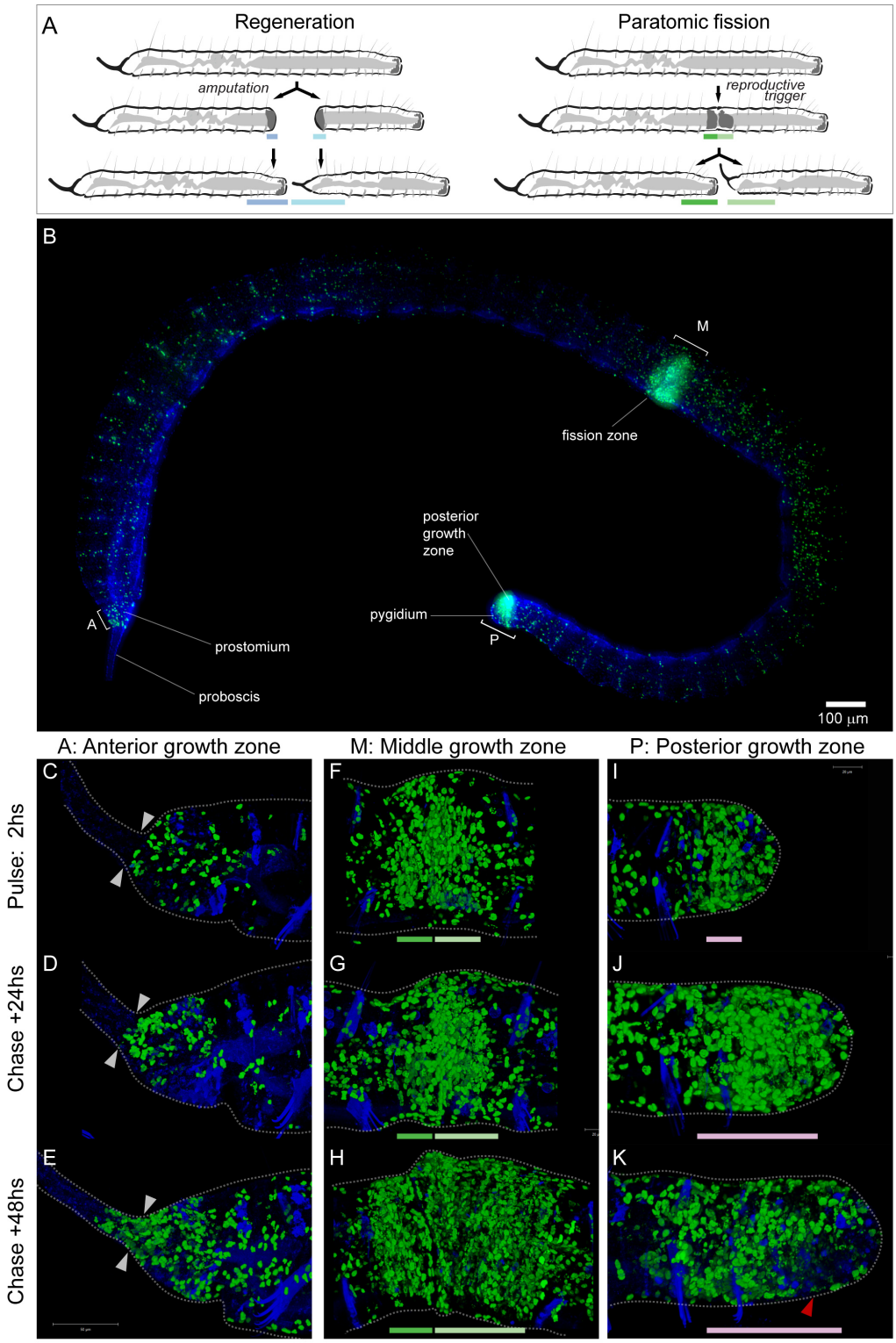
A
Regeneration
amputation
Paratomic fission
reproductive trigger
B
M
fission zone
posterior growth zone
pygidium
P
A
prostomium
proboscis
100 µm
A: Anterior growth zone
M: Middle growth zone
P: Posterior growth zone
Pulse: 2hs
Chase +24hs
Chase +48hs
C
D
E
F
G
H
I
J
K

Figure 3.1

Figure 3.2: Body-wide effects of feeding and amputation on *Pristina leidyi* cell proliferation patterns.

A) Picture of one of the individual worms scored, from the High Food treatment at 48hs, showing segment delimitation as an overlay; segments included in regions A, M and P are highlighted. B) Mean of individual total count of BrdU+ cells by time and treatment (n = 10 per treatment/time); error bars show standard error. Regenerates had on average half the number of segments as uncut worms. C) Plots of absolute counts of BrdU+ cells per segment for six representative individuals of the Low Food and High Food treatments at 4, 24 and 48 hs. The lower right plot correspond to the worm shown in B. D) Curves of relative density of BrdU+ cells along the antero-posterior axis, calculated using R's `density` function on segmental counts pooled by treatment/time. Because worms varied in total segment count, counts at segment s were positioned at s/s_t, with s_t being the total number of segments of that individual. The curves reflect the probability of finding a labeled cell at any given position; the Y-axis is dimensionless. The color-shaded regions correspond approximately to the three growth regions A, M and P. E) Response to feeding level over time for regions A ($s = 0$), M ($15 \leq s \leq 19$) and P ($s = 99^*$); mean segmental count of BrdU+ cells at each of the regions shaded on 3.2A for LF and HF worms. Error bars represent standard error.

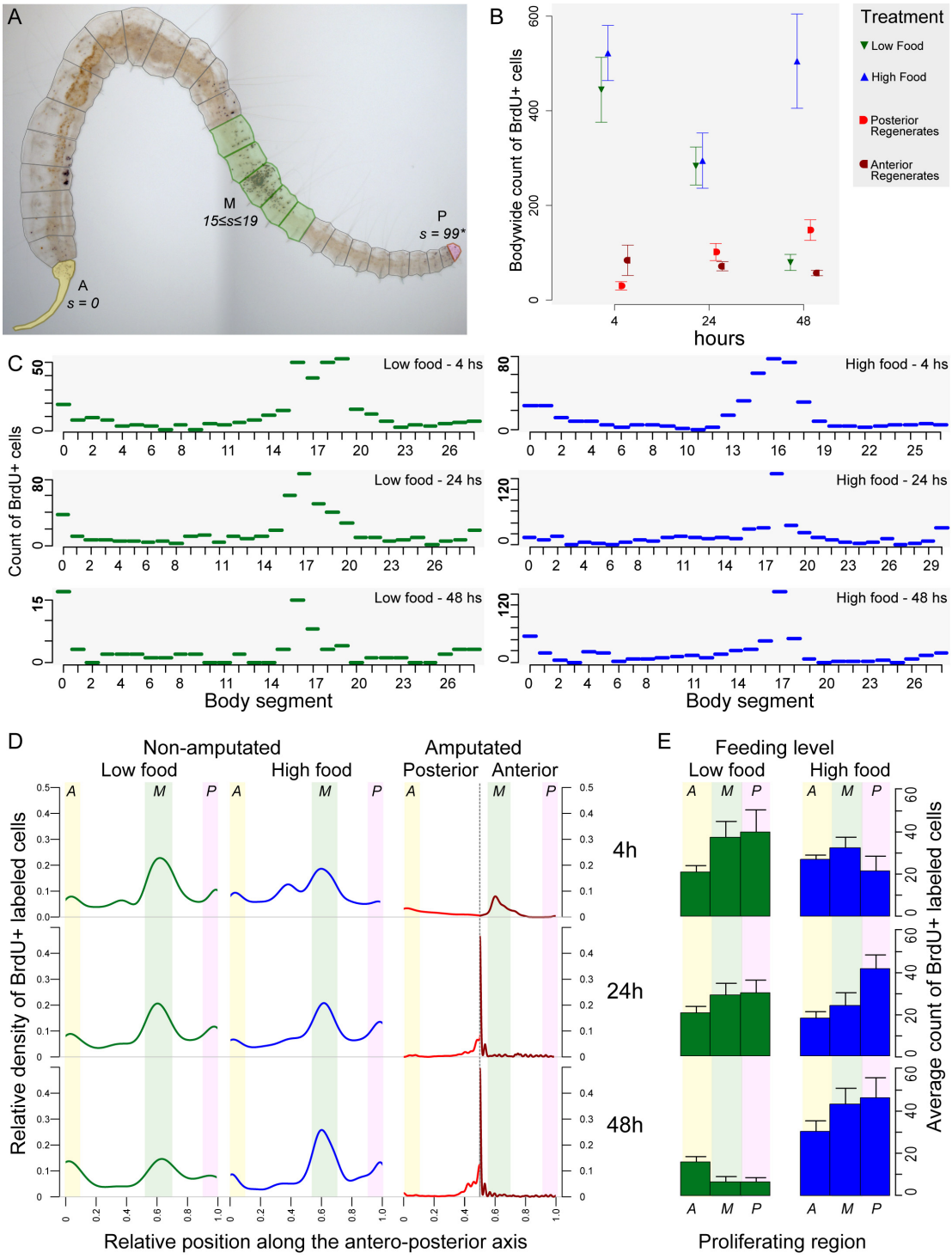
A
M
15≤s≤19
P
s = 99*
A
s = 0
B
Bodywide count of BrdU+ cells
hours
Treatment
Low Food
High Food
Posterior Regenerates
Anterior Regenerates
C
Low food - 4 hs
High food - 4 hs
Low food - 24 hs
High food - 24 hs
Low food - 48 hs
High food - 48 hs
Count of BrdU+ cells
Body segment
D
Non-amputated
Amputated
Low food
High food
Posterior
Anterior
4h
24h
48h
Relative density of BrdU+ labeled cells
Relative position along the antero-posterior axis
E
Feeding level
Low food
High food
Average count of BrdU+ labeled cells
Proliferating region

Figure 3.2

Figure 3.3: Post-amputation shutdown of cell proliferation in the short and long term.

A) Boxplots comparing counts of segmental BrdU+ cells between uncut controls, and posterior or anterior amputees 5-35 or 90-20 minutes after amputation, at different levels of the AP axis. Results from Wilcoxon's rank sum tests for differences between that group and the corresponding control (uncut) are shown as N.S. ($p > 0.05$), * ($p<0.05$), ** ($p<0.005$); n = 10 per treatment/time. B) Average count of BrdU+ cells per segment at 24, 48 and 72 hs after amputation. Segments within each worm were assigned to 10 bins, each $0.1s_t$ wide, with s_t being the total worm length. Prostomium, PGZ+pygidium and regenerating segments were assigned to separate bins. Then, segmental BrdU+ cell counts at each bin were averaged across worms for each timepoint and plotted. Error bars represent standard error of the mean; n = 10 worms per treatment×time.

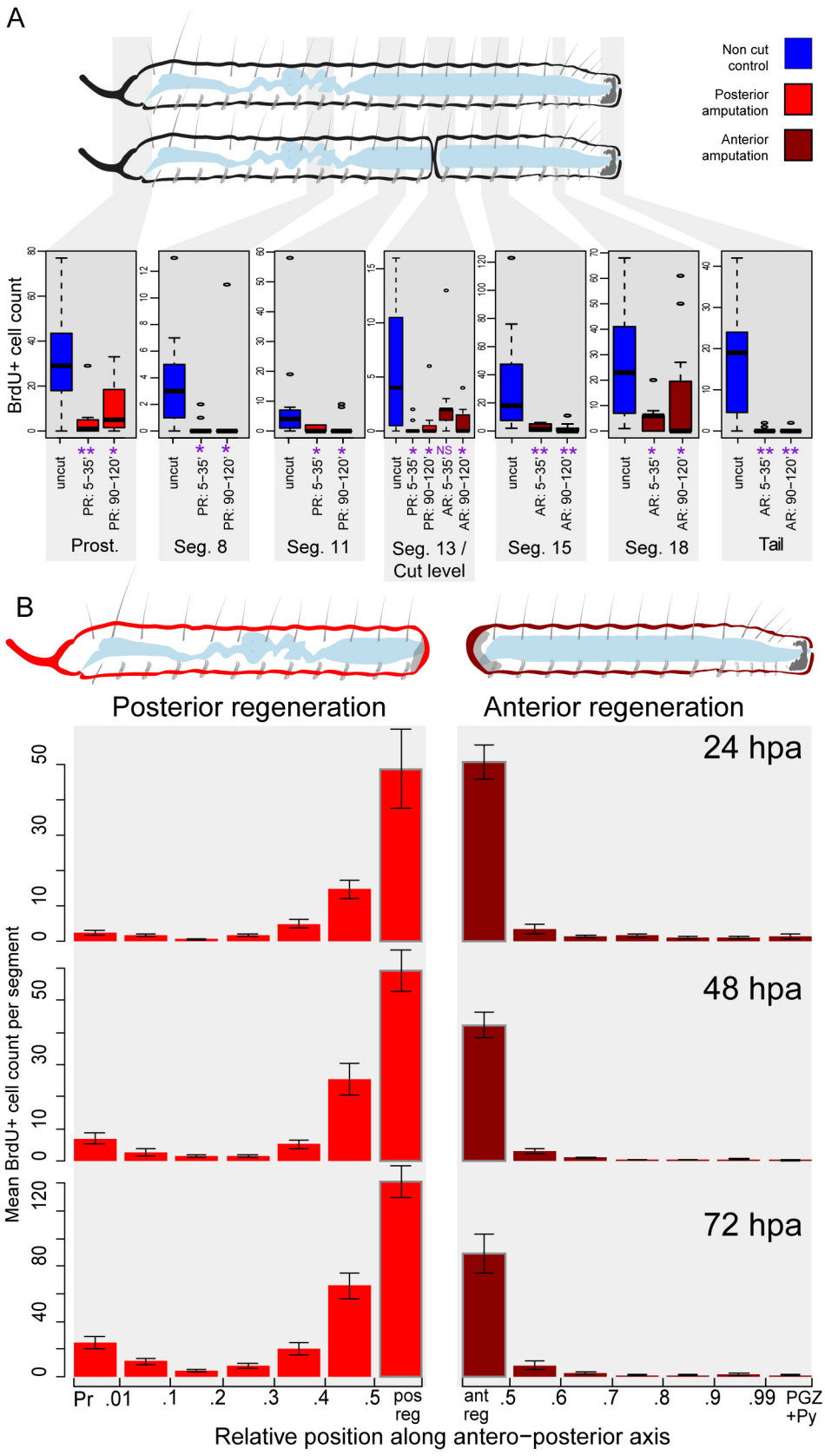
A
Non cut control
Posterior amputation
Anterior amputation
BrdU+ cell count
uncut
PR: 5–35'
PR: 90–120'
AR: 5–35'
AR: 90–120'
NS
Prost.
Seg. 8
Seg. 11
Seg. 13 / Cut level
Seg. 15
Seg. 18
Tail
B
Posterior regeneration
Anterior regeneration
24 hpa
48 hpa
72 hpa
Mean BrdU+ cell count per segment
Pr .01 .1 .2 .3 .4 .5 pos reg
ant reg .5 .6 .7 .8 .9 .99 PGZ +Py
Relative position along antero−posterior axis

Figure 3.3

Figure 3.4: Interactions between regeneration and fission in Pristina leidyi.

A) Schematic diagram of a fissioning *Pristina leidyi* showing the location of the cuts (dashed vertical lines) for each treatment. In each case, the piece underlined by the horizontal color bar was individually kept and the other piece was discarded; thus, FZ-5 and FZ-2 represent anterior amputations, and FZ+2 and FZ+5 represent posterior amputations. Worms were measured immediately after amputation and then every 24hs unitl they had physically split. B) Fraction of individuals per treatment that had split after 24 and 48 hs. C) Fraction of worms showing signs of regeneration at the wound site 24 hs after amputation. D) Mean size of the regenerate at 24 and 48 hs post amputation in worms showing active regeneration; error bars represent standard deviation. E) Developmental trajectories of fission, expressed as 24hs-change vectors in [developing head size]×[developing tail size]-space, and color-coded by treatment. Each arrow joins a point defined by the sizes of the two portions of the FZ at a given time to a point defined by these same measurements 24hs later; worms that had not split 24hs after amputation contributed up to three vectors. The inset at the lower-right represents a scaled-up detail of the boxed area showing trajectories of worms with early FZs. F) Differential interference contrast (DIC) micrographs showing representative individuals at 0 and 24 hs post amputation for each treatment. G) Mean count of BrdU+ cells at the wound site 24 hs post amputation; error bars represent standard error. H-I) Plots of individual counts of BrdU+ cells at the wound site 24 hs post amputation as a function of the log ratio of average BrdU signal intensities measured at the developing tail and head of the FZ (see text). There is no significant correlation for anterior amputees (H), but a significant positive correlation for posterior amputees (I).

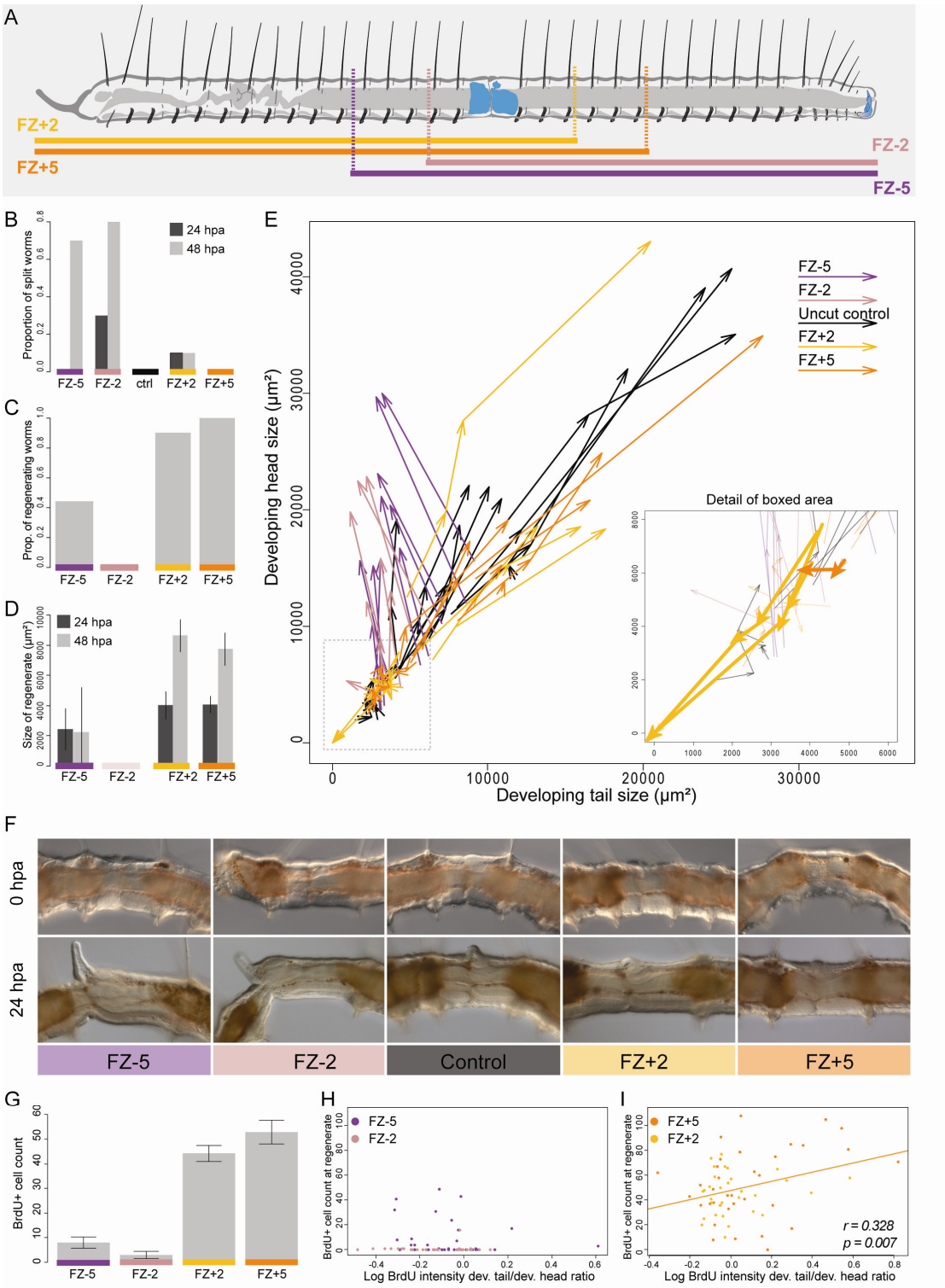
A
FZ+2
FZ+5
FZ-2
FZ-5
B
Proportion of split worms
24 hpa
48 hpa
FZ-5 FZ-2 ctrl FZ+2 FZ+5
C
Prop. of regenerating worms
FZ-5 FZ-2 FZ+2 FZ+5
D
Size of regenerate (µm²)
24 hpa
48 hpa
FZ-5 FZ-2 FZ+2 FZ+5
E
Developing head size (µm²)
Developing tail size (µm²)
FZ-5
FZ-2
Uncut control
FZ+2
FZ+5
Detail of boxed area
F
0 hpa
24 hpa
FZ-5
FZ-2
Control
FZ+2
FZ+5
G
BrdU+ cell count
FZ-5 FZ-2 FZ+2 FZ+5
H
FZ-5
FZ-2
BrdU+ cell count at regenerate
Log BrdU intensity dev. tail/dev. head ratio
I
FZ+5
FZ+2
BrdU+ cell count at regenerate
r = 0.328
p = 0.007
Log BrdU intensity dev. tail/dev. head ratio

Figure 3.4

CHAPTER 4: Convergent evolution of developmental trajectories after independent origins of annelid asexual reproduction by fission

Abstract

Naid annelids, small worms known for their ability to reproduce asexually by paratomic fission, have been recently found to form two clades, Pristininae and Naidinae, likely to have evolved paratomy independently. Yet existing descriptions of fission suggest this trait is highly similar in both groups. The close relationship between regeneration and agametic reproduction have led to the hypothesis that the latter evolved by co-option of the former; thus, co-option of similar regeneration abilities in pristinines and naidines would result in similar fission trajectories. To test this scenario, I conducted a comparative study of regeneration and fission with emphasis on nervous system development in two pristinines, seven naidines and a distantly related outgroup species, using immunocytochemical labeling and confocal microscopy to describe the two trajectories across all species. I found that regeneration trajectories were mostly similar across all species, including formation of blastema, growth of axons from the proximal peripheral nerves, loss of gut ciliation, extension of longitudinal muscle from the stump and re-formation of the central nervous system from outgrowths of the cut ventral nerve cord. Paratomic fission trajectories in pristinines and naidines were also strikingly similar: formation of fission masses, growth of axonal tracts towards the fission plane, retention of gut ciliation and gradual re-routing and separation of longitudinal muscle fibers were seen in all cases. I also found that all species, even the outgroup, have placed the

fission plane at the same interganglionar position. In contrast, I discovered two different modes of reconstructing the central nervous system during paratomic fission: in Type I paratomy, restricted to Pristininae, a new ventral nerve cord along with circumenteric connectives is formed anew from the adjacent ganglion, dorsal to the old cord; in Type II paratomy, restricted to Naidinae, the neuropil of the old ventral nerve cord is "recycled" and the new connectives extend dorsally from it. This study shows that after independent origins of fission a considerable degree of parallel evolution occurred in each lineage. I propose that very similar regenerative capabilities, body plans and functional constraints in stem pristinines and naidines have channeled in parallel the evolution of paratomic fission, resulting in complex traits that are highly alike, yet present some fundamental differences.

Introduction

Agametic reproduction by fission or budding is a very widespread strategy for clonal propagation and resource exploitation (Vorontsova and Liosner, 1960; Hughes, 1987). Among Metazoa, it is frequent both in colonial and solitary taxa, and while in some groups it is shared by most of its members, in others it shows a more "peppered" distribution (Vorontsova and Liosner, 1960; Hughes, 1987; Sköld et al., 2009). In most cases, however, agametically reproductive species are clearly phylogenetically nested within clades displaying strong regenerative abilities (*see Chapter 1*). This pattern led to the hypothesis that evolution of agametic reproduction is facilitated by pre-existing regenerative potential (Morgan, 1901; Vorontsova and Liosner, 1960; Ghiselin, 1987; Zattara and Bely, 2011), since it reduces the problem of generating a novel developmental trajectory to simply re-deploying regenerative

processes in a novel context by swapping an external cue (injury) for an internal cue (e.g., physiological status).

Naid annelid worms included in the family Naididae *sensu* Erseus *et al.* (2008) present an interesting case study for the evolution of agametic reproduction from regenerative abilities. Fissioning naids are freshwater worms characterized by the ubiquitous presence of agametic reproduction by fission. The most common fission type is paratomy, in which new anterior and posterior ends develop within a single mid-body segment and then separate; however, architomy, in which an individual breaks in two or more pieces and develops the missing ends, is also present in the family (Fig. 4.1A). Traditionally, fissioning naid worms were grouped together in the family Naididae and thought to be closely related to the sludge worm family, Tubificidae, in which asexual reproduction is very rare (Brinkhurst and Jamieson, 1971). More recently, molecular phylogenetic studies have shown that naids are polyphyletic and nested along with tubificids and a few other families (Erséus et al., 2002, 2010; Sjolin et al., 2005; Envall et al., 2006); since Naididae was the first family to be formally described, the ICZN codes rule that all species belong now to this family (Erséus et al., 2008). Current phylogenetic consensus places all fissioning naid species in one of two clades, Pristininae and Naidinae, which are separated by a paraphyletic assembly of species without any known mode of asexual reproduction (Fig. 4.1B). Given this new phylogenetic context, paratomy most likely originated twice, once at the base of each clade (Erséus et al., 2002; Bely and Wray, 2004; Envall et al., 2006; Zattara and Bely, 2011).

Is it possible for a trait as complex as making a complete new anterior and posterior end to independently evolve in parallel? Currently available descriptions suggest that paratomic fission is similar between the two clades (Bourne, 1891; Galloway, 1899; Dehorne, 1916; Zattara and Bely, 2011). However, a more in-depth analysis of apparently equal developmental trajectories can reveal significant developmental and evolutionary differences; for example, a detailed study of the naid *Pristina leidyi* (Pristininae) has shown that paratomic fission is distinct from regeneration, despite extensive common processes due to origin of the former by co-option of the later (Zattara and Bely, 2011). Using this same approach, in this paper I extend the analysis of developmental trajectories of regeneration and fission to a second representative of Pristininae and seven species belonging to the Naidinae, plus the outgroup species *Lumbriculus variegatus* (Lumbriculidae). These species represent most main clades within Pristininae and Naidinae and are readily reared in laboratory conditions, making them ideal for comparative studies. The outgroup was selected because it has comparable regeneration ability and asexual reproduction, yet it is phylogenetically distant enough to provide a broader perspective.

My aim in this paper is to determine how regeneration and fission vary between species, and which developmental features of fission have evolved convergently after their respective origins in Pristininae and Naidinae. I placed special emphasis in nervous system development for two main reasons: first, neural structures are readily visualized using immunohistochemical staining in whole mounts; furthermore, recent descriptions of the nervous system of several naids are available (Zattara & Bely, *in prep.*). Second, studies in *P. leidyi* have suggested that

neural features show more fission-specific variability (Zattara and Bely, 2011). If such traits have more freedom to evolve, I expect they will show higher variability across Pristininae, Naidinae and Lumbriculidae.

Materials and Methods

Animal samples

I studied two species belonging to Pristininae (*Pristina leidyi* and *P. aequiseta*), seven species belonging to Naidinae (*Chaetogaster diaphanus, Paranais litoralis, Allonais paraguayensis, Dero digitata, Dero (Aulophorus) furcata, Stylaria lacustris and Nais elinguis*) and one species of the distantly related family Lumbriculidae (*Lumbriculus variegatus*). All species were cultured under conditions described elsewhere (Bely and Sikes, 2010).

Regeneration and fission experiments

For regeneration studies, worms were anesthetized with ice cold spring water and the anterior or posterior third of the removed with a scalpel, and allowed to regenerate for 1 to 5 days at 25°C. Daily samples were separated, relaxed and fixed as described below. Fission was usually induced by moving worms into new cultures and feeding them. In all paratomic species, fission zones could be seen as whitish, thickened rings around a mid-body segment within a few days. *Lumbriculus* and *Allonais* reproduced instead by architomic fission, in which they split in two pieces, each piece regrowing the missing head or tail. I collected worms with fission zones at different stages, and relaxed and fixed as described below.

Relaxation, fixation and immunocytochemistry

Prior to fixation, the worms were relaxed 10 min with either cold (4°C) 10mM $MgCl_2$/5mM NaCl/1mM KCl/8% ethanol solution (pristinines), or with 0.1% chloretone in spring water (naidines and lumbriculids). After relaxation, animals were fixed with 4% formaldehyde in 0.75x PBS, and rinsed in 1x PBS. After permeabilization with 0.1% Triton-X in PBS (PBTx) and blocking for 1h in 10% normal goat serum (NGS) in PBTx, they were incubated 15–20 h at 4°C with mouse anti-acetylated-α-tubulin monoclonal antibody (T6793, Sigma, St. Louis, MO, USA) and rabbit anti-serotonin polyclonal antibodies (S5545, Sigma), both diluted 1:100 in blocking solution. Specimens were then washed with PBTx and incubated 15–20 h at 4C in blocking solution containing Alexa-Fluor-647-conjugated goat anti-mouse IgG(H+L) antibodies (1:200, A21236, Invitrogen, Carlsbad, CA, USA) and Cy3-conjugated goat anti-rabbit IgG antibodies (1:200, 111-166-003, Jackson Immunoresearch ,West Grove, PA, USA), 60 nM Alexa-Fluor-488 phalloidin (A12379, Invitrogen) and 10μg/mL DAPI. After washing with PBTx and PBS, specimens were transferred through a graded glycerol series and mounted in 25 mM *n*-propyl-gallate (02370 Sigma) in 75% glycerol/25% PBS.

Imaging and image analysis

Mounted animals were imaged under a Leica SP5X confocal laser scanning microscope (Leica, Wetzlar, Germany), using 20x or 40x oil immersion lenses. Z-stacks with steps 0.5-1.0μm were acquired using the Leica LAS AF software, and analysed using ImageJ (Bethesda, MD, USA) (Abramoff et al., 2004) and Zen 2009 LE (Zeiss, Oberkochen, Germany). I imaged all species in lateral and ventral views.

Additional specimens were examined in a Zeiss Axioplan 2 epifluorescence microscope.

Results

I examined developmental trajectories during regeneration and fission of ten annelid species: two Pristininae species (*Pristina leidyi* and *P. aequiseta*), seven Naidinae species (*Chaetogaster diaphanus, Paranais litoralis, Allonais paraguayensis, Dero digitata, Dero (Aulophorus) furcata, Stylaria lacustris* and *Nais elinguis*), and one outgroup species, *Lumbriculus variegatus*. Overall, both types of developmental trajectories were very similar to the ones described elsewhere for *Pristina leidyi* (*see Chapter 2*); thus, I present here the main variations resulting from comparative observations, and refer the reader to the aforementioned description for general details.

Regeneration

The developmental trajectory of regeneration was similar for all species, and can be divided in three phases: wound healing, blastema formation and blastema differentiation. Upon amputation, the wound is closed by muscular contraction and an internal wound plug, and covered by a thin epithelium; 12-24hs later, the blastema, a mass of hyaline tissue, starts growing at the stump; eventually, the blastema becomes fractioned in portions that differentiate into the tissues and organs of the regenerated end. In posterior regeneration, the anal pore is reopened before or during blastema formation; in contrast, in anterior regeneration the mouth reopens later, during blastema differentiation.

All ten species are capable of regenerating a posterior end formed by a pygidial cap, posterior growth zone and a variable number of segments, but species vary in their ability to regenerate an anterior end. Both pristinine species make a new head composed by a non-segmental cap (prostomium and peristomium) and 4 segments bearing ventral and dorsal chaetal bundles. Five out of 7 naidine species also make a new head comprised by non-segmental cap and 4 segments bearing ventral chaetae, but with no dorsal chaetal bundles, except for *Dero furcata*, which develops paired dorsal bundles at segment 4. The naidines *Chaetogaster diaphanus* and *Paranais litoralis* failed to regenerate an anterior structure. The outgroup *Lumbriculus* makes a new head formed by non-segmental cap and 7 chaetae-bearing segments. Except for smaller size and less pigmentation, regenerated ends are similar to the original ones in structure and chaetal bundle distribution.

In pristinines and naidines, anterior regeneration is associated with a loss of gut ciliation that extends backwards from half to three or more segments (Fig.4.S1). In *Lumbriculus*, this loss of gut cilia was not observed. No loss of gut cilia was seen during posterior regeneration in any species.

Anterior body wall muscle regeneration is similar in all species (Fig.4.S1): starting at the blastema formation phase, longitudinal muscle fibers extend from edge of the stump over the blastema, eventually reaching the anterior tip and crisscrossing to form the prostomial musculature; circular muscle forms seemingly *de novo* over the longitudinal fibers. Posterior body wall muscle regeneration follows a similar sequence, except that musculature at the pygidial cap forms before longitudinal fibers have extended all the way back from the stump. This difference between anterior and

posterior muscle regeneration was observed for all pristinine and naidine species, but was more obvious in naidines with larger pygidia like *Dero* sp. and *Stylaria lacustris*. The outgroup *Lumbriculus* shows a similar developmental sequence.

Regeneration of the peripheral nervous system was similar across all species (Fig.4.2). All species have a number of segmental peripheral nerves that branch laterally from the ventral nerve cord ganglia. Starting at the blastema formation phase, a number of tubulin-immunoreactive (TIR) axonal tracts originate perpendicularly from nearest peripheral nerves and extend towards the wound site and over the blastema (Fig. 4.2A). This TIR tract outgrowth was observed in all species, during both anterior and posterior regeneration.

Regeneration of the anterior central nervous system involves formation of a new stretch of ventral nerve cord, circumenteric connectives and a cerebral ganglion (Fig. 4.2B-C). Starting at the wound healing phase, sets of serotonin-immunoreactive (SIR) nerves grow forward from the cut end of the old ventral cord. Upon reaching the anteroventral edge of the newly forming blastema, they deviate dorsally, becoming the primordial neuropil of the new connectives, and connect dorsally into a loop that becomes the transverse cerebral commisure. During blastema differentiation, this neuropil becomes denser by addition of SIR and TIR nerves, and the ventral nerve cord and cerebral ganglia form around it. A number of SIR cell bodies develop in the new cord ganglia, ventral to the neuropil, and in the cerebral ganglion. No obvious difference between species was observed along this developmental process.

Fission

Both pristinine species and 6 naidine species reproduce asexually by paratomy. Paratomy is noticeable by the presence of a fission zone within a single segment, and can be divided in three phases: fission mass formation, fission mass differentiation and splitting. Early fission mass formation is detected as a ring of epidermis thickens around a transverse groove delineating the fission plane; later, the fission mass, a hyaline mass of cell similar to blastemal tissue, forms underneath the thickened region; during fission mass differentiation, the fission mass grows and divides in portions that differentiate into tissues and organs of the new anterior and posterior ends. After differentiation, the newly formed ends separate through the fission plane.

One naidine species, *Allonais paraguayensis*, and the outgroup species, *Lumbriculus variegatus*, reproduced instead by architomy, spontaneously breaking in two pieces and following a sequence similar to the one described above for post-amputation regeneration.

The new posterior and anterior ends comprise a non-segmental cap plus a variable number of segments. The number of posterior segments made during fission varies both between and within species, and it was not further analyzed. In contrast, the number of anterior segments varies between species but is fixed within a species. Both pristinine species make 6 segments bearing ventral and dorsal chaetal bundles; all naidine species make 4 segments, except *Paranais litoralis,* that makes 3 segments. New anterior segments in 5 naidine species have ventral but not dorsal chaetal bundles; *Dero furcata* develops paired dorsal bundles at segment 4, while

Chaetogaster diaphanus makes ventral chaetae only at segments 1 and 4, and no dorsal chaetae at all. The outgroup *Lumbriculus variegatus* makes 7 anterior segments, all bearing ventral and dorsal chaetae. Except for smaller size and less pigmentation, ends developed within a fission zone are similar to the original ones in structure and chaetal bundle distribution.

In all paratomic species, no loss of gut cilia was observed at or near the fission zone during paratomy. In contrast, loss of gut cilia similar to that seen during anterior regeneration was observed during architomy in the naidine *Allonais paraguayensis*. In the outgroup *Lumbriculus variegatus*, gut ciliation was not lost during architomy; thus, architomy resembles regeneration also in *Lumbriculus*.

During fission in both pristinine species and the six paratomic naidinae species, body wall longitudinal musculature remains continuous across the fission zone. During fission mass formation, longitudinal body wall muscle bands are pushed inwards by the fission furrow and thickening epidermis; during fission mass differentiation, a number of longitudinal muscle fibers are re-directed to the developing prostomium and pygidium, and the density of fibers that cross the fission plane is gradually reduced, so a "break line" is eventually formed. While a difference between muscle fibers was not evident from microscopy data, during manipulation of fixed specimens I noticed that both pristinine species were less prone to break at the fission plane than any of the naidine species at a comparable fission stage.

Body wall muscle development during architomy in the naidine *Allonais paraguayensis* and the outgroup *Lumbriculus variegatus* was similar to that described for regeneration.

Development of the nervous system during fission showed interesting patterns, as did the spatial relation between fission zones and the pre-existing peripheral nerves (Fig. 4.3). In both pristinine species and the six paratomic naidinae species, the fission plane is located between rather than within consecutive ventral nerve cord ganglia. The fission zone's anterior boundary is level with the last peripheral nerve of the preceding ventral nerve cord ganglion, while the posterior boundary is level with the first peripheral nerve of the following ganglion (Fig. 4.3A). Architomic species (*Allonais* and *Lumbriculus*) split before showing any fission mass; however, they always break apart at a stereotypical position located between two consecutive VNC ganglia and then form anterior and posterior fission masses. The proximal boundaries of these post-separation fission masses are level respectively with the last segmental nerve of the preceding ganglion and with the first nerve of the following ganglion (Fig 4.4). In other words, despite the swap in the order of fission mass formation and splitting between paratomy and architomy, the fission plane and the fission mass forms at the same position relative to the nervous system in all 10 species.

In both pristinine species and the six paratomic naidinae species, tubulin immunoreactive (TIR) axonal tracts originating at the peripheral nerves bounding the fission zone grow towards the fission plane (Fig. 4.3A). This TIR tract outgrowth is similar to the one seen during regeneration, although noticeably less dense; in contrast to regeneration, no TIR tracts originate from beyond the bounding nerves. In the architomic pristinine *Allonais paraguayensis* and the outgroup *Lumbriculus variegatus*, TIR tract growth after splitting originates not only from the nearest nerve,

but from several others (Fig. 4.4); tract density is noticeably high in *Allonais*. Interestingly, the fission plane in *Lumbriculus* coincided with the location of a serotonin immunoreactive epidermal ring; this structure was not seen at any of the other species.

Development of the central nervous system during paratomic fission presented the most striking difference to regeneration, and also showed marked differences between pristinine and naidine species. In all species, the portion of ventral nerve cord neuropil within a fission zone stretches but maintains continuity across the fission plane throughout the whole process and until physical separation (Fig. 4.3B-C). In both pristinine species, the ventral nerve cord of the developing head and tail forms *de novo* by serotonin-immunoreactive (SIR) axonal outgrowths that originate from the adjacent ganglia and grow dorsal to the old cord towards the fission plane (Fig. 4.3B, upper two panels). In the developing head, the new tracts deviate dorsally before reaching the plane, forming the circumenteric connectives, and reaching the cerebral ganglion primordia. The new cord ganglia differentiate from fission cell masses ventral to the new neuropil and dorsal to the old one (Fig. 4.3C, upper two panels). In contrast, in all paratomic naidine species, no new ventral nerve cord tracts are made; the circumenteric connectives grow out of the old neuropil as perpendicular lateral extensions originating right behind the fission plane, deviate dorsally and reach the cerebral ganglion primordia (Fig. 4.3B, lower two panels). The new cord ganglia differentiate ventral to the old neuropil and attach directly to it (Fig. 4.3C, lower two panels). Thus, pristinine and naidine species present two clearly different modes of central nervous system development during fission, which I denominate Type I and II

respectively (Fig. 4.5). I did not find in any species a developmental mode intermediate between these two types, and there was no variation in this feature within either Pristininae or Naidinae.

Discussion

Despite considerable variation from group to group, most annelids seem to possess a shared basal suite of regenerative abilities (*see Chapter 1*), and it has been proposed that fission can evolve by co-option of these abilities (Morgan, 1901; Vorontsova and Liosner, 1960; Ghiselin, 1987; Zattara and Bely, 2011). This idea has been tested in the pristinine *Pristina leidyi* by a detailed analysis of developmental trajectories during regeneration and paratomic fission. Since paratomic fission is likely to have originated independently in lineages leading to Pristininae and Naidinae species (Erséus et al., 2002, 2010; Bely and Wray, 2004; Envall et al., 2006; Zattara and Bely, 2011), I made a comparative study of regeneration and fission in another pristinine species, seven naidine species and one distantly related outgroup species, describing the main similarities and differences to gain insight in how these developmental trajectories have evolved.

Regeneration trajectories track adult morphologies

Regeneration developmental trajectories were mostly similar across all pristininae, naidinae and outgroup species. Except for the retention of gut ciliation in the outgroup, differences relate directly to morphological characteristics of each species: for example, while pristinine species have dorsal chaetal bundles on all segments, most naidine species lack dorsal chaetae on the four anterior-most

segments, except for *Dero furcata*, where only three segments lack them, and *Chaetogaster diaphanus*, which has no dorsal chaetae at all. While not unexpected, this observation highlights the fact that regeneration trajectories track evolutionary changes in embryonic development leading to changes in adult morphology. Yet regeneration and embryogenesis are considered two separate developmental trajectories (Hessling and Westheide, 1999; Myohara, 2004; Zattara and Bely, 2011). How are they kept synchronized? It can be proposed that this occurs because of the extensive pleiotropy caused by re-deployment during regeneration of embryogenetic developmental modules. In this "modular" scenario, changes underlying morphological evolution occur at the module level, and thus affect all trajectories calling upon modified modules. Alternatively, the cause could be a "homeostasis" scenario, where regeneration trajectories are an extension of a homeostatic process returning a perturbed system to its stable morphological equilibrium established during embryogenesis. More research on the developmental architecture of regeneration, fission and embryogenesis trajectories would be needed to tell these scenarios apart.

Blastemal innervation from peripheral nerves is a novel trait of clitellate regeneration

Outgrowth of axons from proximal peripheral nerves was seen during regeneration in all species. Since a similar phenomenon was also described in enchytraeid species (Müller, 2004; Myohara, 2004), my observations confirm it as a regeneration feature common to clitellates annelids but not seen during polychaete regeneration (Müller, 2004), and supports its proposed use as an autopomorphic trait

of clitellate regeneration (Zattara and Bely, 2011). Nerve dependence is a common feature of regeneration in many systems and has been suggested to promote blastema formation through release of growth factors or other mitogens (Brockes and Kumar, 2008). If this pattern of temporary innervation is indeed a novel feature of clitellate regeneration, then it could be hypothesized that it evolved as a mechanism to enhance or accelerate the epimorphic component of regeneration. This idea could be formally tested by quantifying the correlation between innervation density and regeneration rate across species, or by experimentally modulating axonal growth within a single species and measuring the resulting regenerative response. While elucidating the role of temporary innervation will require further research, my current observations support its use as a useful diagnostic trait of clitellate-specific regeneration trajectories.

Architomic fission trajectories are most similar to regeneration

Analysis of fission in the naidine *Allonais paraguayensis* and the outgroup *Lumbriculus variegatus* supports a closer relationship of architomy to regeneration than to paratomy. This is evidenced not only by the lack of obvious differences between the two, but by the fact that certain traits of paratomy, like retention of gut ciliation, were not seen in *Allonais*. Gut ciliation was not lost in *Lumbriculus*, but this is also the case during regeneration in this species. More similarity between regeneration and architomy is not unexpected, considering that except for the initial steps (external trauma versus internally induced autotomy) most challenges are similar for both trajectories. Furthermore, architomy has been proposed as a first step in the evolution of fission (Zattara and Bely, 2011), and is the only fission mode

present in other groups of clitellates like enchytraeids, tubificines and lumbriculids (*see Chapter 1*). However, none of the most recent phylogenetic scenarios place *Allonais* as a basal clade within the Naidinae (Bely and Sikes, 2010; Erséus et al., 2010). Instead, architomy in *Allonais* must be interpreted either as a reversion from paratomy (if the step-wise scenario holds true) or a re-evolution of architomy. Besides *Allonais*, a few species of *Dero* are also known to reproduce by architomy (Sperber, 1948), suggesting that *Allonais* does not represent the only shift away from paratomy and that, once their phylogenetic relationships are clear, naidines will offer interesting insights into the evolution of fission modes.

Independent origins of fission exhibit widespread convergent evolution

I found that paratomic fission trajectories in pristinines and naidines were strikingly similar: formation of fission masses, growth of axonal tracts towards the fission plane, retention of gut ciliation and gradual re-routing and separation of longitudinal muscle fibers were seen in all cases. Why have these two independently gained trajectories evolved so many convergent traits? Convergence of some traits is clearly due to co-option of the regeneration trajectory: fission mass cells are most likely homologous to blastemal cells, while axonal growth towards the fission plane is a less intense manifestation of the blastemal innervation seen during regeneration (Zattara and Bely, 2011). In contrast, other shared traits like retention of gut cilia and longitudinal muscle bands are less related to regeneration, but reflect parallel adaptations of the paratomic trajectory to cope with the common problem of maintaining body functionality across a developing fission zone. These observations suggest that a considerable degree of parallel evolution is expected when lineages

independently evolve traits co-opting the same preexisting developmental components and facing similar challenges.

A more unexpected finding is that clitellates have independently placed fission planes in the same interganglionar position. The fission plane is located between the last segmental nerve of the preceding ventral nerve cord ganglion and the first nerve of the following one; this holds true for all pristinine, naidine and outgroup species studied, irrespective of their fission mode or fission origin. Convergence in placement of the fission plane is a striking finding, especially when considering that mesodermal structures that usually define segmental compartment boundaries, like septa, vary in their position relative to the segmental units of the nervous system (Zattara & Bely, *in prep.*). Furthermore, in the distantly related *Enchytraeus japonensis*, representing another independent gain of fission, fragmentation also occurs along a stereotypical position that is located between nerves of two consecutive ganglia (Yoshida-Noro et al., 2000). Is this convergence due to co-option of a feature that is common to all clitellates? Both *Lumbriculus* and *Enchytraeus* have autotomy reflexes by which they split at a particular "autotomy plane" within a segment (Lesiuk and Drewes, 1999; Yoshida-Noro et al., 2000); I have found a serotonin immunoreactive ring at that autotomy plane in *Lumbriculus*. *E. japonicus* also presents post-amputational corrective autotomy, so that if cut elsewhere along the segment, it will pinch off at the stereotypical location closest to the wound and discard the distal tissue portion (Kawamoto et al., 2005). However, no autotomy reflex has been described so far for any of the pristinine or naidine species in this study, including *Allonais*. Furthermore, I have not found any morphological or

immunochemical markers of an autotomy plane in any of them, and amputation experiments in several species have shown no evidence of corrective autotomy taking place (A.E. Bely and E.E.Z., unpublished data). Thus, convergence in the position of fission planes can not be explained by a common pre-existing stereotypical autotomy mechanism.

Why then is the fission plane always located between consecutive ventral nerve cord ganglia? One possibility is the existence of a strong constraint preventing the animals from spontaneously breaking apart a neural ganglion. Another reason could be the presence of morphological feature at that position that can be readily co-opted as a fission plane "organizer"; a distinctive nerve fiber attached to peculiar ventral cells has been described at the future fission plane in the naidine *Nais pseudoobtusa* (Reyners, 1969), and a distinctive serotonergic ring can be seen in *Lumbriculus*. Yet another hypothesis is that even in the absence of corrective autotomy, the existence of a fixed position from which regeneration is effectively initiated strongly channels the placement of the fission zone every time fission evolves. If any of the above explanations holds true, then independent placement of fission planes in the same location would represent a good example of the role of pre-existing traits in convergent evolution.

Central nervous system development during paratomy is a novel challenge solved in different ways by pristinines and naidines

Building a new central nervous system while maintaining neural integration across a developing fission zone is a problem unique to paratomy with no parallel during regeneration or architomy. Worms cope with this challenge by deploying one

of two different solutions (Fig. 4.5): in Type I paratomy, a new ventral nerve cord along with circumenteric connectives forms anew dorsal to the old one from the adjacent ganglion; in Type II paratomy, the neuropil of the old cord is "recycled" and the connectives form anew from it. Type I development had been recently described for *Pristina leidyi* (Zattara and Bely, 2011), and now for *Pristina aequiseta*, both pristinine species. Type II corresponds to paratomic central nervous system development described for the naidines *Dero vaga* (Galloway, 1899) and *Chaetogaster diaphanus* (Dehorne, 1916); this paper has shown it is also the type found in the naidine species *Paranais litoralis, Dero digitata, Dero (Aulophorus) furcata, Stylaria lacustris* and *Nais elinguis*. I found no intermediate or alternative modes of making a new central nervous system among the species I studied. While both types are of necessity adequate enough to allow successful completion on asexual reproduction, they are unlikely to be functionally identical: the presence of a complete new cord in Type I fission minimizes the potential for functional interference with the old cord; on Type II fission, however, new segmental ganglia develop and connect to it during the process. Nerve impulse conduction is slightly slowed down and dampened after crossing a fission zone in *Dero digitata,* a Type II species (Drewes and Fourtner, 1991).No other neurophysiological studies have been conducted in any other paratomic naid species; I expect future comparative studies to uncover functional differences between these two fission types.

Fission Type I is found only in pristinine species; conversely, fission Type II is only found in naidine species (Fig. 4.6). Thus, each type corresponds to one independent origin of paratomy. Considering the large degree of evolutionary

convergence between pristinine and naidine paratomic fission trajectories described above, the stark difference between Types I and II is outstanding. Why might the reasons invoked to explain widespread parallelism not apply in this case? A likely explanation is that making a new CNS during paratomy is a novel problem that can not be solved by direct redeployment of a pre-existing regenerative process, nor is strongly constrained into a single possible solution. CNS development during regeneration requires the presence of an amputated nerve cord; however, autonomous section of the nerve cord at the onset of paratomy has never been reported in any annelid. Thus, co-option of regeneration does not impose a particular location for the new cord to form from. Furthermore, in contrast to other unique traits of paratomy like gut ciliation and longitudinal muscle band continuity, how the new CNS is made does not seem to be strongly constrained by the need to maintain functional integrity across the developing worm. In other words, a less restrictive context makes variation in CNS development strategies between independent paratomy trajectories more likely.

Developmental channeling as a predictive framework

Through comparative analysis of developmental trajectories of regeneration and fission presented in this work, I have shown that despite their independent origin, paratomic trajectories in pristinine and naidine annelids show remarkable convergence, yet present some notable differences. These data suggest that extreme cases of parallel evolution can be explained in part by recruitment of the same old developmental processes of regeneration, and in part by the constraints imposed by the common challenge of maintaining integrity across a fission zone. On the other

hand, I have found a clear-cut difference between the two groups in how each reconstructs the central nervous system, likely due to lessened constraints, and that agrees with the hypothesis that neural features are more likely to show differences between regeneration and fission trajectories.

I propose that after independent gains of fission in stem pristinines and naidines, very similar regenerative capabilities, body plans and potential constraints have channeled in parallel their respective evolutionary trajectories, resulting in complex traits that are highly alike. This supports the idea that pre-existing developmental capabilities can markedly bias evolutionary trajectories, and that presence of strong developmental channeling can be used as a predictive framework capable of generating testable hypotheses. Given the wide phylogenetic distribution of regeneration and agametic asexual reproduction, we should have plenty of opportunities to explore the evolutionary role of developmental channeling and test its predictions.

Chapter 4 Figures

Figure 4.1: Post-embryonic developmental trajectories types and phylogenetic distribution in clitellate annelids.

A) Clitellates present three related developmental trajectories: reparative regeneration (left), architomic fission (centre) and paratomic fission (right). All three imply development of terminal structures: in regeneration, this occurs in response to an external event resulting in transverse amputation or autotomy; in contrast, both types of fission result from an internal stimulus. During architomy, the animal splits first and then re-develops the missing ends; in paratomy, development precedes the physical separation of daughter worms. The dark and light color bars mark new posterior and anterior tissues respectively (green for regeneration, blue for fission). B) Phylogenetic relationships between the main clitellate clades, and distribution of regeneration (green squares) and fission (blue squares). A half filled square indicates the trait is present only in a few members of the group.

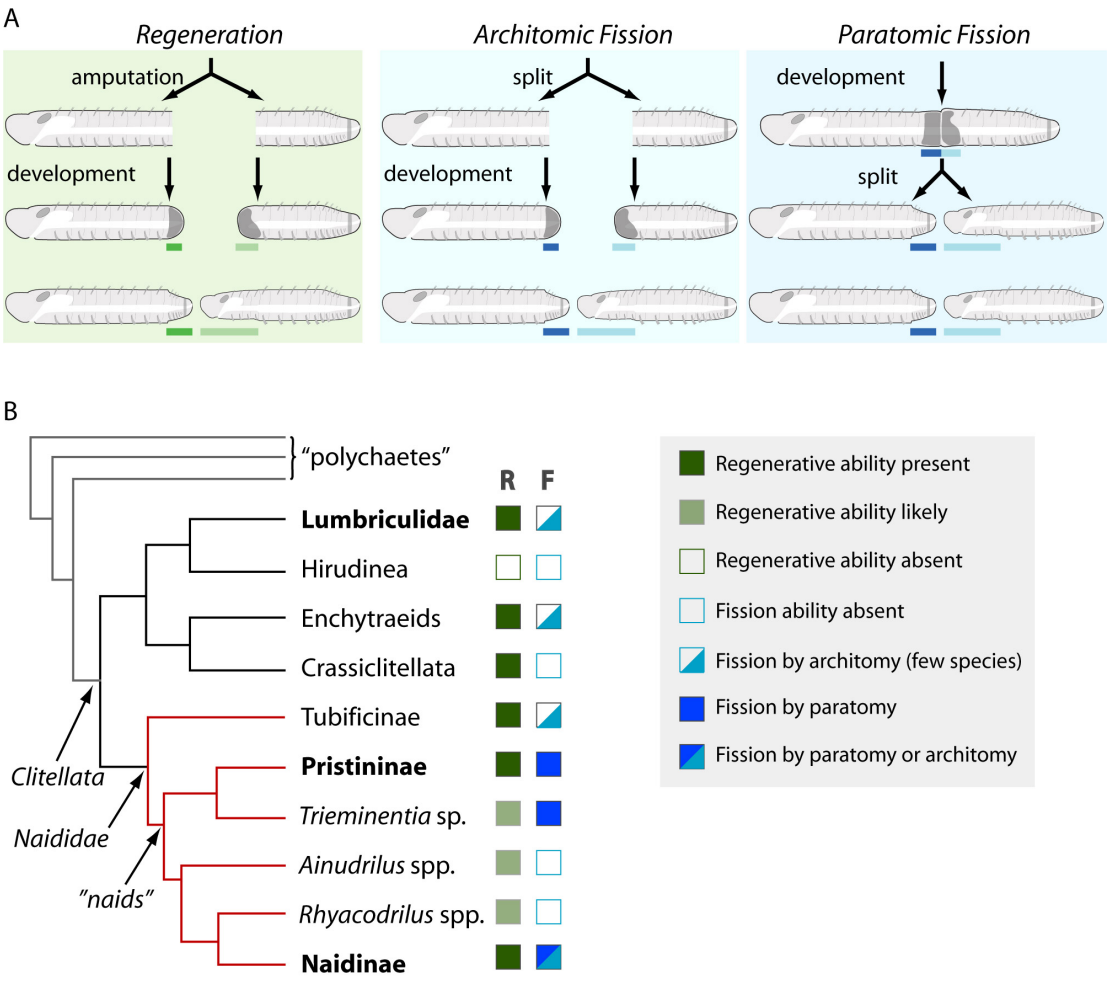
A
Regeneration
amputation
development
Architomic Fission
split
development
Paratomic Fission
development
split
B
"polychaetes"
R F
Lumbriculidae
Hirudinea
Enchytraeids
Crassiclitellata
Tubificinae
Pristininae
Trieminentia sp.
Ainudrilus spp.
Rhyacodrilus spp.
Naidinae
Clitellata
Naididae
"naids"
Regenerative ability present
Regenerative ability likely
Regenerative ability absent
Fission ability absent
Fission by architomy (few species)
Fission by paratomy
Fission by paratomy or architomy

Figure 4.1

Figure 4.2: Anterior nervous system development during anterior regeneration in Pristininae and Naidinae.

Anterior is to the left in all panels; the light green bar marks new anterior tissues. A) Peripheral nerves extend perpendicular tracts (open arrowheads point to some examples) over the blastema. Anterior regenerates at the blastema formation phase. Maximum intensity projection of CLSM Z-stacks of acetylated alpha-tubulin immunoreactive axons and nephridial cilia (TIR, green) and a nuclear counterstain (DAPI, blue). B-C) Development of the anterior central nervous system. Anterior regenerates at the blastema formation (B) or blastema differentiation (C) phase. Maximum intensity projection of CLSM Z-stacks of serotonin immunoreactive axons and perykaria (SIR, yellow) and a nuclear counterstain (DAPI, blue). The filled arrowheads indicate the anterior limit of the original ventral nerve cord. np: nephridium; pn: peripheral nerve; cg: cerebral ganglion; cec: circumenteric connective; *: ventral ganglia.

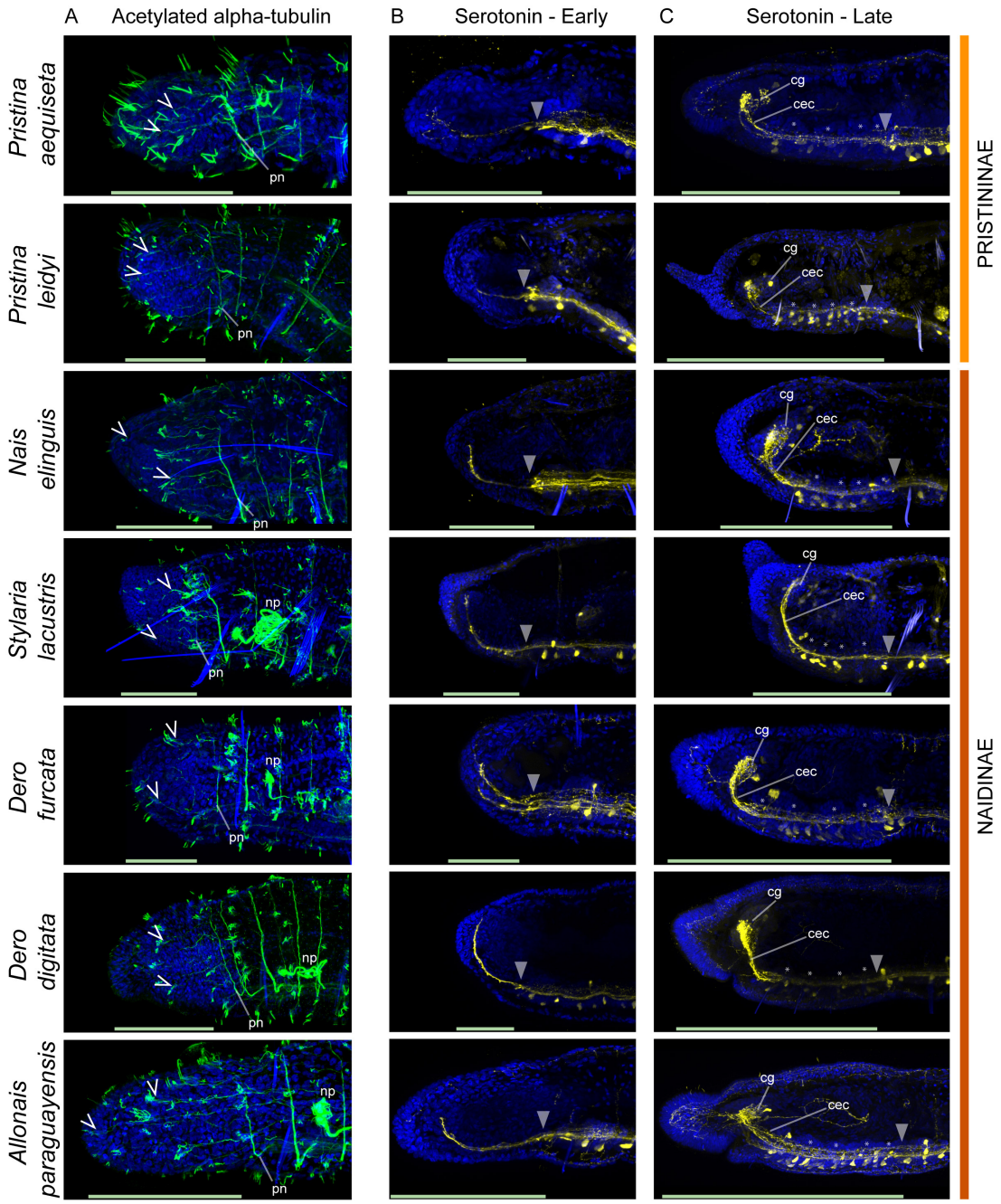
A Acetylated alpha-tubulin
B Serotonin - Early
C Serotonin - Late
Pristina aequiseta
Pristina leidyi
Nais elinguis
Stylaria lacustris
Dero furcata
Dero digitata
Allonais paraguayensis
PRISTININAE
NAIDINAE
cg
cec
pn
np

Figure 4.2

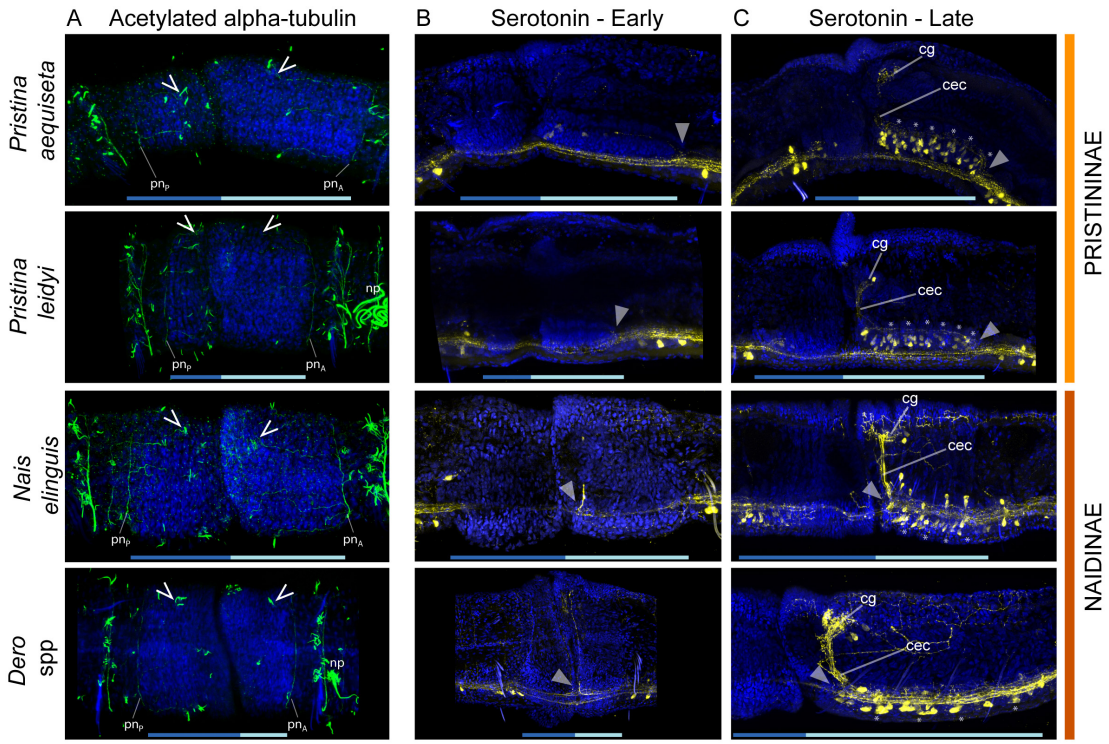

Figure 4.3: Nervous system development during paratomic fission in Pristininae and Naidinae.

Anterior is to the left in all panels; light and dark blue bars mark new posterior and anterior tissues respectively. A) The fission zone is bound by the posterior-most nerve from the preceding ganglion (pn_P) and the anterior-most from the following ganglion (pn_A); each of these nerves sends perpendicular tracts towards the fission plane (open arrowheads point to some examples). Fission zones at early fission mass differentiation. Maximum intensity projection of CLSM Z-stacks of acetylated alpha-tubulin immunoreactive axons and nephridial cilia (TIR, green) and a nuclear counterstain (DAPI, blue). B-C) Development of the new central nervous system occurs by extension from the adjacent ganglia of a new ventral nerve cord dorsal to the old one in Pristininae (top two rows), but by recycling of the old cord in Naidinae. Fission zones at early (B) or late (C) fission mass differentiation. Maximum intensity projection of CLSM Z-stacks of serotonin immunoreactive axons and perykaria (SIR, yellow) and a nuclear counterstain (DAPI, blue). The arrowheads indicate the branching point of the new CNS. Np: nephridium; pn: peripheral nerve; cg: cerebral ganglion; cec: circumenteric connective; *: ventral ganglia.

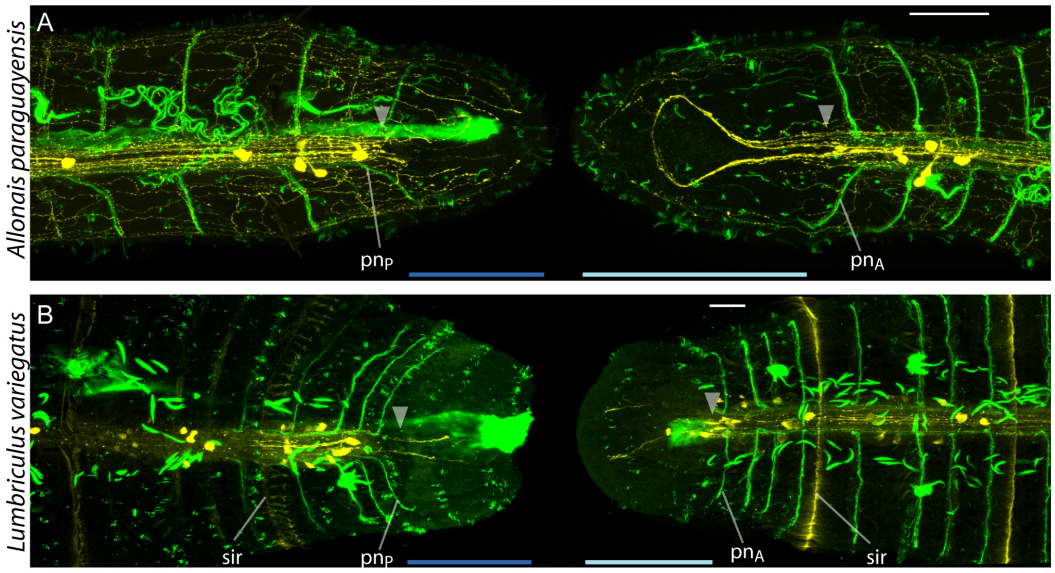

Figure 4.4: Architomic fission "break planes" convergently evolved into the same interganglionar position.

Anterior is to the left in all panels; light and dark blue bars mark new posterior and anterior tissues respectively. Ventral views of anterior and posterior pieces of *Allonais paraguayensis* (A) and *Lumbriculus variegatus* (B) ~1 day after splitting apart; note that the developing fission masses are bound by the posterior-most nerve from the preceding ganglion (pn_P) and the anterior-most from the following ganglion (pn_A). In *Lumbriculus variegatus* the fission plane coincides with the presence of an epidermal serotonin immunoreactive ring (sir). Maximum intensity projection of CLSM Z-stacks of acetylated alpha-tubulin immunoreactive axons, and gut and nephridial cilia (TIR, green), and serotonin immunoreactive axons and perykaria (SIR, yellow). The arrowheads indicate the limits of the original ventral nerve cord.

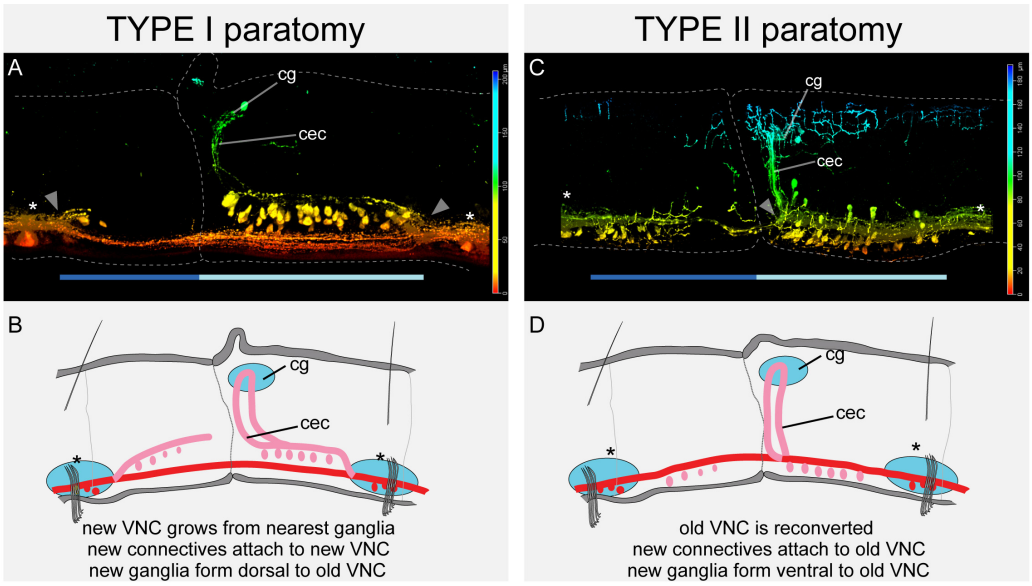

Figure 4.5: Paratomic fission types in naid annelids.

Naid worms present two distinct paratomy types based on how they develop the new central nerve system within a fission zone. A and C are lateral view projections of CLSM Z-stacks of serotonin immunoreactive (SIR) axons and perykaria, color coded from ventral (red) to dorsal (blue) positions. B and D are schematic representations of A and C. Anterior is to the left in all panels; light and dark blue bars mark new posterior and anterior tissues respectively. A-B) Type I paratomy in *Pristina aequiseta.* The new SIR neuropil branches off dorsally (arrowhead) in front of the adjacent ganglion (marked with *); SIR perykarya form ventral to the new cord, but dorsal to the old.start differentiating dorsal to the old cord before the new cord neuropil reaches them. C-D) Type II paratomy in *Dero furcata*. No new nerve cord tracts are made; instead, neuropil forming the circumenteric connectives branch laterally from the cord right behind the fission plane (arrowhead) and extends dorsally to form the cerebral ganglion commisure; SIR perykaria form ventral to the old cord. Cec: circumenteric connectives; cg: cerebral ganglion; *: ventral nerve cord ganglia adjacent to the fission zone.

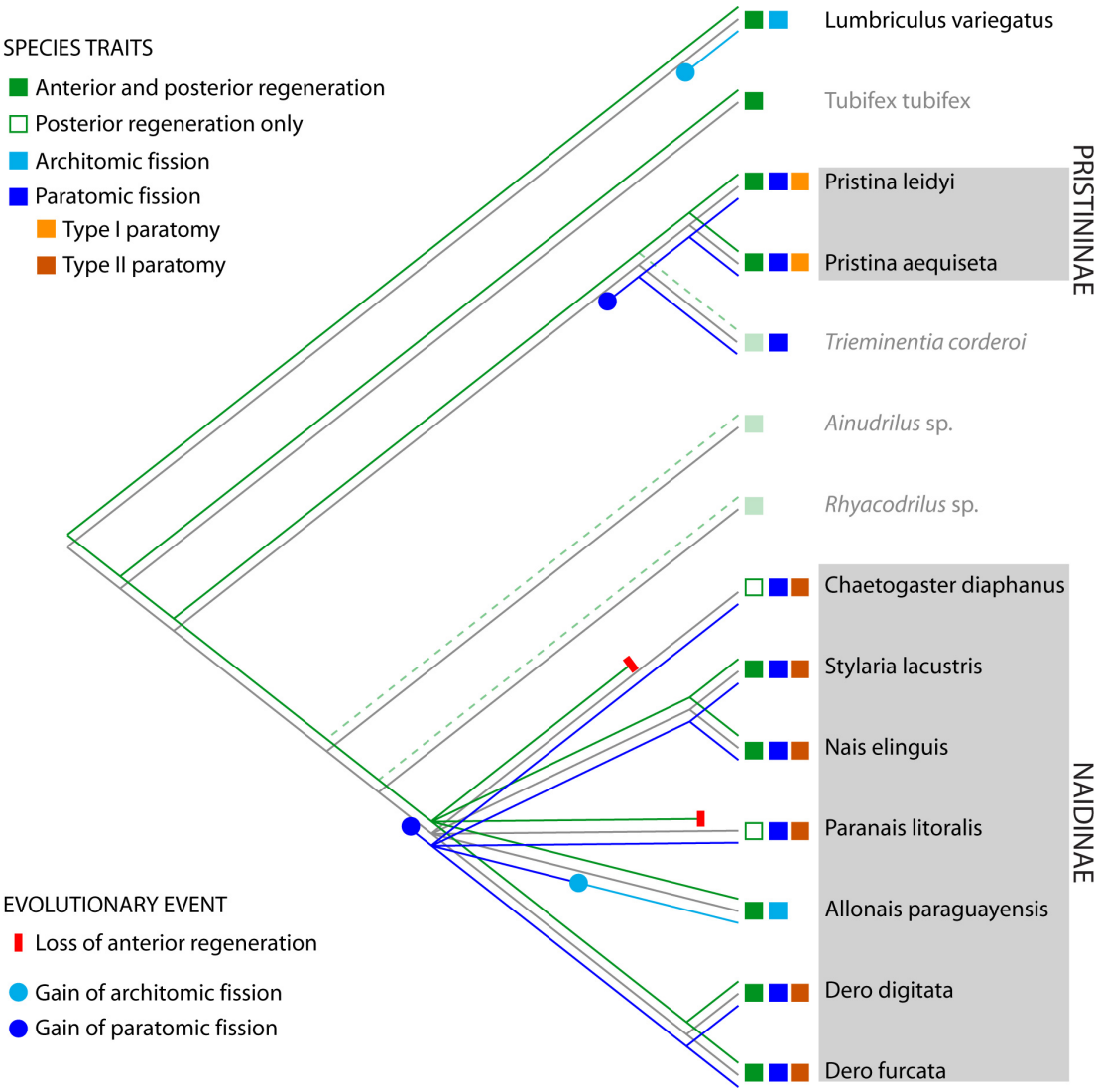

Figure 4.6: Phylogenetic distribution of regeneration and fission in Naididae.

Presence of anterior regeneration (green lines) and architomic and paratomic fission (light and dark blue lines respectively) are mapped on top of the species relationship tree (grey lines). Dashed lines and ghosted boxes indicate inferred but untested regenerative abilities; ghosted names belong to species not studied in this paper. Phylogenetic relationships are presented as consensus of data from Bely and Wray (2004), Envall *et al.* (2006) and Erséus *et al.* (2010). The mapping of character gains and losses shown in this tree is arbitrary and reflects only one example of several possible scenarios.

Figure 4.S1: Supplementary Figures – Regeneration series

Series of anterior and posterior regeneration in the lumbriculid *Lumbriculus variegatus*, the pristinine *Pristina aequiseta*, and the naidines *Stylaria lacustris*, *Nais elinguis*, *Allonais paraguayensis*, *Dero (Aulophorus) furcata* and *Dero digitata*. The two left columns represent color coded projections of CLSM Z-stacks of Alexa-Fluor 488 phalloidin showing muscle development; the two right columns show maximum intensity projection of CLSM Z-stacks of acetylated alpha-tubulin immunoreactive structures (axons of the nervous system, gut ciliation and nephridia, green), serotonin immunoreactive structures (central nervous system axons and perykaria, yellow), and DAPI as a nuclear counterstain (DNA, blue). Rows represent 1 day intervals, starting from 1 day after amputation. The light and dark green bars mark new anterior and posterior tissues respectively

LUMBRICULUS VARIEGATUS

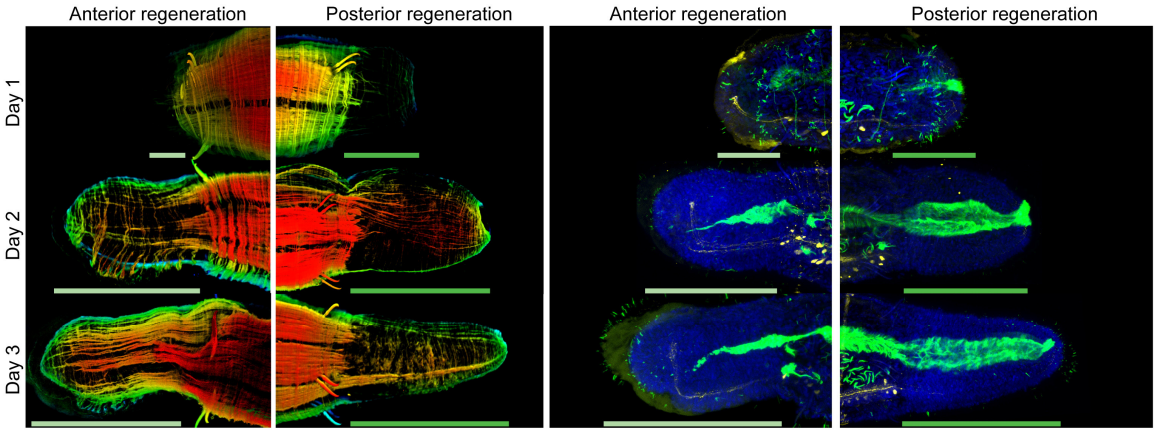

PRISTINA AEQUISETA

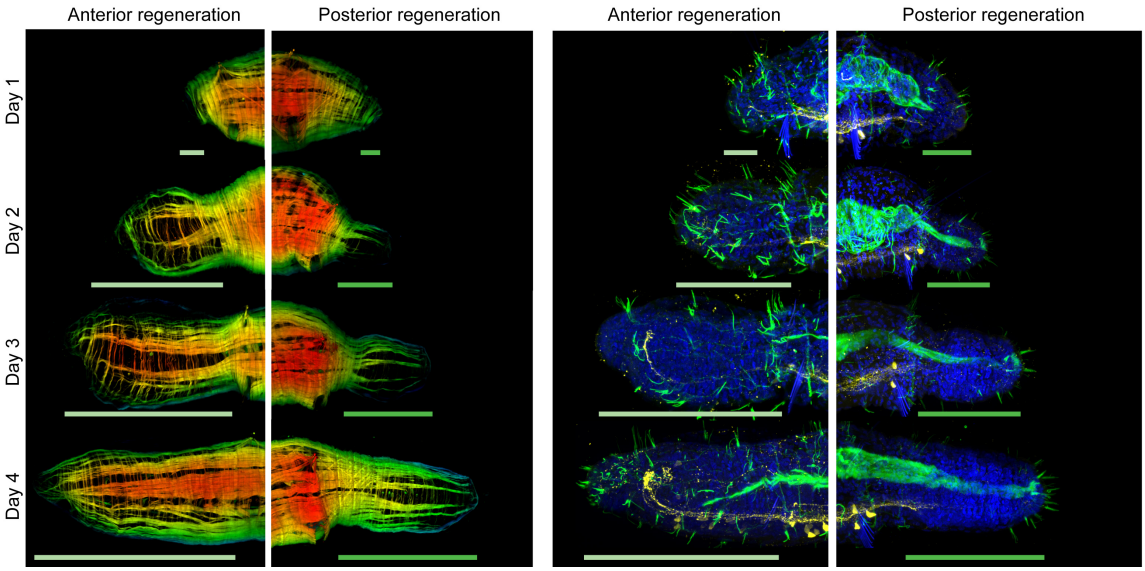

STYLARIA LACUSTRIS

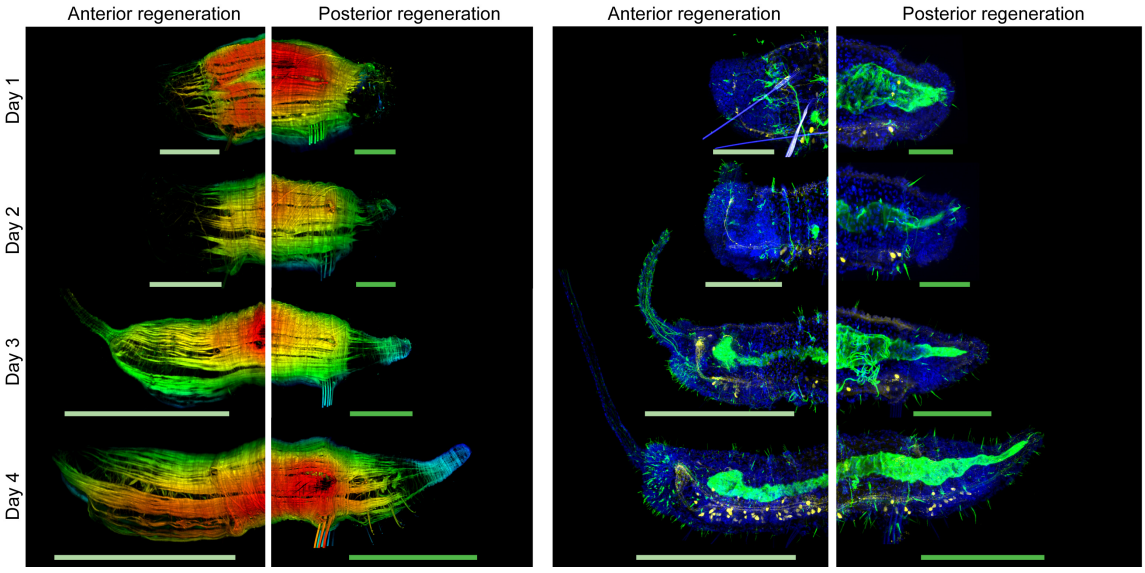

NAIS ELINGUIS

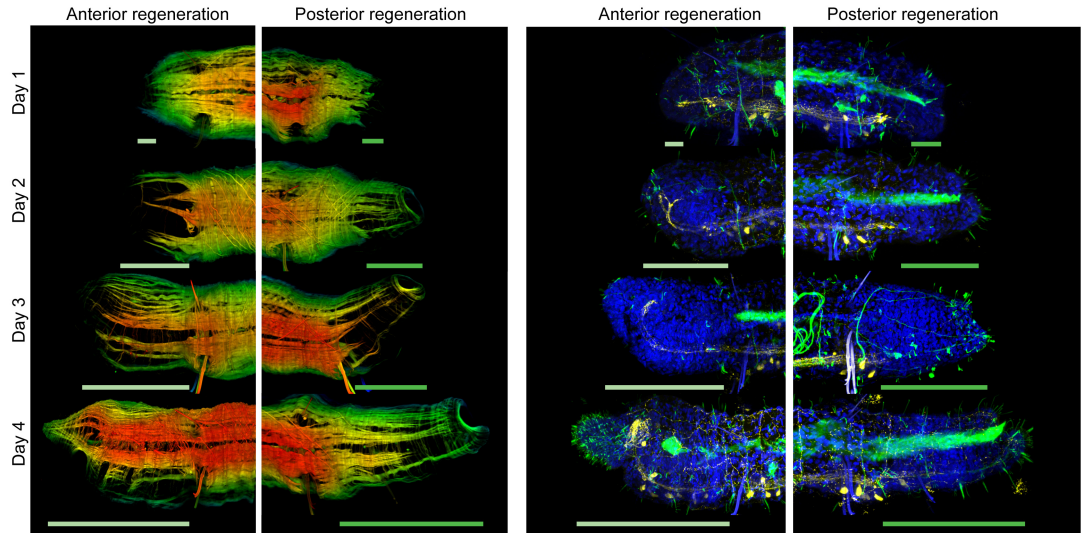

ALLONAIS PARAGUAYENSIS

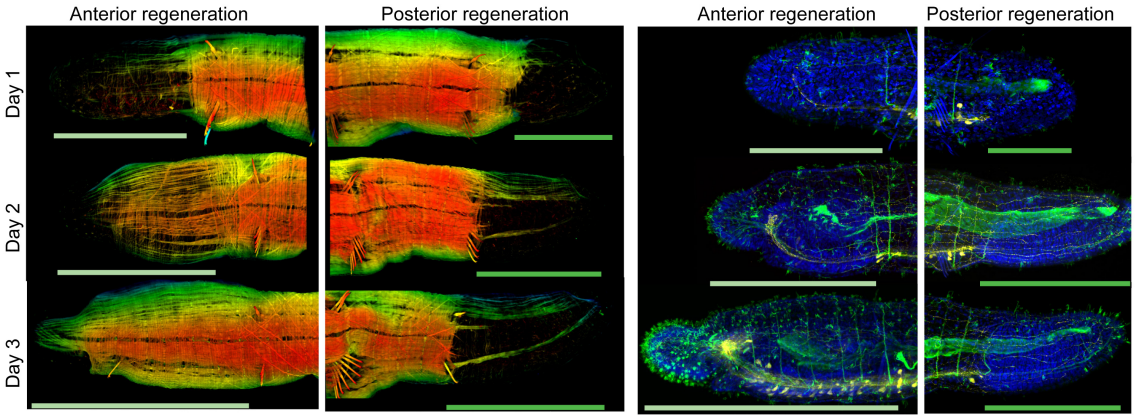

DERO DIGITATA

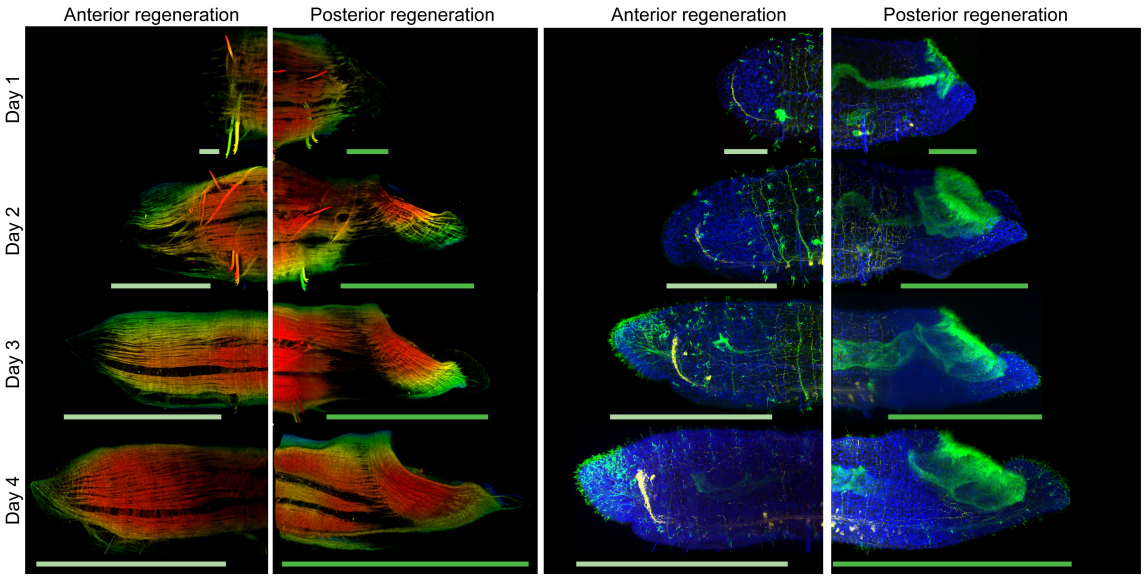

DERO FURCATA

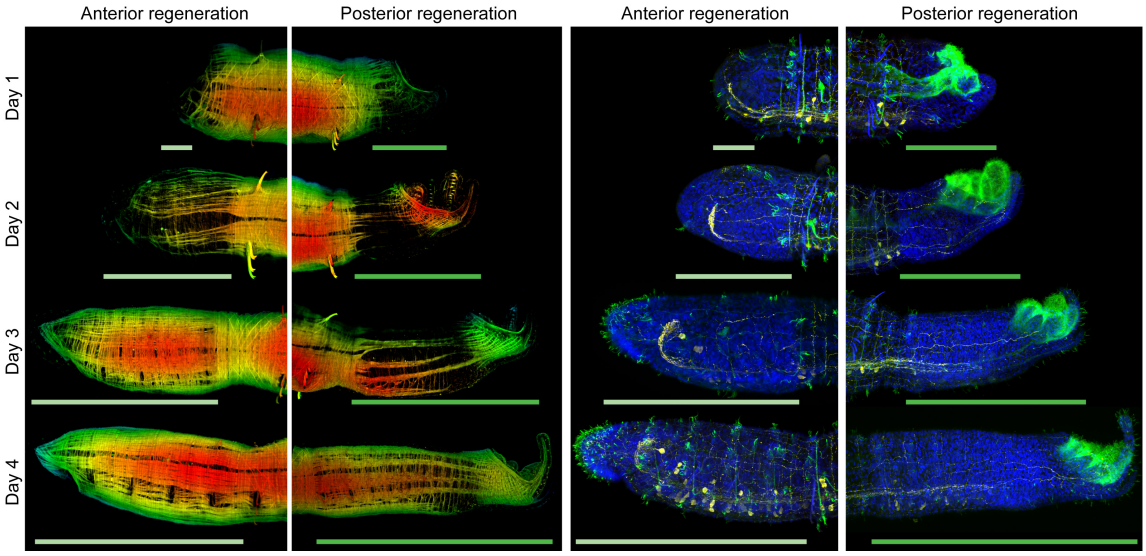

CHAPTER 5: Cell tracing and 4D imaging reveal complex cell movements during annelid regeneration

Abstract

Studies on the cellular basis of annelid regeneration, a topic of study for more than a century, stalled because static approaches used to infer a dynamic model failed to yield conclusive data. With renewed interest in stem cells and regeneration across animals, it has become critical to develop new approaches to study this issue. Using the naid annelid *Pristina leidyi* as a regeneration model, I tested the potential of thymidine analogue incorporation and carbocyanine cell labeling as reliable cell fate tracers, and developed a novel technique for long-term *in vivo* high-resolution time-lapse (4D) imaging to provide new answers to century-old questions in annelid regeneration. Results from thymidine analogue pulse-chase experiments show that there is no window during anterior regeneration where cell proliferation is restricted enough to allow for reliable labeling of a single cell population; however, analysis of differential label dilution revealed interesting patterns, including an early birthdate of cells forming the lateral line of the regenerate. Carbocyanine cell tracing provided evidence that the anterior prostomial cap derives completely from dorsal epidermis, and that cells labeled away from the wound can migrate into the regenerate; however, its potential was limited due to a significant amount of cell re-arrangement and migration during regeneration. High levels of cell migration were confirmed and studied using 4D imaging, revealing the existence of at least six migratory cell categories of diverse morphology and behavior; one of these populations showed a

statistically significant tendency to move toward the wound site during posterior regeneration. These cells moved sliding along the ventral nerve cord, and showed morphology similar to neoblasts, putative migratory stem cells which have been described during clitellate annelid regeneration; this would imply the first direct evidence of annelid neoblast migration, so far inferred only from counts on histological sections and dubious irradiation experiments. My findings indicate that even if extensive cell proliferation and migration limit the potential of thymidine analogues and carbocyanine labeling to trace individual cells, high resolution 4D microscopy has proven capable of providing a rich, dynamic picture of regeneration, making of *Pristina* a unique system to study *in vivo* cell dynamics during regeneration.

Introduction

Despite the broad distribution of regenerative capabilities across animals (Morgan, 1901; Vorontsova and Liosner, 1960; Alvarado and Tsonis, 2006; Bely, 2010), relatively few species have been studied in enough detail to address the question of cell origins and fates during regeneration, and even fewer have yielded well supported answers. That the main reason for this knowledge gap is limited availability of experimental tools for cell lineage tracing is evidenced by the fact that most breakthroughs have been achieved using novel techniques (Tanaka and Reddien, 2011). Recent work has shown the presence of three types of pluripotent stem cells in *Hydra* and a single type of totipotent stem cell in planaria (Tanaka and Reddien, 2011); on the other hand, studies on amphibians and zebrafish have proven that cells within the limb, tail and fin regeneration blastemas conserve their original cell type

identity, contrary to the traditional view that blastemal cells were multipotent (Kragl et al., 2009; Stewart and Stankunas, 2012). Whether those cells truly de-differentiate is still unclear in many cases.

In Annelida, a phylum with widespread regenerative abilities (Bely, 2006), the origin and fate of cells has been hotly debated for more than a century (Berrill, 1952; Herlant-Meewis, 1964; Hill, 1970). Most workers agree that the regenerate's ectodermal and endodermal derivatives originate from the old epidermis and gut lining respectively. However, the origin of mesodermal tissues has been more contentious: while some ascribed an ectodermal origin of all mesoderm (Semper, 1876; Hepke, 1897; Michel, 1898; von Wagner, 1900, 1906; Abel, 1902; Nusbaum, 1908), others supported a mesodermal origin instead (Randolph, 1891, 1892; Krecker, 1910, 1923; Sayles, 1927; Stone, 1932, 1933; Turner, 1934, 1935; O'Brien, 1946; Foulkes, 1953; Christensen, 1964; Herlant-Meewis, 1964; Hill, 1970; Cornec et al., 1987). Even within the latter, there is considerable disagreement about what cells make each tissue; a particular cell type, the neoblast, has been proposed as being anything from a "mere" detached peritoneal cell to a reserve pluripotent stem cell line. There is no consensus on what tissues derive from neoblasts: some authors only attribute them with replacing the peritoneal lining and a restricted number of other tissues (Randolph, 1892; Foulkes, 1953; Bilello and Potswald, 1974), while others concluded they make most or all mesodermal derivatives (Krecker, 1910, 1923; Sayles, 1927; Stone, 1932; Turner, 1934, 1935; O'Brien, 1946; Christensen, 1964). Presence of neoblasts in non-clitellate annelids is also controversial (Hill, 1970; Potswald, 1972; Bilello and Potswald, 1974). Furthermore, a basic neoblast feature,

long distance migration to the wound site, has been inferred purely from static "snapshots" through examination of histological sections of fixed material, but never directly demonstrated *in vivo*. Despite this, the migrating neoblast model is being assumed as fully tested in newer annelid regeneration literature (Myohara et al., 1999; Tadokoro et al., 2006; Sugio et al., 2012). This fact emphasizes the need for a more critical review of older literature and the use of new technical approaches to study cell origins and fates in annelid regeneration.

To begin investigating the cellular basis of annelid regeneration, I studied *Pristina leidyi* (Clitellata: Naididae), a small freshwater species whose transparency and ease of culture make a good system for *in vivo* studies. I used pulse-chase tracing by thymidine analogue incorporation and detection, adapted carbocyanine iontophoretic cell labeling used in embryonic studies, and developed a novel method for long-term time-lapse imaging. I addressed three issues: a) which tissues show cell proliferation during anterior regeneration?; b) is it possible to trace the fate of labeled cells in anterior regenerates?; c) are there neoblasts migrating to the wound site, and are they the only migratory cell type?

Materials and Methods

Animal collection, culturing and amputation

Specimens of *Pristina leidyi* Smith used during these experiments descend from samples collected from an artificial pond at the University of Maryland campus (35°59'48"N, 76°56'25"W). Worms were cultured in the laboratory at room temperature in artificial spring water (0.35 g/L InstantOcean aquarium mix) in glass

bowls and fed dried powdered *Spirulina*. Under those conditions, worms reproduce asexually indefinitely; no sexual individuals were observed during the course of these experiments. Amputations were performed under a dissection scope using a surgical scalpel on worms anesthetized with 50μM nicotine or ice cold spring water; worms paralyzed with TTX (see below) were cut without anesthetization. Amputees were kept at 25°C until fixation. Throughout this paper, I use the regeneration staging system introduced in Chapter 2 (Zattara and Bely, 2011): Stage 1, wound healing; Stage 2, blastema formation; Stage 3, blastema patterning; Stage 4, early differentiation; Stage 5, late differentiation; Stage 6, growth.

Thymidine analogue incorporation assays

To label cells undergoing DNA replication, I used either 5-Bromo-2′-deoxyuridine (BrdU, B5002 Sigma) or 5-ethynyl-2′-deoxyuridine (EdU, A10044 Invitrogen) incorporation assays. Worms were incubated in BrdU or EdU in artificial spring water (SpW) according to each experimental design. For the first experiment (Fig. 5.2A), anteriorly amputated worms were incubated in 300 μM EdU from 4 to 22 hpa; some were fixed at 22hpa (pulse), and the rest were moved to BrdU-containing water for 24 hs to chase out any EdU not incorporated into replicating DNA during the pulse, and then into clean fresh water. Samples were taken at 48, 72 and 96 hpa and assayed for EdU and acetylated α-tubulin detection (see below). For the second experiment, amputated worms were incubated in 800 μM BrdU from 22 to 48 hpa were moved from the BrdU labeling medium straight into fresh water. Samples were fixed at 48 hpa (pulse), 72hpa and 96hpa (chases, Fig. 5.3A) and immunoassayed for detection of BrdU and phospho-histone H3 (see below).

BrdU labeled worms were relaxed 10 minutes in cold 100 mM MgCl2, 5 mM NaCl, 1 mM KCl, 8% ethanol solution, fixed with 4% formaldehyde in 0.75x PBS for 40 minutes, washed 3 times with PBS, incubated in 6M HCl at 37C for 1:45hs, washed with PBS, then PBTx (0.1% Triton-X in PBS) several times, blocked in 10% Normal Goat Serum in PBTx for 3hs and incubated overnight at 4C in anti-BrdU mouse monoclonal primary antibodies (G3G4, DSHB) diluted 1:25 in blocking solution, and anti-phosphorylated histone H3 (06-570, Millipore, Darmstadt, Germany) diluted 1:200. Then the samples were washed several times with PBTx over 3 hs, incubated overnight at 4C in FITC-conjugated goat anti-mouse IgG secondary antibodies (Jackson Immunoresearch, West Grove, PA), washed with PBTx and PBS, transferred through a graded glycerol series (25%, 50% and 75% in PBS) and mounted in 25 mM *n*-propyl-gallate (02370 Sigma) in 75% glycerol/25% PBS for fluorescent imaging. EdU labeled worms were fixed as described above, assayed with the Click-iT® EdU Alexa Fluor® 594 Imaging Kit (C10339 Invitrogen, Carlsbad, CA) using the manufacturers instructions, counterstained with 4, 6-diamidino-2-phenylindole HCl (DAPI; D9542 Sigma, St. Louis, MO), and mounted as above.

Carbocyanine (DiI, DiOC, DiD) iontophoretic labeling

To label patches of tissue and groups of cells, I adapted iontophoretic carbocyanine labeling techniques used in embryos and neurons (Hodor and Ettensohn, 1998; Gan et al., 1999; Henry et al., 2001; Sweet et al., 2004; Meyer and Seaver, 2009) for use in adult worms. Iontophoresis is based on “pushing” of a charged molecule by an electric field; carbocyanine compounds have an overall

positive charge, so they can be loaded in a pulled microneedle threaded with a platinum electrode connected via a needle holder to the + terminal of a device that can deliver varying current; a ground anode is placed in contact with the media (see Fig. 5.3A for a circuit diagram). The needle holder was mounted on a standard micromanipulator and operated under a dissecting microscope. I used three different carbocyanine compounds: DiI (ex.550, em.565), DiOC (ex.480, em.501), and DiD (ex.644, em.665). Each compound was diluted to saturation in ethanol and back-loaded in microneedles made with thin wall borosilicate capillary glass (BF100-78-10, Sutter Instruments, Novato, CA) pulled with a P-90 puller (Sutter Instruments). Worms anesthetized with nicotine or paralyzed with TTX (see below) were labeled by pressing the tip of the needle against a patch of tissue and closing the circuit for 30 seconds to a few minutes. Due to the low conductance of the spring water medium, usually the lower resistance settings (4.4-1.3kΩ) were needed to obtain satisfactory labeling. Label was applied either over an epidermal patch by pressing the needle against the worm, or internally by piercing the body wall. Patches were labeled on worms just amputated, or 24 hours after amputation; in some experiments uncut worms were labeled at a ventral ganglion and amputated one or two segments away from the labeled area. Labeled worms were immediately observed under an epifluorescence microscope to verify incorporation of dye, and then imaged daily under a Leica SP5X confocal microscope (see below). A total of 35 worms were labeled and followed daily for up to ~90hpa.

Confocal laser scanning microscopy

Live, or fixed and stained worms were imaged with a Leica SP5X confocal laser scanning microscope (Leica, Wetzlar, Germany) equipped with motorized XY-stage and Z-servo, a white light laser and a high-speed resonance scanner. Images were acquired using 20x or 40x oil immersion lenses. Live imaging was done using the resonance scanner on three channels: transmitted light, a "signal" channel tuned to the excitation/emission spectrum of the tracer dye (DiI, DiOC or DiD) and a "control" channel tuned to control autofluorescence (see below). For stained samples, multi-channel sequential acquisition was optimized to capture each fluorochrome (typically a combination of DAPI, FITC, Cy3, Alexa-Fluor 594 and/or Alexa-Fluor 647). Confocal stacks were visualized and analyzed using ImageJ v1.46 (NIH, Bethesda MD, USA).

Worms present at least two types of autofluorescence sources: the first are granules within cells of the chloragogen tissue that covers the gut, which due to their location and relatively low levels of autofluorescence were not likely to be confused with labeled cells; the second source are granules included in eleocytes, large round coelomocytes usually found attached to septa, but also distributed throughout the animal. Eleocyte granules are filled with a strongly autofluorescent compound, likely a riboflavonoid (Koziol et al., 2006), excited in the 405-488nm range and presenting an emission spectrum with a peak at 560nm and a broader shoulder down to 520nm. This spectrum has significant overlap with DiOC and DiI; while eleocytes are morphologically distinctive, similar granules are often seen in smaller cells. Thus, when labeling using DiOC or DiD, imaging included an additional autofluorescence

control channel to separate labeled cells from autofluorescence; granule autofluorescence can be seen as double signal (Fig. 5.3F-H). DiD has no spectral overlap with these granules, but requires for examination a far red light source and filter set that is not usually available in most epifluorescence microscope setups.

Worm paralyzation and long-term 4D imaging

Worms were paralyzed by incubation for 2-24hs in ~3-10 μM tetrodotoxin (TTX) in spring water. TTX is a potent sodium channel blocker (Carroll et al., 2003; Feldman et al., 2010; Chau et al., 2011), and exposure to it results in inhibition of skeletal muscle voluntary contractions, most likely due to blockade of TTX-sensitive channels in neurons that innervate them; however, TTX does not noticeably affect periodic contractions of the gut and blood vessels, or nephridial and gut lumen ciliary beating implied in excretion, digestion and gas exchange, thus allowing for prolonged survival of the immobilized specimens. In pilot trials, I found no effect of TTX on post-amputation survival; worms treated with the drug were alive past 10 days after incubation and may live much longer, eventually dying by starvation. TTX paralysis has no detectable effect on regeneration developmental trajectory, except for a possible slight decrease in final regenerate size which may be a fixation artifact.

Paralyzed worms were amputated and placed on a regular glass slide coated with Rain-X (ITW Global Brands, Houston TX, USA) in warm liquid 1% low-melt agarose (SeaPlaque, #50101 Lonza, Basel, Switzerland) and positioned as desired. A cover glass, supported by four “feet” of rolled molding clay to prevent squashing, was quickly placed over the slide and pushed down until the worm’s edges were firmly in contact with both glass surfaces. The sides of the cover glass were then sealed with

halo-carbon oil (FLY-7000 LabScientific, Livingstone NJ, USA) seal to prevent water evaporation while allowing gas exchange. Mounted worms were imaged under DIC optics in a Zeiss Axioplan2 microscope equipped with a Zeiss AxioCam HRc camera using the 6D Acquisition module of AxioVision v4.8.2 (Zeiss, Oberkochen, Germany). Full Z-stacks comprising focal planes spaced 3μm apart were acquired every 2 minutes for over 100 hours post-amputation, resulting in high spatiotemporal resolution 4D (XYZT-dimensional) datasets covering the full process of regeneration.

4D dataset analysis

Datasets from a total of 15 worms were scored, including at least 3 each of anterior, posterior and non -amputated controls worms. Each 4D dataset was analyzed during up to 24hpa with AxioVision, or imported using ImageJ. Moving cells were identified, measured, described and tracked frame-by-frame by scoring by hand their XYZT coordinates. While worms were positioned so that the antero-posterior and dorso-ventral axes where aligned with the X and Y axes respectively, they tend to curl ventrally, resulting in a slight curvature. Thus, XY coordinates only approximate actual AP and DV positions. Scoring of coordinates resulted in 12383 XYZT coordinates corresponding to 423 individual cell "tracks". These tracks were the units of analysis: each is composed by a XYZT series of variable length representing the position of a given cell at each timepoint during the interval I was able to reliably follow that particular cell. Within each track, "instantaneous" displacement and speed at each timepoint but the first were calculated based on the difference in coordinates between two consecutive timepoints. Then, each track was characterized by overall mean speed (the average of instantaneous movements across the complete track),

maximum instant speed (the maximum value of instantaneous movements across the complete track), total displacement (difference between the first and last timepoints of the track) and overall velocity (total displacement divided the track duration). A subset of 290 tracks from 3 anterior amputees, 5 posterior amputees and 2 uncut worms was further characterized: I re-examined the cell in each track and measured size, morphological characteristics, in particular cell shape, presence of locomotive structures, attachment mode to substrates and presence and amount of cytoplasmic granules; I then used these characteristics to categorize each cell and its track into six types. Statistical differences from zero for the center of displacement and velocity distributions were tested using the non-parametric Wilcoxon rank sum test; the standard α=0.05 was used as confidence level. Data statistical analysis and graphic representations were performed in R (R Development Core Team, 2011).

Results

Thymidine analogue incorporation shows cell proliferation at most cell layers

To determine which cell layers undergo cell proliferation during regeneration, I incubated anteriorly amputated worms in BrdU at three different 6-hs intervals within Stage 1: 0-6, 6-12 and 12-18 hours post amputation (hpa). Using CLSM-generated Z-stacks (n = 4 per interval), I counted BrdU positive cells found in the cut segment (0) and three proximal segments (1 to 3), sorting them by tissue (Fig. 5.1). Proliferating cells were detected in derivatives of ectoderm (epidermis and chaetal sacs), endoderm (gut) and putative mesodermal cells (coelomocytes, wound plug) at all intervals (Fig. 5.1A-C). Initially, the number and distribution of BrdU positive

cells across tissues is roughly similar between cut and proximal segments, but later a marked increase in proliferation of epidermal and wound plug cells is seen at the wound site (Fig. 5.1D).

Pulse-chase experiments show that the lateral line and peritoneal lining of the regenerate derive from cells born during the first day (Fig. 5.2). Cell proliferation patterns in worms pulsed for 18hs (4-22 hpa, Fig. 5.2A) in EdU and fixed at 22hpa (pulse, Fig. 5.2B) match observations described above for 6 hs pulses: most EdU+ cells are at the epidermis, gut and wound plug, but a number are also found around the coelomic cavity and at the chaetal sacs. Epidermal labeling is more abundant at the anterior surface of the stump, around the wound site, but extends back as lateral irregular patches. The gut shows weak but ubiquitous signal that extend for several segments behind the cut plane. The strongest labeling is seen in the wound plug, located between the closed wound and the blind gut end. Within individuals fixed during the chase (Fig. 5.2C-F), labeled cells become separated in two clear fractions: some with weaker, more fragmented signal apparently resulting from label dilution due to continuing cell division, and others conserving a strong signal, attributed to relatively few divisions after the EdU pulse. Cells belonging to the first fraction were found throughout the regenerate's epidermis, gut, pharyngeal sac and coelomic cells; they were also present in a small subset of cells within the ventral nerve cord ganglia, particularly at the anterior end (Fig. 5.2C'-F'). Cells in the second fraction showed two interesting patterns: at the body wall, they form a clear lateral line that can be seen to be continuous with an unlabeled subepidermal lateral cell line on the adjacent segments (Fig 5.2D-F); internally, they are found at early stages forming the

peritoneal linings of the prostomium and peristomium, and at later stages also participating in the peritoneum of new segments (Fig. 5.2C'-F'). Cells of this type are also found at the base of the cerebral ganglion, at the internal ventral edge of the prostomium, dorsal to the stomodeal invagination, and in front of the anterior edge of the ventral nerve cord. Label was rarer or absent within the ventral nerve cord ganglia, stomodeal invagination and dorsal tissues of the brain. While it is not possible to confidently assign most cell fates from this pulse-chase experiment given the relatively large number of cells initially incorporating the label, results strongly suggest that the lateral line and peritoneal lining derive from cells born during regeneration's first day and that many of these cells undergo little proliferation after the first 24 hs.

Results from the second set of pulse-chase experiments show that most cells forming a regenerated head descend from cells born after the first day. Given that a considerable fraction of cells forming the regenerated head were not labeled after a pulse based on the first day post-amputation, I repeated the above experiment, this time labeling with BrdU from 22 to 48 hpa. Worms fixed at 48hpa (pulse, Fig. 5.3B) had extensive BrdU positive labeling throughout the gut, extending several segments behind the wound, including a cell mass located dorsally over the gut; at the primordia of the cerebral ganglion, circumenteric connectives and anterior-most ventral nerve cord ganglia; and at the anterior and lateral epidermis and body wall of the regenerate. Fewer labeled cells were present at the dorsal and ventral epidermis. Worms fixed during the chase (Fig. 5.3C-E) presented labeled cells throughout most of the regenerate's tissues, with the exception of labeled nuclei showing the typical

peritoneal morphology; however, due to incompatibility between BrdU detection and most DNA markers, it was not possible to confidently verify the absence of label at those cells. In contrast to the above EdU experiment, labeled cells had a rather continuous range of signal intensity; nonetheless, stronger signal was evident at the ventral side of the prostomium and towards the posterior-most region of the proliferating epidermis. This experiment shows that proliferation occurs at all germ-layer derivatives after 22hpa, and that most new tissues are formed from cells born during that time or its descendants.

Pristina cells can be labeled with carbocyanine and traced throughout regeneration

Due to the large number of proliferating cells in different tissues during regeneration, thymidine-analogue labeling is not precise enough for cell fate tracing. I used iontophoretic transfer (Fig. 5.4A) to label patches of tissues with carbocyanine-based dyes. I dyed and followed a total of 35 worms; results were highly variable, and worms usually required application of relatively high voltages during up to 1-2 min to achieve satisfactory dye transfer. Animals show strong signal after the procedure, but strength and apparent numbers of labeled cells decline over time. Carbocyanine dyes intercalate within the lipophilic core of cell membranes and are not horizontally transferred, but it is not possible to rule out phagocytic ingestion of free dye or necrosed dyed cells.

After anterior regeneration, the anterior wound surface is replaced by the prostomium. Is the prostomium a dorsal, ventral or mixed derivative? Examination of 5 anterior amputees labeled at the anterior surface epidermis showed that patches

located dorsal to the mid-longitudinal plane were fully incorporated into the developing prostomium (Fig. 5.4B-E, *n=3*), while patches ventral to that plane were pushed down and backwards by the developing prostomium and do not contribute to it (Fig. 5.4F-I; *n=2*). This suggests that dorsal and ventral identities are conserved during regeneration.

During anterior regeneration, new anterior ventral nerve cord, circumenteric connectives and cerebral ganglion are made. Carbocyanine dyes are particularly useful to label nerves, because once the dye enters the cell membrane, it will diffuse throughout the cell. Four worms were labeled at a ventral ganglion before amputation and showed neural staining along the ventral nerve cord extending far away from the injection point. In one of them, labeled axons can be seen extending anteriorly from the cut plane into the regenerate, and forming part of the new nerve cord, circumenteric connectives and cerebral ganglion neuropil (Fig. 5.4I-K). Since the dye does not transfer between cells, then these labeled axons necessarily originated in the original ventral nerve cord, showing that at least part of the regenerate's neuropil is formed by outgrowth of axons extending from the old ventral nerve cord.

Cells labeled behind the cut site migrate forward and are incorporated into the regenerate. I labeled 3 worms at a subepidermal patch of cells located between the ventral chaetae and made an anterior cut one segment away from the labeled patch (Fig. 5.5A-B). I imaged the worms a few hours after amputation to ensure no labeled cells were present near the wound, and then daily for up to 75 hpa. Most labeled cells remained at their original location during the regeneration process, but ~5-10 cells were found dorsal to the original labeling location. In two worms, 3 labeled cells were

observed at position anterior to the amputation plane (Fig. 5.5A-B, 20-75hpa). The third worm got a larger ventral patch labeled, and showed a much larger number of cells (19) located anterior to the amputation plane (data not shown). A fourth worm was labeled at the epidermis within the same location; no cells were found away from the original location after 46 hpa. These results suggest that cells found below the epidermis can migrate over more than one segment and enter the regenerating area.

4D imaging reveals the presence of multiple migratory cell types

Cell tracing experiments evidenced a significant amount of cell re-arrangement and migration during regeneration. Since abundant cell migration complicates interpretation of cell labeling experiments, I developed a novel worm immobilization and mounting technique to allow continuous imaging of regenerating animals over very long periods of time (from hours to several days) using tetrodotoxin (TTX), a potent sodium channel blocker. Worms treated with TTX become permanently paralyzed, but are not otherwise affected and can stay alive for more than a week. Thus, TTX-induced paralysis allows for long-term continuous high-resolution imaging of regenerating worms.

Analysis of 4D datasets of 6 anterior and 6 posterior amputees, along with 3 non-amputated controls, shows extensive cell migration. Cells of different types can be clearly seen moving across the animal in both amputated and non-amputated worms. Detectability and traceability of cells vary depending on the moving cell's size, morphology and location. For example, cells floating in the coelomic cavity or crawling along the inner side of the body wall (particularly near the mid-sagital plane) are easier to detect and follow; on the other hand, cells embedded within more

compact tissues or obscured by overlying structures like chaetal sacs are difficult or impossible to distinguish. Despite these detection biases, enough moving cells are present to allow for a preliminary description of morphological types and their behavior.

To characterize migratory cell types, a 4D dataset subset of 3 anterior amputees, 5 posterior amputees and 2 uncut worms was analyzed during up to 24hpa (see methods). Based on this data, I tentatively grouped the moving cells in six different types (Fig. 5.6): eleocytes, "carriers", amoebocytes, "hyalinocytes", "rollers" and "sliders". The names in quotes have been coined here as temporary placeholders until further evidence on their nature and homologies becomes available.

Eleocytes (Fig. 5.6A-B): Large (usually 11-13μm, but up to 20 μm), round cells, containing a globular cluster of orange/brown granules. Usually found singly or in clusters attached to septa, gut, or chaetal sac muscles, but can be found at different places within the coelomic cavity. They tend to stay attached to nearby tissues, but can "jump" quickly after detaching from their anchor points, attaining instant velocities of up to 35 μm/min; they can also crawl along the peritoneal lining. Very common and easy to see even when not moving.

Carriers (Fig. 5.6C-D): Medium size (8-10 μm) cells of variable, irregular shape containing few to several orange/brown granules. Located anywhere within the worm's coelom, they move by a combination of sliding and pseudopodial "walking", at variable mean speeds ranging from 1 to up 7 μm/min, but capable of instant speeds of up to 20 μm/min. Very common, harder to detect if not moving; may be actually comprised of similar morphological stages of different cell types.

Amoebocytes (Fig. 5.6E): Large (16-22 μm) amoeboid cells usually found stretched along the inner side of the body wall, containing usually 1-2 large orange/brown granules, sometimes more or none. They are frequently found crawling over the dorsal peritoneum, but can move laterally or ventrally. They move by extending long pseudopodia, stretching as much as 50 μm or more; their average speed is relatively low, averaging 2-3 μm/min, but can occasionally show bursts of 8-30 μm/min. Some amoebocytes were seen moving quickly by "swinging" forward while alternately attaching to ventral or dorsal peritoneum. Relatively common.

Hyalinocytes (Fig. 5.6F-G): Medium to large (8-18 μm), round or oblong shaped cells with smooth texture and clear appearance; no granules or obvious cytoplasmatic elements. No obvious motility structures, usually seen swinging from an attached edge; average moving speed of ~5 μm/min, with bursts of up to 11 μm/min. Relatively rare; round and oblong cells may be very different cell types.

Rollers (Fig. 5.6H-I): Medium size (7-9 μm), round cells, usually with none or one orange/brown granule, occasionally two. Normally with only a small contact with their substrate or detached; they often show a small number of filopodial extensions and move relatively fast, with average speeds of 6-8 μm/min and bursts of up to 20 μm/min. Observations of 4D datasets suggest they move by rolling over the substrate aided by filopodia (hence the name), but imaging at a higher temporal resolution is needed to confirm this behavior. Relatively common.

Sliders (Fig. 5.6J): Small to medium (7-10 μm) spindle shaped cells, usually with no granules (rarely one). Usually with a large surface in contact with the substrate, often seen over the ventral nerve cord or moving over the lateral

peritoneum. They move by sliding over the substrate at relatively low average speeds (1-3 μm/min), with maximum instantaneous speeds ranging from 3-8 μm/min. Relatively uncommon except after posterior amputation.

Migratory cells show a wide range of behaviors, average speeds and overall movement trends. Total displacement varied within and between cell type and treatment; in most cases, there was no statistically significant preference either towards the anterior or posterior (Fig. 5.6K; Wilcoxon rank sum tests of difference from zero overall X-axis directionality), except for carriers in uncut animals which moved preferentially towards the anterior end ($p = 0.01$; $n = 19$), amoebocytes in anterior amputees which moved preferentially towards the anterior end ($p = 0.03$; $n = 13$) and sliders in posterior amputees which moved preferentially towards the posterior end ($p < 0.001$; $n = 55$). Since track durations ranged from less than 10 minutes to several hours depending on how easy it was to follow a particular cell, I divided total X-displacement by track duration for each cell to reduce this potential detection bias. X-displacement in these datasets approximates antero-posterior movement. Histograms of distribution of cell overall X-axis velocity across 2 anterior and 3 posterior amputees show negative skewness ($g_1 = -0.417$) on the former and positive skewness ($g_1 = 0.428$) on the latter (Fig. 5.7A). Despite skew towards anterior migration, the center of distribution of X-velocities on anterior amputees is not significantly different from zero (Wilcoxon rank sum test, $p = 0.107$). On the other hand, the center of distribution of X-velocities on posterior amputees is significantly higher than zero (Wilcoxon rank sum test, $p = 7E\text{-}7$), reflecting a preponderance of posterior migration towards the wound site.

To find whether this posterior migration trend was common to all cell types, I repeated the analysis on data from 3 posterior amputees, stratified by cell type (Fig. 5.7B). Even though frequency distributions for all but rollers had a positive skewness, differences from zero were not significant except for sliders, most of which were found moving along the dorsal surface of the ventral nerve cord, usually toward the wound (Fig. 5.8A). While most of these ventral sliders were moving posteriorly, some moved in the opposite direction, sometimes changing direction during the track. Sliders moved at varying speeds; a few non moving cells were also seen over the nerve cord (not scored). In summary, migrating cells can move both towards and away from a wound; the only cells that showed a strong and statistically significant directional preference were sliders moving towards the wound site in posterior amputees.

Migrating cells can stop moving and change shape to undergo mitosis. I found two cases where the complete process of mitotic division in a migrating slider-type cell could be followed (Fig. 5.9; corresponding to a slider moving along the inner surface of the lateral body wall in an anterior amputee). In the case shown in Fig. 5.9, the slider slowed down to a stop (designated as t=0), and adopted at 6 min a rounder shape. At 12 min, a vertical structure is seen, likely a metaphase chromosomal plate; the structure is gone at 14 min, and by 16 min the cell has undergone cytokinesis through the vertical plane. After 20 min, the two daughter cells begin to flatten against the substrate and by 30 min have recovered the slider morphology and resume movement. If prophase does not start until the cell has changed shape and cytokinesis occurs at or towards the end of mitosis, then the whole M-phase took 12 minutes or

less, with a 6 min prophase, 2 min or less metaphase, and 4 min anaphase plus telophase. It is interesting to note that while undergoing mitosis, a cell that would be described as a slider temporarily adopts a morphology similar to that of a roller; this shows that cell type categorization requires a dynamic picture where both shape and behavior are taken into account.

Discussion

The cellular basis of annelid regeneration has been a topic of study and debate for more than a century; controversies have been due to lack of conclusive data because static technical approaches were being used to infer a dynamic model. With a renewed interest in regeneration and the distribution of stem cells across animals, it has become critical to develop new approaches to study these issues. In this study, I tested the potential of thymidine analogue incorporation and detection, carbocyanine cell labeling and tracing, and long-term *in vivo* high-resolution time-lapse (4D) imaging to provide new answers to century-old questions in annelid regeneration. In particular, I tested the ability of thymidine analogue pulse-chase detection assays as reliable cell fate tracers, the potential of carbocyanine labeling as an *in vivo* cell tracer, and whether migrating cell populations in general and neoblasts in particular can be directly observed and characterized *in vivo* in regenerating worms.

Widespread cell proliferation during *Pristina* regeneration limits the power of thymidine analogues as cell fate tracers

Thymidine analogues like [^{3}H]thymidine, bromodeoxyuridine (BrdU) or ethynildeoxyuridine (EdU) are routinely used to label and trace neuronal progenitors

and their descendents in mammalian systems (Miller and Nowakowski, 1988); however, accurate cell fate tracing depends on the ability to label a restricted known set of cells. When using systemic labels like BrdU or EdU, achieving specific labeling depends on cell proliferation being restricted to a single tissue or cell population at the time of labeling. Is there such a window of opportunity during annelid regeneration? While early studies of annelid regeneration proposed that most, if not all, new material in regenerated tissues originated in epidermal cell proliferation (Hepke, 1897; Michel 1898; Abel, 1902; von Wagner, 1900, in Sayles, 1927; Nusbaum, 1908; and Stone, 1933 in Hill, 1970), most workers agreed that all germ layers replace their own (Randolph, 1892; Stone, 1932, 1933; Turner, 1934, 1935; Christensen, 1964; Herlant-Meewis, 1964; Hill, 1970). Nonetheless, regeneration in some annelid species may present spatio-temporal patterns of proliferation enabling the use of BrdU/EdU as tracers. For example, in *Enchytraeus japonensis*, BrdU pulses revealed no positive cells between 0-6 hours post amputation (hpa), proliferation was restrictedo to segmentally iterated coelomic cells between 6-12 hpa, and ectodermal proliferation only near the wound site after 12 hpa (Sugio et al., 2012). These patterns allowed using BrdU pulse-chase experiments for cell fate tracing in that species. However, such windows were not found in *Pristina*: S-phase cells are present at multiple tissues and cell types at all times. A clear shift however can be seen from the initial even distribution of proliferation across segments to a sharp preponderance of proliferation at the wounded segment. At later time-points, proliferation in *Pristina* becomes even more widespread within derivatives of all three layers. There is no time window at which cell cycling is restricted to just a

single tissue layer or cell type. This makes it unfeasible to exclusively label a restricted cell population, severely limiting the power of BrdU/EdU pulse-chase experiments for cell fate tracing.

Despite these limitations of thymidine analogue tracing, analysis of differential signal dilution during the chase revealed an interesting pattern. Most cell proliferation at the body-wall between 4-22hpa was located laterally and anteriorly at a diffuse band along the mid-longitudinal plan; while weakly labeled cells resulting form several rounds of cell division can be seen at later stages, a group of cells arranged along a lateral band shows a much stronger signal, suggesting they have not undergone many divisions since the original pulse. These cells are continuous with a lateral row of subepidermal cells that runs the whole length of the worm, known as the lateral line. First described in Naididae by Semper (1876) as a putative homologue of the vertebrate lateral line system and later found in most oligochaetes and maybe even capitellid polychaetes (Eisig 1887, in Brode, 1898), it has been interpreted as a parasympathetic nerve or an aggregation of nuclei from circular muscles (Vejdosvsky, 1879, Hesse, 1893, Eisig, 1887, in Brode, 1898; Keyl, 1913). Despite its widespread distribution, the nature of the lateral line remains a mystery: since Brode (1898) and Keyl (1913), it has been mostly ignored except as a morphological marker. Interestingly, a number of genes putatively involved in patterning and signaling are expressed in segmentally iterated lateral spots located along the lateral line both in uncut regenerating worms (A.E. Bely and B.D.Ozpolat, unpublished data). Such observations, together with fact that cells fated to the lateral line in the regenerate form very early during regeneration, hint that this structure may be more

than just a "problematic cell cord of doubtful significance" (Eisig, 1887 in Brode, 1898) and that further research into the function of this mysterious structure is long overdue.

Carbocyanine labeling and time-lapse imaging reveal a highly dynamic picture of annelid regeneration

Past descriptions of annelid regeneration based on histological sectioning of developing specimens gave relatively little attention to migration of "coelomocytes", a heterogeneous category of cells roaming the coelomic cavity. Although several workers have proposed a role for them in regeneration, most of the attention has been devoted to the oligochaete migrating neoblasts (Herlant-Meewis, 1964). Data obtained from carbocyanine labeling and time-lapse imaging paint a more complex and dynamic picture of cell movements during annelid regeneration: internal cells labeled together at one spot in regenerating animals were often found later widely spread out; furthermore, direct observation of 4D datasets show rampant migration by several cell types. While such high levels of cell migration make difficult the use of iontophoretic carbocyanine labeling as a reliable cell fate tracer, this challenge can be overcome by combining this technique with high resolution time-lapsing. The combination is made even more powerful with the use of confocal microscopy: confocal Z-stacks of fluorescently labeled cells are amenable to computer-aided analysis with the use of segmentation algorithms, as done in zebrafish embryos (Keller et al., 2008). A pilot set of proof-of-concept short time-lapse datasets of worms injected with droplets of DiD diluted in soybean oil imaged under a high-speed confocal microscope (E.E.Z., unpublished data) confirms the feasibility of this

approach and should allow a more dynamic approach to the study of cell movements and role in regenerative processes.

Directional migration of ventral sliders provides the first direct evidence of neoblast migration

The existence of motile coelomocytes and their possible role in annelid regeneration has been discussed for more than a century (see Herlant-Meewis, 1964 for a review). Why then did neoblasts, described from fixed material as putative migratory stem cells since Randolph's foundational paper (1891, 1892), receive such disproportionate attention? In many cases, the reason is that other cell types were considered to be performing non-morphogenetic functions, like immunity, phagocytosis of damaged cells or nutrient transport (Herlant-Meewis, 1964). While this separation of "physiological" versus "developmental" roles may be more in the mind of researchers than in the actual worms, which (if any) of these cell types actually serves as tissue progenitor in the regenerate is still an open question. While my 4D datasets were not able to trace cells to their final destination, cells fated to form part of the regenerate are expected to show a mostly unidirectional migration towards the wound site. I found only one cell population showing a statistically significant directional bias toward the wound: sliders in posterior amputees, most of which were seen moving along the ventral nerve cord. The shape, location and directional behavior of these ventral sliders strongly suggest that they are the neoblasts mentioned by other authors. If so, then these observations would to my knowledge be the first direct evidence of their migratory behavior. Interestingly, very few ventral sliders and no strong directionality was observed in anterior amputees.

Posterior, but not anterior migration of neoblasts has been described for *Tubifex*, *Limnodrilus* and *Allonais* (Naididae); in contrast, migration to both anterior and posterior wounds was reported in *Dero* (Naididae) and *Lumbriculus* (Lumbriculidae) (Krecker, 1910, 1923; Sayles, 1927; Stone, 1932, 1933; Turner, 1934, 1935; O'Brien, 1946; Foulkes, 1953). Since my cell-tracking analysis only encompassed the first 24hpa, later migration cannot be discarded. In any case, having found the first direct evidence of a model proposed more than century ago proves that dynamic descriptions of cell behavior based on 4D datasets are a powerful tool not only to directly test century-old models, but also to inform interpretation of assays made on fixed material (e.g. immunostaining, *in situ* RNA hybridization, etc.).

Concluding remarks

The origin and fate of cells involved in annelid regeneration has been a controversial topic during the last couple centuries. Persistence of this debate can be traced to the fact that most conclusions were derived from dynamic interpretations of static data. In this work, I have evaluated the capabilities and limitations of three newer techniques (thymidine analogue incorporation and detection, carbocyanine iontophoretic labeling and high-resolution 4D imaging) to offer novel insights on cell behavior during the post-amputation regenerative response of the naid *Pristina leidyi*. My findings indicate that extensive cell proliferation and migration limit the potential of BrdU/EdU assays and carbocyanine labeling to reliably trace individual cells; on the other hand, high resolution 4D microscopy has proven a powerful tool capable of providing a rich, dynamic picture of the regenerative process. Combining 4D imaging with carbocyanine labeling and confocal microscopy is a promising avenue for future

research that could make of *Pristina leidyi* a unique system to study *in vivo* cell dynamics, during regeneration and otherwise; indeed, long term 4D imaging of adult animals has to date only been reported for zebrafish (Kamei and Weinstein, 2005), a species only capable of regenerating some appendages. Insight from these techniques will also help inform interpretation of results from fixed materials. Last but not least, the ability for long term *in vivo* imaging will no doubt redouble its worth when transgenic methods become available for this species.

Chapter 5 Figures

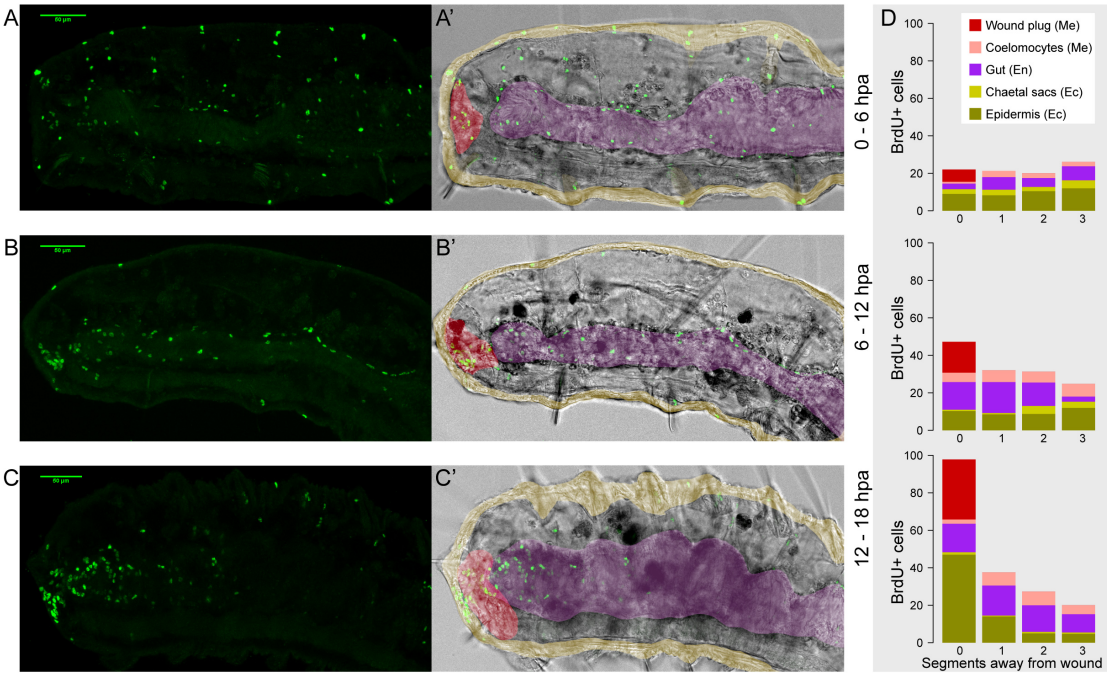

Figure 5.1: Cell proliferation occurs at all three germ layers during early regeneration.

Anterior is to the left in all panels. A-C) Distribution of BrdU+ cells in anterior amputees fixed after incubation in 0.8mM BrdU 0-6 (A), 6-12 (B) and 12-18 (C) hours post amputation (hpa). Each image set shows the reflected light (A-C, green, BrdU) or a merge (A'-C') at a mid-sagital thick optical section of reflected (green, BrdU) and transmitted (grayscale, morphology) light channels. False-color indicates epidermis (ectodermal, yellow), gut (endodermal, purple) and wound plug (mesodermal, red). C) Average count of BrdU+ cells stratified by tissue type and distance from the wounded segment (n= 4 worms per time-point).

Figure 5.2: Cells born during the first 24 hours post amputation form the lateral line and internal coelomic linings.

Anterior is to the left in all panels. A) Diagram showing the approximate distribution of anterior regeneration stages and the design of pulse-chase experiment. Letters correspond to panels in this figure. B-F) Early regeneration EdU/BrdU pulse-chase; surface and mid-sagital thick optical sections showing EdU+ nuclei (red), acetylated-tubulin (green, showing peripheral nervous system and gut ciliation) and all nuclei (blue, DAPI). Anterior amputees were incubated in 0.3mM EdU from 4-22 hpa and fixed or chased with 0.8mM BrdU for 24hs, fixed at various stages, stained and imaged under CLSM. A-A') Stage 2 at 22 hpa; B-B') Stage 3 at 48 hpa; C-C') Stage 4 at 72 hpa; D-D') Stage 5 at 72 hpa; E-E') Stage 6 at 96 hpa.

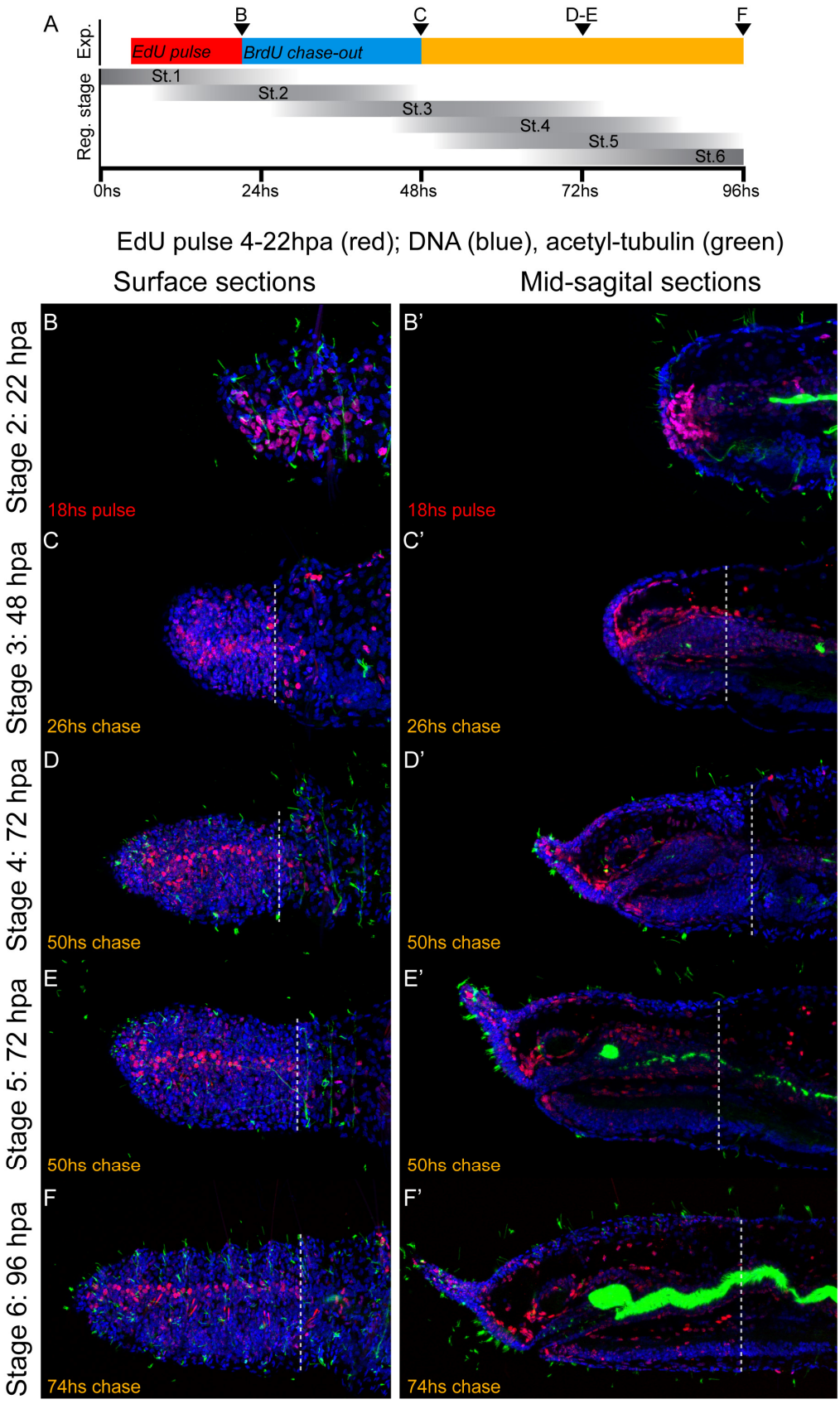
A
B
C
D-E
F
Exp.
EdU pulse
BrdU chase-out
Reg. stage
St.1
St.2
St.3
St.4
St.5
St.6
0hs
24hs
48hs
72hs
96hs
EdU pulse 4-22hpa (red); DNA (blue), acetyl-tubulin (green)
Surface sections
Mid-sagital sections
Stage 2: 22 hpa
Stage 3: 48 hpa
Stage 4: 72 hpa
Stage 5: 72 hpa
Stage 6: 96 hpa
B
B'
18hs pulse
C
C'
26hs chase
D
D'
50hs chase
E
E'
50hs chase
F
F'
74hs chase

Figure 5.2

Figure 5.3: Cells born during the second day of regeneration make up most of the anterior regenerate.

Anterior is to the left in all panels. A) Diagram showing the approximate distribution of anterior regeneration stages and the design of pulse-chase experiment. Letters correspond to panels in this figure. B-E) Mid regeneration BrdU pulse-chase; surface and mid-sagital thick optical sections showing BrdU+ nuclei (red), and phospho-histone H3(blue, used here as morphology counterstain). Anterior amputees were incubated in 0.83mM BrdU from 22-48 hpa and fixed at various stages, stained and imaged under CLSM. F-F) Stage 3 at 48 hpa; G-G') Stage 4 at 72 hpa; H-H') Stage 5 at 72 hpa; I-I') Stage 6 at 96 hpa.

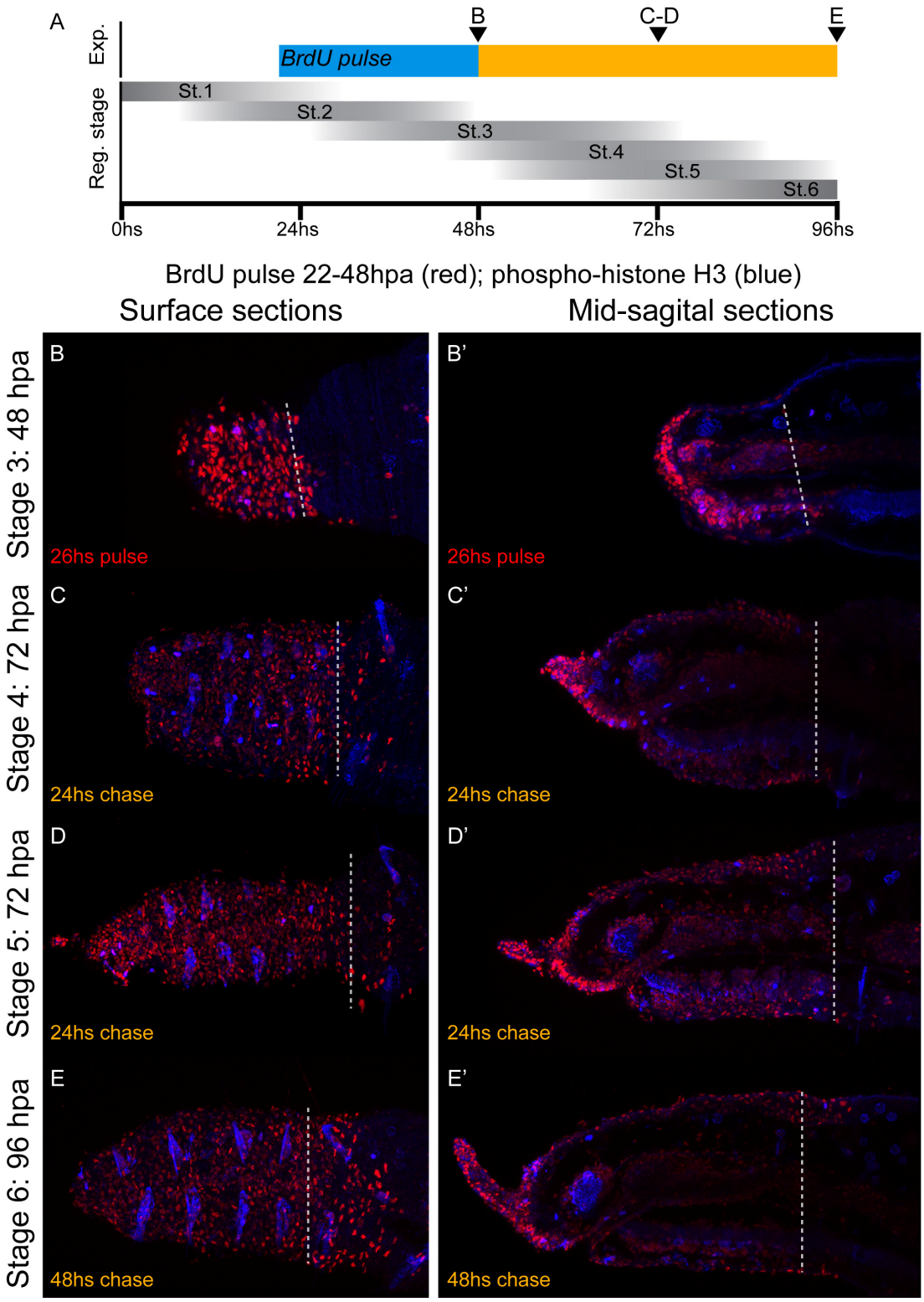
A
Exp.
B
C-D
E
BrdU pulse
Reg. stage
St.1
St.2
St.3
St.4
St.5
St.6
0hs
24hs
48hs
72hs
96hs
BrdU pulse 22-48hpa (red); phospho-histone H3 (blue)
Surface sections
Mid-sagital sections
Stage 3: 48 hpa
Stage 4: 72 hpa
Stage 5: 72 hpa
Stage 6: 96 hpa
B
B'
26hs pulse
C
C'
24hs chase
D
D'
24hs chase
E
E'
48hs chase

Figure 5.3

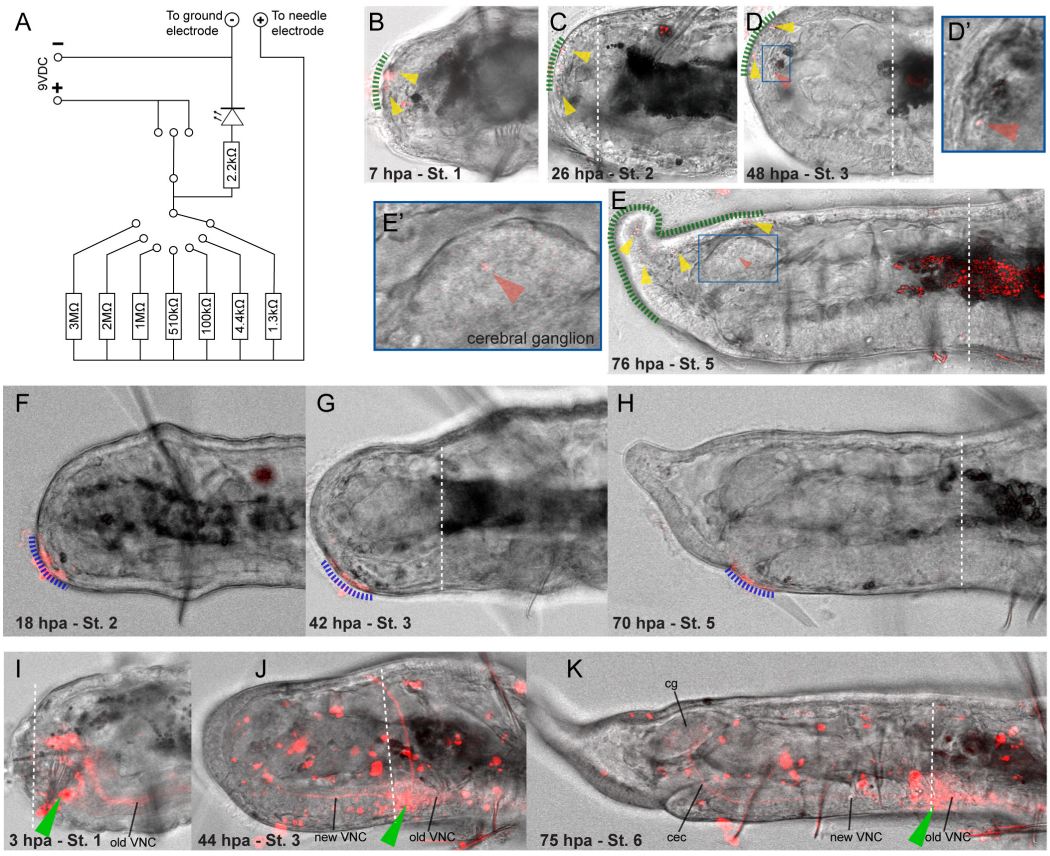

Figure 5.4: Carbocyanine cell labeling and tracing.

A) Circuit diagram of the iontophoretic dye injection device. B-K) Confocal images of representative experiments Merge of reflected (red, peak emission of DiI, DiOC or DiD) and transmitted (grayscale, morphology) light channels. Anterior is to the left in all panels. B-E) DiI labeled cells (yellow arrowheads) at an antero-dorsal epidermal patch (green dashed line); an internal labeled cell (red arrowhead) is found at later stages (inset of boxed areas). B) Stage 1, 7hpa; C) Stage 2, 26hpa; D) Stage 3, 48 hpa; D') Detail of boxed area in D; E) Stage 5, 76 hpa. E') Detail of boxed area in E. F-H) Labeling of epidermal anteroventral patch (blue dashed line) showing postero-ventral displacement. F) Stage 2, 18 hpa; G) Stage 3; 42 hpa; H) Stage 5; 70 hpa. I-K) DiI labeling of neurons within the ventral nerve cord shows incorporation of neuronal elements from the old cord into the regenerates new CNS. I) Stage 1, 3hpa; J) Stage 3, 44 hpa; K) Stage 6, 75 hpa. Green arrowhead shows position of the dye injection; VNC: ventral nerve cord; cec: circumenteric connectives; cg: cerebral ganglion.

Figure 5.5: Carbocyanine labeling shows migration of cells into the anterior regenerate.

Merge of reflected (red, peak emission of DiI, DiOC or DiD) and transmitted (grayscale, morphology) light channels. Green arrowheads indicate injection site; white dashed lines indicate amputation plane; asterisks indicate autofluorescent eleocytes; blue arrowheads highlight labeled cells found anterior to the amputation plane. Anterior is to the left in all panels. A) Anterior regeneration series at 4, 20, 45 and 75 hpa of a worm labeled behind the ventral chaetae and amputated one segment ahead of the injection site; labeled cells are found from 20 hpa within the regenerated tissues, away from the original injection location. The upper left inset shows for the first time-point a merge of the tracer dye channel (red) with a channel capturing light from autofluorescent emissions at wavelengths not overlapping the tracer dye's emission spectrum (green). Overlap allows spectral separation of autofluorescent (yellow) and tracer dye labeled (red) cells. B) A replicate of the experiment shown in A. Labeled cells in the regenerate are found at the anterior edge of the new ventral ganglia, near the stomodeal invagination and around the new gut.

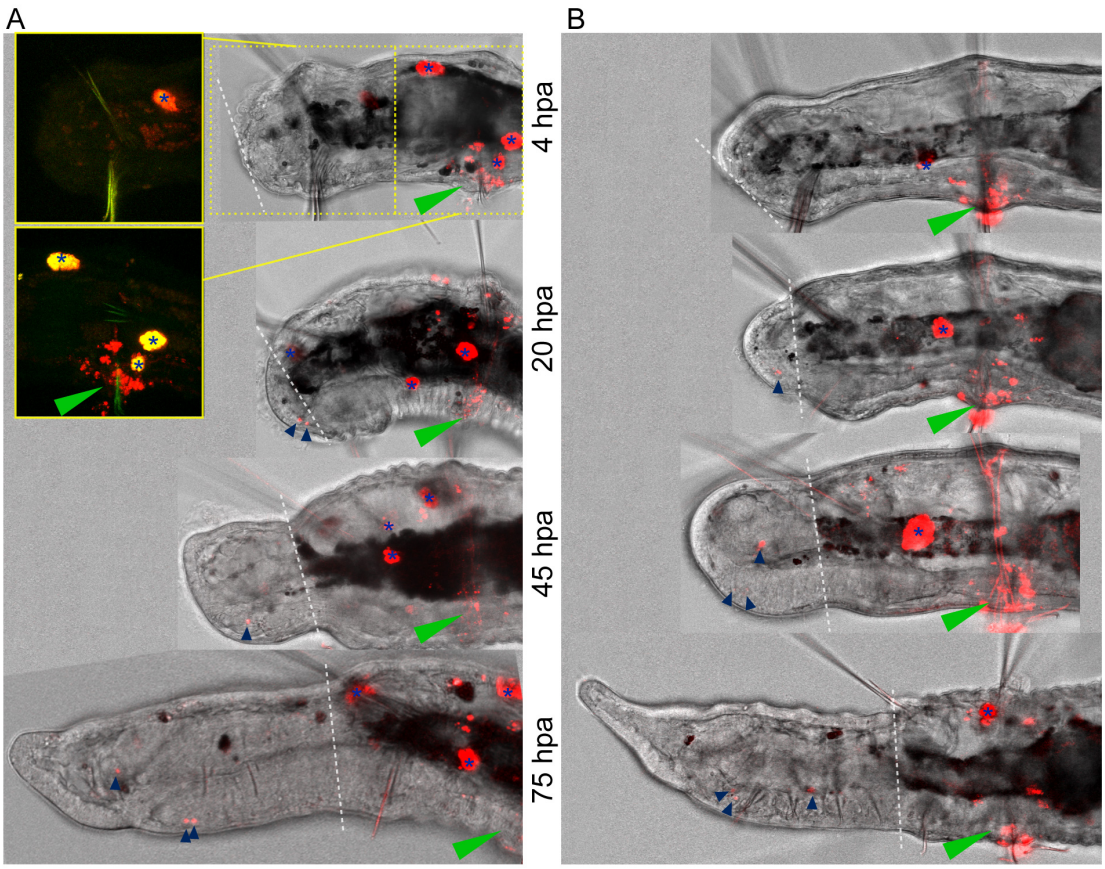

Figure 5.5

Figure 5.6: Analysis of 4D microscopy datasets

Analysis of 4D microscopy datasets shows the presence of at least six migratory cell populations. A-J) Examples of different cell types; white arrowheads indicate migrating cell; scale bars: 20μm. A) Round eleocytes clinging from a septum and chaetal muscles. B) A migrating eleocyte sliding along the dorsal body wall. C) Two carrier cells near the ventral surface of the coelome; notice the variable morphology and the presence of one to many granular inclusions. D) An carrier moving along the ventral body wall. E) An amoebocyte moving along the dorsal body wall; they can be distinguished from amoeboid carriers by their larger size and behavior. F) A fusiform hyalinocyte, clinging by one end from the dorsal body wall. G) A round hyalinocyte, attached at one edge to the dorsal body wall. H) A roller with granular inclusions moving along the dorsal body wall. I) A roller without inclusions moving along the dorsal body wall; notice the fine filopodia. J) Two sliders moving along the surface of the ventral nerve cord. K) Vector plot of overall cell XY plane displacement by cell type and amputation treatment. Each arrow represents the difference between XY coordinates measured at the start and end of the track of one cell; longer arrows represent larger total displacements; all plots are at the scale shown at the lower left. Vectors are not corrected for track duration. Sample size n is indicated for each vector group; p shows the p-value of Wilcoxon rank sum tests for the average X displacement being significantly different from zero in each group (only for groups where $n > 5$). Representative drawings of each cell type are shown next to the corresponding plots.

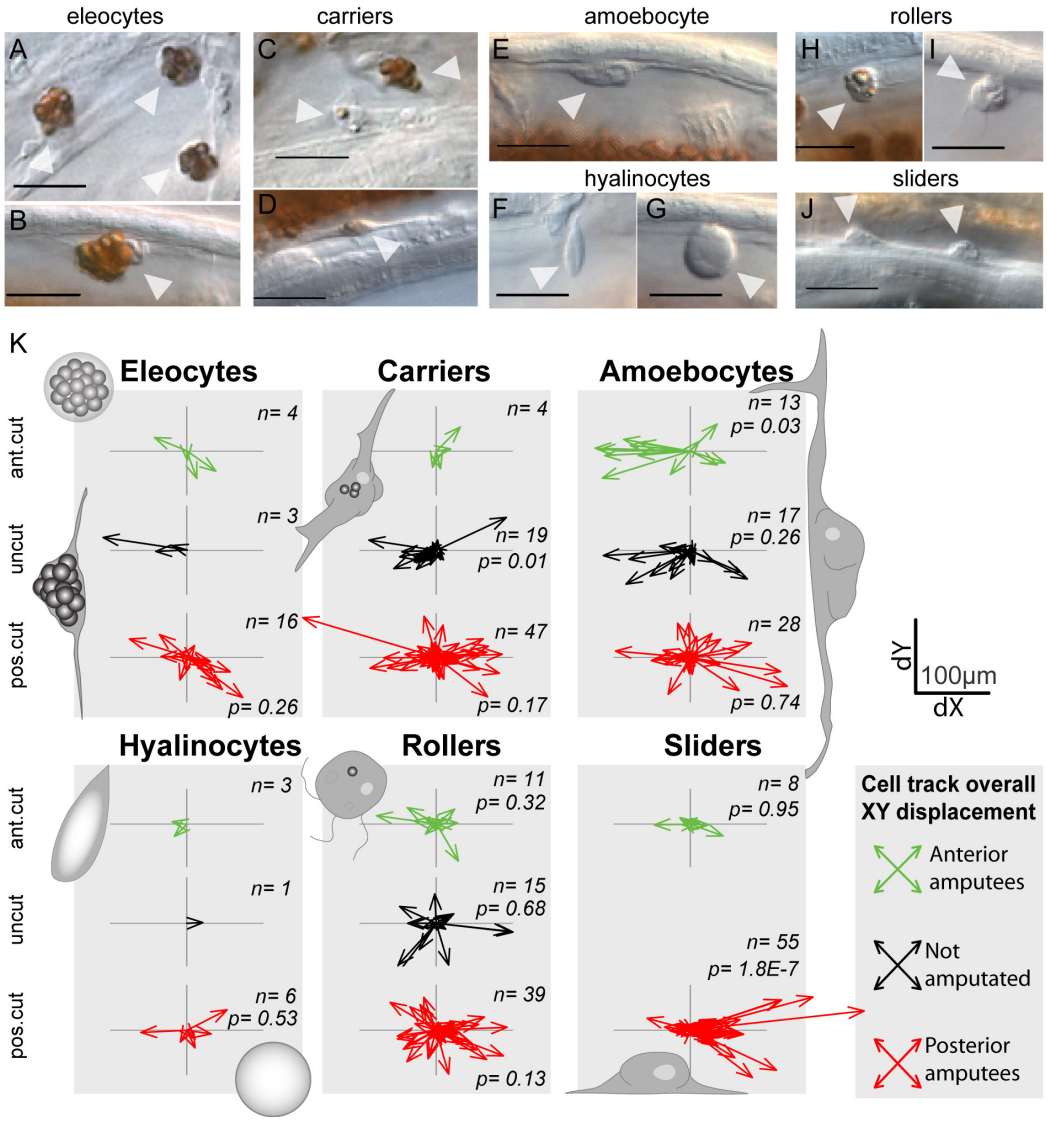
eleocytes
carriers
amoebocyte
rollers
A
B
C
D
E
H
I
hyalinocytes
sliders
F
G
J
K
Eleocytes
Carriers
Amoebocytes
ant.cut
uncut
pos.cut
n= 4
n= 3
n= 16
p= 0.26
n= 4
n= 19
p= 0.01
n= 47
p= 0.17
n= 13
p= 0.03
n= 17
p= 0.26
n= 28
p= 0.74
dY
100µm
dX
Hyalinocytes
Rollers
Sliders
n= 3
n= 1
n= 6
p= 0.53
n= 11
p= 0.32
n= 15
p= 0.68
n= 39
p= 0.13
n= 8
p= 0.95
n= 55
p= 1.8E-7
Cell track overall
XY displacement
Anterior
amputees
Not
amputated
Posterior
amputees

Figure 5.6

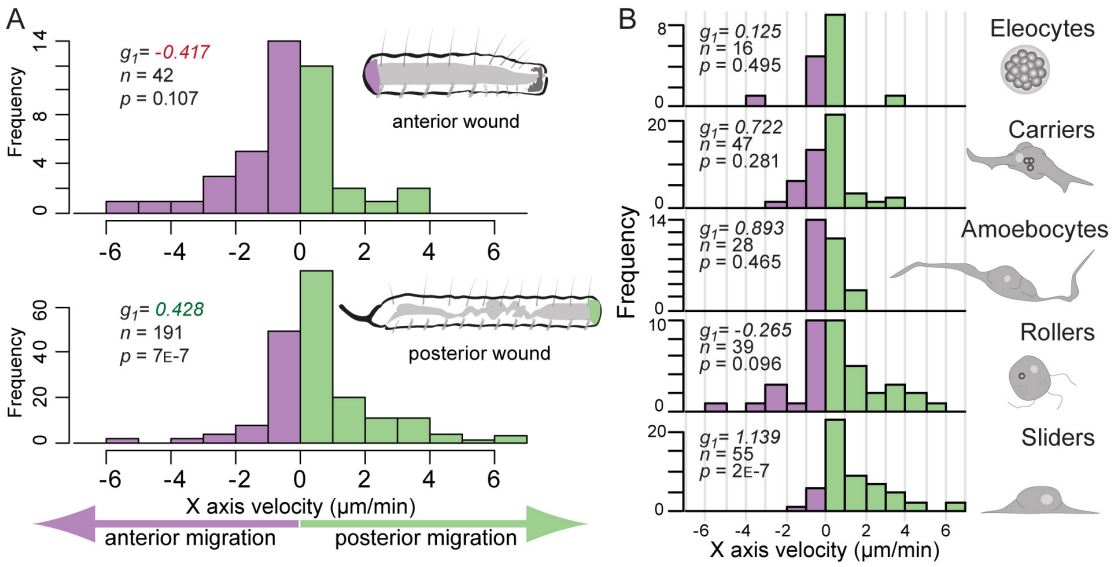

Figure 5.7: Frequency distribution of horizontal cell velocities

Analysis of 4D microscopy datasets reveal preferential posterior migration of sliders during posterior regeneration. A) Frequency distribution of cell total X-axis velocities, measured as overall X displacement along a track divided the track total duration, for cells measured in 2 anterior (top) and 3 posterior (bottom) amputees. Purple bars represent anterior migration (negative values) and green bars, posterior migration (positive values). B) Frequency distribution of cell X-axis velocities for cells scored in 3 posterior amputees, grouped by cell type. Hyalinocytes were not included due to low sample size. Statistics as in A. Cell diagrams not to scale. g_1: skewness; *n*: number of cell tracks; *p*: p-value for the Wilcoxon rank sum test.

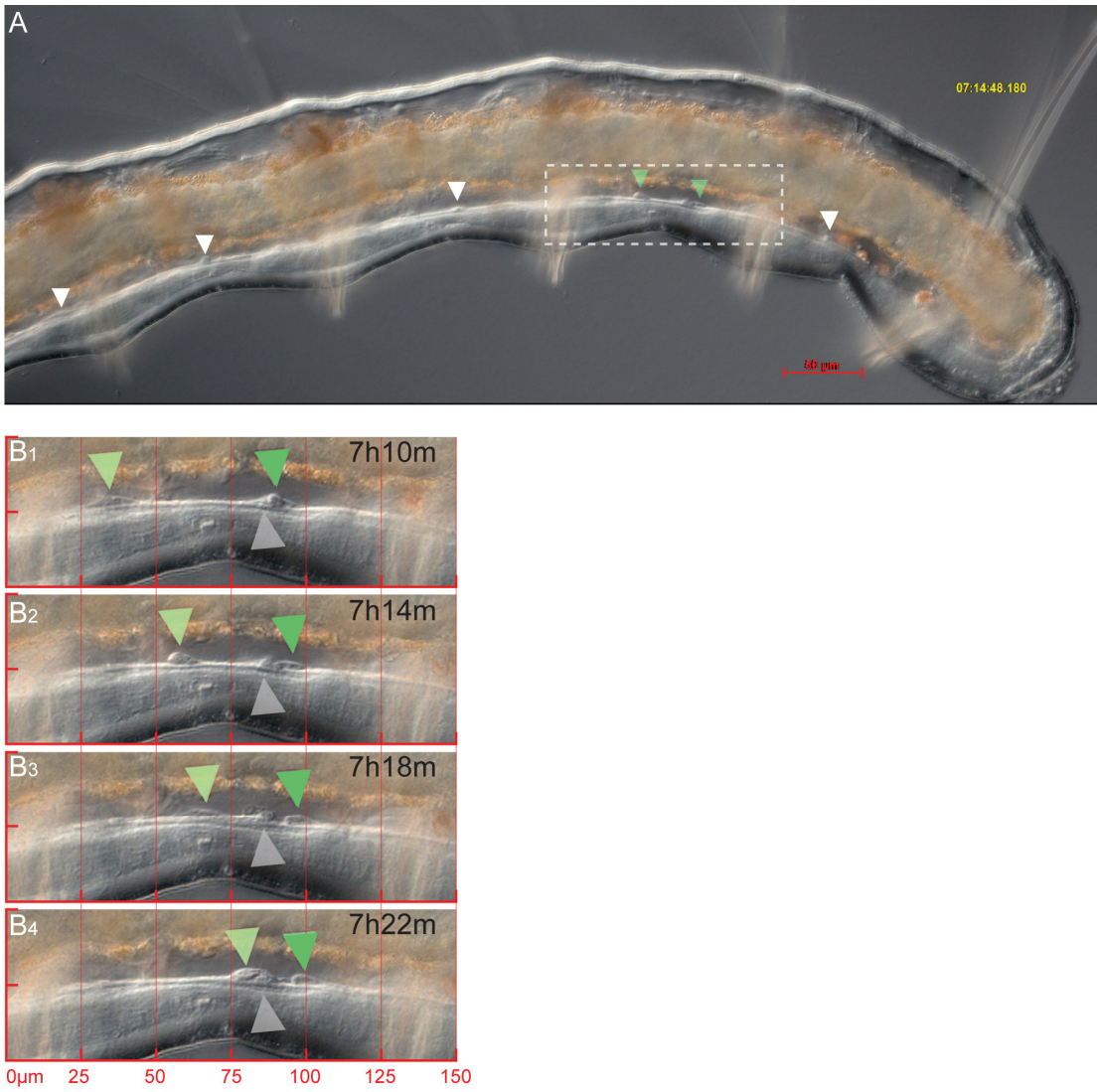

Figure 5.8: Sliders move over the ventral nerve cord during posterior amputation.

A) Sample XY frame from a 4D dataset of a posterior amputee; mid-sagital plane, approximately 7:30hpa. Anterior is to the left in all panels. Arrowheads show migrating dorsal sliders; the green arrowheads highlight sliders shown in B. B) Detail of four frames, spaced 4 minutes apart, corresponding to the boxed area in A. The two ventral sliders (green arrowheads; same ones in C) are moving posteriorly at different speeds (light green: faster, dark green: slower). A third cell of about the same size as the sliders (grey arrowhead) remains in the same spot.

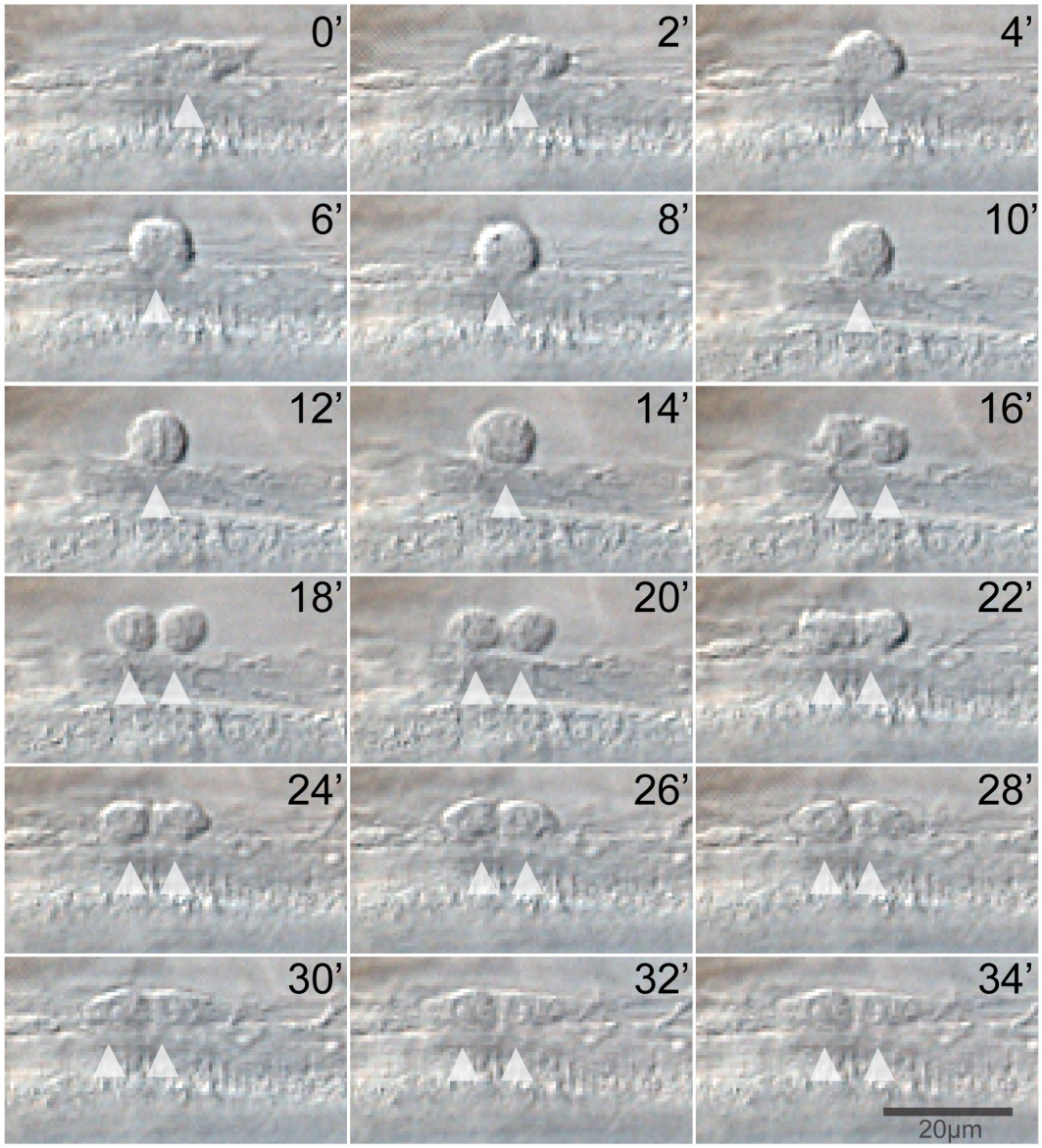

Figure 5.9: Time-lapse imaging can capture *in vivo* mitotic events.

Detail of 34 minutes from a time-lapse recording of an anterior amputee; a slider previously moving in anterior direction over the body wall stops, changes shape from spindle to round, and divides by mitosis; the two daughter cells then regain the spindle shape. Notice the transient vertical structure at 12’, presumably a metaphase plate.

Conclusions

An analysis of the phylogenetic distribution of regeneration and fission among metazoans in general and annelids in particular supports the hypothesis that regeneration is a pre-requisite to evolve agametic asexual reproduction, and that this reproductive mode has originated independently many times.

A detailed comparison of morphogenesis during regeneration and paratomic fission in the naid annelid worm *Pristina leidyi* revealed extensive similarities between both developmental trajectories, including evidence for a synapomorphy in peripheral nervous system development apparently not shared with embryogenesis. It also uncovered that important differences occur throughout the trajectories, manifested by temporal shifts in developmental events and by the presence of elements unique to only one process. These findings provide strong support for the hypothesis that fission is derived from regeneration, and indicate that the two trajectories have diverged from each other by accumulating differences along their entire developmental course.

A quantitative analysis of cell proliferation and growth in *Pristina leidyi* has demonstrated that: a) there is a baseline non-linear gradient of proliferative potential that is independent of resource availability; b) starting within minutes upon amputation, regeneration can significantly shift resource allocation within the worm; c) competitive interactions between somatic growth, regeneration and fission are stronger in anterior than in posterior amputees, possibly because removal of the head, but not the tail, causes the worm to behave as a closed developmental system. Since similar results were reported for naidine annelids and catenulid flatworms, it can be

concluded that given independent gains of paratomic fission, convergent evolution of resource allocation strategies can be driven by similar developmental and physiological contexts.

A comparative study of morphogenesis during regeneration and fission in 10 annelid species (2 pristinines, 7 naidines and one outgroup lumbriculid) has shown that: a) regeneration developmental trajectories are very similar across all 10 species; b) clitellate annelids have convergently placed the plane of division at the same interganglionar position; c) architomic fission trajectories are closer to regeneration than to paratomic fission; d) paratomic fission trajectories in pristinines and naidines are strikingly similar in many morphogenetic aspects. However, there are two different modes of reconstructing the central nervous system during paratomic fission, one only found in pristinines, the other restricted to naidines. Together, this data suggest that after independent origins of fission a considerable degree of parallel evolution occurred in each lineage.

I tested the potential of three techniques to study the cellular basis of annelid regeneration. Thymidine analogue pulse-chase experiments showed limited potential for cell tracing, but differential label dilution can be informative, for example by highlighting early formation of lateral line cells in the regenerate. Carbocyanine cell labeling provided evidence for a dorsal origin of the prostomium and long distance migration of cells into the regenerate. High-resolution 4D imaging revealed six migratory cell categories, including cells found sliding along the ventral nerve cord toward the wound site during posterior regeneration, whose morphology was similar that of neoblasts, putative migratory stem cells described from histological studies.

My findings indicate that even if extensive cell proliferation and migration limit the potential of thymidine analogues and carbocyanine labeling to trace individual cells, high resolution 4D-microscopy can provide a rich, dynamic picture of regeneration.

Altogether, these results strongly support that fission originated multiple times by repeated co-option of regenerative abilities; furthermore, the striking convergences of fission developmental trajectories and resource allocation strategies suggest that a combination of similar regenerative capabilities, functional constraints and ecophysiological context can channel evolutionary trajectories into closely parallel paths, both in phylogeneticaly close and distant lineages.

Bibliography

Abel, M., 1902. Beiträge zur Kenntnis der Regenerationsvorgänge bei den limicolen Oligochäten. *Zeitschrift fur Wissenschlaftliche Zoologie* 73, 1–74.

Abramoff, M.D., Magalhaes, P.J., Ram, S.J., 2004. Image processing with ImageJ. *Biophotonics International* 11, 36–42.

Åkesson, B., Gschwentner, R., Hendelberg, J., Ladurner, P., Müller, J., Rieger, R., 2002. Fission in *Convolutriloba longifissur*a: asexual reproduction in acoelous turbellarians revisited. *Acta Zoologica* 82, 231–239.

Akimenko, M.A., Johnson, S.L., Westerfield, M., Ekker, M., 1995. Differential Induction of Four *Msx* Homeobox Genes During Fin Development and Regeneration in Zebrafish. *Development* 121, 347–357.

Allen, W.E., 1911. A study of the relation of tissue differentiation to rate of growth during regeneration. *The Biological Bulletin* 21, 187–2061.

Alonso-Bedate, M., Sequers, E., 1985. Suggested regulatory mechanisms for caudal regeneration in *Allolobophora molleri* (Annelida: Oligochaeta). *Comparative Biochemistry and Physiology Part A: Physiology* 81, 225–228.

Alvarado, A.S., Tsonis, P.A., 2006. Bridging the regeneration gap: genetic insights from diverse animal models. *Nature Reviews Genetics* 7, 873–884.

Alvariño, A., 1994. Chaetognatha. In K.G. Adiyodi and R.G. Adiyodi (eds.). *Reproductive Biology of Invertebrates. Vol. VI Part B, Asexual propagation and reproductive strategies*. John Wiley & Sons, Chichester, UK, 329-338.

Azariah, J., 1994. Cephalochordata. In K.G. Adiyodi and R.G. Adiyodi (eds.). *Reproductive Biology of Invertebrates. Vol. VI Part B, Asexual propagation and reproductive strategies*. John Wiley & Sons, Chichester, UK, 395-401.

Bell, A.W., 1959. *Enchytraeus fragmentosus*, a New Species of Naturally Fragmenting Oligochaete Worm. *Science* 129, 1278–1278.

Bely, A.E., 1999. Decoupling of fission and regenerative capabilities in an asexual oligochaete. *Hydrobiologia* 406, 243–251.

Bely, A.E., 2006. Distribution of segment regeneration ability in the Annelida. *Integrative and Comparative Biology* 46, 508–518.

Bely, A.E., 2010. Evolutionary Loss of Animal Regeneration: Pattern and Process. *Integrative and Comparative Biology* 50, 515 –527.

Bely, A.E., Sikes, J.M., 2010. Latent regeneration abilities persist following recent evolutionary loss in asexual annelids. *Proceedings of the National Academy of Sciences* 107, 1464–1469.

Bely, A.E., Wray, G.A., 2001. Evolution of regeneration and fission in annelids: insights from *engrailed*- and *orthodenticle*-class gene expression. *Development* 128, 2781–91.

Bely, A.E., Wray, G.A., 2004. Molecular phylogeny of naidid worms (Annelida: Clitellata) based on *cytochrome oxidase I*. *Molecular Phylogenetics and Evolution* 30, 50–63.

Benazzi, M., Benazzi-Lentati, G., 1993. Platyhelminthes - Turbellaria. In K.G. Adiyodi and R.G. Adiyodi (eds.). *Reproductive Biology of Invertebrates. Vol. VI Part A, Asexual propagation and reproductive strategies*.Oxford & IBH Publishing, New Delhi, 107-141.

Berrill, N.J., 1931. Regeneration in *Sabella pavonina* (Sav.) and other sabellid worms. *Journal of Experimental Zoology* 58, 495–523.

Berrill, N.J., 1952. Regeneration and budding in worms. *Biological Reviews* 27, 401–438.

Berrill, N.J., 1978. Induced segmental reorganization in sabellid worms. *Journal of Embryology and Experimental Morphology* 47, 85–96.

Bilello, A.A., Potswald, H.E., 1974. A cytological and quantitative study of neoblasts in the naid *Ophidonais serpentina* (Oligochaeta). *W. Roux' Archiv f. Entwicklungsmechanik* 174, 234–249.

Birnbaum, K.D., Alvarado, A.S., 2008. Slicing across Kingdoms: Regeneration in Plants and Animals. *Cell* 132, 697–710.

Blackstone, N., 2009. Mitochondria and the redox control of development in cnidarians. *Seminars in Cell & Developmental Biology* 20, 330–336.

Bourne, A.G., 1891. Notes on the Naidiform Oligochaeta; containing a Description of New Species of the Genera *Pristina* and *Pterostylarides*, and Remarks upon Cephalization and Gemmation as Generic and Specific Characters in the Group. *Quarterly Journal of Microscopical Science* s2-32, 335–356.

Brinkhurst, R.O., Jamieson, B.G.M., 1971. *Aquatic Oligochaeta of the World*. Oliver & Boyd, Edinburgh.

Brockes, J.P., Kumar, A., 2008. Comparative Aspects of Animal Regeneration. *Annual Review of Cell and Developmental Biology* 24, 525–549.

Brode, H.S., 1898. A contribution to the morphology of *Dero vaga*. *Journal of Morphology* 14, 141–180.

Brusca, R.C., Brusca, G.J., 1990. *Invertebrates*. Sinauer, Sunderland, MA.

Burton, P., Finnerty, J., 2009. Conserved and novel gene expression between regeneration and asexual fission in *Nematostella vectensis*. *Development Genes and Evolution* 219, 79–87.

Carlson, B.M., 2007. *Principles of Regenerative Biology*. Academic Press, Burlington, MA.

Carlson, M.R.J., Komine, Y., Bryant, S.V., Gardiner, D.M., 2001. Expression of *Hoxb13* and *Hoxc10* in Developing and Regenerating Axolotl Limbs and Tails. *Developmental Biology* 229, 396–406.

Carroll, S., McEvoy, E.G., Gibson, R., 2003. The production of tetrodotoxin-like substances by nemertean worms in conjunction with bacteria. *Journal of Experimental Marine Biology and Ecology* 288, 51–63.

Carroll, S.B., Grenier, J.K., Weatherbee, S.D., 2005. *From DNA to diversity: molecular genetics and the evolution of animal design*, Second ed. Blackwell Publishing, Malden, MA.

Casellato, S., 1984. Life-cycle and karyology of *Branchiura sowerbyi* Beddard (Oligochaeta, Tubificidae). *Hydrobiologia* 115, 65–69.

Chau, R., Kalaitzis, J.A., Neilan, B.A., 2011. On the origins and biosynthesis of tetrodotoxin. *Aquatic Toxicology* 104, 61–72.

Child, C., 1903. Studies on regulation. III. Regulative destruction of zooids and parts of zooids in *Stenostoma*. *Archiv f. Entwickelungsmechanik* 17, 1–40.

Child, C.M., 1906. The relation between regulation and fission in planaria. *The Biological Bulletin* 11, 113–123.

Child, C.M., 1915. *Individuality in organisms*. The University of Chicago press, Chicago, IL.

Child, C.M., Hyman, L.H., 1919. The Axial Gradients in Hydrozoa. I. Hydra. *Biological Bulletin* 36, 183–223.

Christen, B., Beck, C.W., Lombardo, A., Slack, J.M.W., 2003. Regeneration-specific expression pattern of three posterior Hox genes. *Developmental Dynamics* 226, 349–355.

Christensen, B., 1964. Regeneration of a new anterior end in *Enchytraeus bigeminus* (Enchytraeidae, Oligochaeta). *Vidensk Medd Dan Natrur Foren* 127, 259–273.

Christensen, B., 1994. Annelida - Clitellata. In K.G. Adiyodi and R.G. Adiyodi (eds.). *Reproductive Biology of Invertebrates. Vol. VI Part B, Asexual propagation and reproductive strategies*. John Wiley & Sons, Chichester, UK, 1-23.

Chu, J., Pai, S., 1944. The relations between natural fission and regeneration in *Stylaria fossularis* (Annelida). *Physiological Zoology* 17, 159–166.

Chuang, S.H., 1994. Brachiopoda. In K.G. Adiyodi and R.G. Adiyodi (eds.). *Reproductive Biology of Invertebrates. Vol. VI Part B, Asexual propagation and reproductive strategies*. John Wiley & Sons, Chichester, UK, 315-328.

Clark, R.B., Bonney, D.G., 1960. Influence of the Supra-oesophageal Ganglion on Posterior Regeneration in *Nereis diversicolor*. *Journal of Embryology and Experimental Morphology* 8, 112–118.

Clark, R.B., Clark, M.E., 1959. Role of the Supra-oesophageal Ganglion during the Early Stages of Caudal Regeneration in Some Errant Polychaetes. *Nature* 183, 1834–1835.

Clavier, J., 1984. Production due to regeneration by *Euclymene oerstedi* (Claparède) (Polychaeta: Maldanidae) in the maritime basin of the Rance (Northern Britanny). *Journal of Experimental Marine Biology and Ecology* 75, 97–106.

Coe, W.R., 1934. Analysis of the regenerative processes in nemerteans. *The Biological Bulletin* 66, 304–315.

Consoli, L., 1923. La rigenerazione in rapporto con la strobilazione negli Oligocheti limicoli. *Bull Ist Zool Palermo* 1, 23–47.

Cornec, J.-P., Cresp, J., Delye, P., Hoarau, F., Reynaud, G., 1987. Tissue responses and organogenesis during regeneration in the oligochete *Limnodrilus hoffmeisteri* (Clap.). *Canadian Journal of Zoology* 65, 403–414.

Darwin, C., 1868. *The variation of animals and plants under domestication*. John Murray, London.

David, A.A., Williams, J.D., 2011. Asexual reproduction and anterior regeneration under high and low temperatures in the sponge associate *Polydora colonia* (Polychaeta: Spionidae). *Invertebrate Reproduction & Development* 1–10.

Dehorne, L., 1916. Les naidimorphes et leur reproduction asexuée. *Archives de Zoologie Experimentale et Générale* 56, 25–157.

Drewes, C.D., Fourtner, C.R., 1991. Reorganization of escape reflexes during asexual fission in an aquatic oligochaete, *Dero digitata*. *Journal of Experimental Zoology* 260, 170–180.

Dunn, C.W., Hejnol, A., Matus, D.Q., Pang, K., Browne, W.E., Smith, S.A., Seaver, E., Rouse, G.W., Obst, M., Edgecombe, G.D., Sorensen, M.V., Haddock, S.H.D., Schmidt-Rhaesa, A., Okusu, A., Kristensen, R.M., Wheeler, W.C., Martindale, M.Q., Giribet, G., 2008. Broad phylogenomic sampling improves resolution of the animal tree of life. *Nature* 452, 745–749.

Envall, I., Källersjö, M., Erséus, C., 2006. Molecular evidence for the non-monophyletic status of Naidinae (Annelida, Clitellata, Tubificidae). *Molecular Phylogenetics and Evolution* 40, 570–584.

Erséus, C., 2005. Phylogeny of oligochaetous Clitellata. *Hydrobiologia* 535-536, 357–372.

Erséus, C., Envall, I., Marchese, M., Gustavsson, L., 2010. The systematic position of Opistocystidae (Annelida, Clitellata) revealed by DNA data. *Molecular Phylogenetics and Evolution* 54, 309–313.

Erséus, C., Kallersjo, M., Ekman, M., Hovmoller, R., 2002. 18S rDNA phylogeny of the Tubificidae (Clitellata) and its constituent taxa: Dismissal of the Naididae. *Molecular Phylogenetics and Evolution* 22, 414–422.

Erséus, C., Wetzel, M.J., Gustavsson, L.N., 2008. IZCD rules - a farewell to Tubificidae (Annelida, Clitellata). *Zootaxa* 1744, 66–68.

Feldman, C.R., Brodie, E.D., Brodie, E.D., Pfrender, M.E., 2010. Genetic architecture of a feeding adaptation: garter snake (*Thamnophis*) resistance to tetrodotoxin bearing prey. *Proceedings of the Royal Society B: Biological Sciences* 277, 3317 –3325.

Fell, P.E., 1993. Porifera. In K.G. Adiyodi and R.G. Adiyodi (eds.). *Reproductive Biology of Invertebrates. Vol. VI Part A, Asexual propagation and reproductive strategies*. Oxford & IBH Publishing, New Delhi, 1-44.

Finogenova, N.P., Arkhipova, N.R., 1994. Morphology of some species of the genus *Aulodrilus* Bretscher. *Hydrobiologia* 278, 7–15.

Fischer, A., Dorresteijn, A., 2004. The polychaete *Platynereis dumerilii* (Annelida): a laboratory animal with spiralian cleavage, lifelong segment proliferation and a mixed benthic/pelagic life cycle. *BioEssays* 26, 314–325.

Foulkes, R.H., 1953. Regeneration of the Anterior End of *Aulophorus furcatus* (Naididae) with Special Reference to Effect of X-Rays. *Biological Bulletin* 105, 80–86.

Fry, C.L., 2006. Juvenile hormone mediates a trade-off between primary and secondary sexual traits in stalk-eyed flies. *Evolution & Development* 8, 191–201.

Galloway, T.W., 1899. Observations on non-sexual reproduction in *Dero vaga*. *Bulletin of the Museum of Comparative Zoology* 35, 1–140.

Gan, W.B., Bishop, D.L., Turney, S.G., Lichtman, J.W., 1999. Vital imaging and ultrastructural analysis of individual axon terminals labeled by iontophoretic application of lipophilic dye. *J. Neurosci. Methods* 93, 13–20.

Gardiner, D.M., Blumberg, B., Komine, Y., Bryant, S.V., 1995. Regulation of *HoxA* Expression in Developing and Regenerating Axolotl Limbs. *Development* 121, 1731–1741.

Gates, G.E., 1927. Regeneration in a Tropical Earthworm *Perionyx excavatus* E. Perr. *Biological Bulletin* 53, 351–364.

Gates, G.E., 1949. Regeneration in an Earthworm, *Eisenia foetida* (Savigny) 1826. I. Anterior Regeneration. *Biological Bulletin* 96, 129–139.

Ghiselin, M.T., 1987. Evolutionary aspects of marine invertebrate reproduction. In Giese, A.C., Pearse, J.S., Pearse, V.B. (Eds.). *Reproduction of Marine Invertebrates.* Blackwell Scientific, Palo Alto, CA.

Ghosh, S., Roy, S., Séguin, C., Bryant, S.V., Gardiner, D.M., 2008. Analysis of the expression and function of *Wnt-5a* and *Wnt-5b* in developing and regenerating axolotl (*Ambystoma mexicanum*) limbs. *Development, Growth & Differentiation* 50, 289–297.

Gibson, G.D., Paterson, I.G., 2003. Morphogenesis during sexual and asexual reproduction in *Amphipolydora vestalis* (Polychaeta: Spionidae). *New Zealand Journal of Marine and Freshwater Research* 37, 741–752.

Gilbert, J.J., 1993. Rotifera. In K.G. Adiyodi and R.G. Adiyodi (eds.). *Reproductive Biology of Invertebrates. Vol. VI Part A, Asexual propagation and reproductive strategies*. Oxford & IBH Publishing, New Delhi, 231-263.

Glasby, C.J., Schroeder, P.C., Aguado, M.T., 2012. Branching out: a remarkable new branching syllid (Annelida) living in a *Petrosia* sponge (Porifera: Demospongiae). *Zoological Journal of the Linnean Society* 164, 481–497.

Goldfarb, A.J., 1909. The influence of the nervous system in regeneration. *Journal of Experimental Zoology* 7, 643–722.

Gurley, K.A., Rink, J.C., Alvarado, A.S., 2008. β-Catenin Defines Head Versus Tail Identity During Planarian Regeneration and Homeostasis. *Science* 319, 323–327.

Haag, E.S., Lenski, R.E., 2011. L'enfant Terrible at 30: The Maturation of Evolutionary Developmental Biology. *Development* 138, 2633–2637.

Hanelt, B., Bolek, M.G., Schmidt-Rhaesa, A., 2012. Going Solo: Discovery of the First Parthenogenetic Gordiid (Nematomorpha: Gordiida). *PLoS ONE* 7, e34472.

Harman, W.J., Loden, M.S., 1978. *Bratislavia unidentata* (Oligochaeta: Naididae), a Re-Description. *The Southwestern Naturalist* 23, 541–544.

Harms, J.W., 1948. Über ein inkretorisches Cerebralorgan bei Lumbriciden, sowie Beschreibung eines verwandten Organs bei drei neuen Lycastis-Arten. *Development Genes and Evolution* 143, 332–346.

Harper, E.H., 1904. Notes on regulation in *Stylaria lacustris*. *The Biological Bulletin* 6, 173–190.

Harris, M.P., Williamson, S., Fallon, J.F., Meinhardt, H., Prum, R.O., 2005. Molecular evidence for an activator-inhibitor mechanism in development of embryonic feather branching. *Proceedings of the National Academy of Sciences of the United States of America* 102, 11734–11739.

Heino, Kaitala, 1999. Evolution of resource allocation between growth and reproduction in animals with indeterminate growth. *J Evolution Biol* 12, 423–429.

Henry, J.Q., Tagawa, K., Martindale, M.Q., 2001. Deuterostome evolution: early development in the enteropneust hemichordate, *Ptychodera flava*. *Evolution & Development* 3, 375–390.

Hepke, P., 1897. Uber histo- und organogenetische Vorgange bei den Regenerationsprocessen der Naiden. *Zeitschrift fur Wissenschlaftliche Zoologie* 63, 263–291.

Herlant-Meewis, H., 1964. Regeneration in annelids. *Advances in morphogenesis* 4, 155–215.

Hessling, R., Westheide, W., 1999. CLSM analysis of development and structure of the central nervous system of *Enchytraeus crypticus* ("Oligochaeta", Enchytraeidae). *Zoomorphology* 119, 37–47.

Hill, S.D., 1970. Origin of the Regeneration Blastema in Polychaete Annelids. *American Zoologist* 10, 101–112.

Hodor, P.G., Ettensohn, C.A., 1998. The dynamics and regulation of mesenchymal cell fusion in the sea urchin embryo. *Developmental Biology* 199, 111–124.

Hori, I., Kishida, Y., 1998. A fine structural study of regeneration after fission in the planarian *Dugesia japonica*. *Hydrobiologia* 383, 131–136.

Hori, I., Kishida, Y., 2001. Further observation on the early regenerates after fission in the planarian *Dugesia japonica*. *Belgian Journal of Zoology* 131.

Hughes, R.N., 1987. The Functional Ecology of Clonal Animals. *Functional Ecology* 1, 63–69.

Hughes, R.N., 1989. *A Functional Biology of Clonal Animals*, Functional Biology Series. Chapman and Hall, London.

Hummon, M.R., Hummon, W.D., 1993. Gastrotricha. In K.G. Adiyodi and R.G. Adiyodi (eds.). *Reproductive Biology of Invertebrates. Vol. VI Part A, Asexual propagation and reproductive strategies*. Oxford & IBH Publishing, New Delhi, 265-277.

Hyman, L.H., 1916. An analysis of the process of regeneration in certain microdrilous oligochaetes. *Journal of Experimental Zoology* 20, 99–163.

Hyman, L.H., 1938. The fragmentation of *Nais paraguayensis*. *Physiological Zoology* 11, 126–143.

Hyman, L.H., 1940. Aspects of Regeneration in Annelids. *The American Naturalist* 74, 513–527.

Jacob, F., 1977. Evolution and Tinkering. *Science* 196, 1161–1166.

Jacobs, D.K., Hughes, N.C., Fitz-Gibbon, S.T., Winchell, C.J., 2005. Terminal addition, the Cambrian radiation and the Phanerozoic evolution of bilaterian form. *Evolution & Development* 7, 498–514.

Jeffery, W.R., Strickler, A.G., Yamamoto, Y., 2004. Migratory neural crest-like cells form body pigmentation in a urochordate embryo. *Nature* 431, 696–699.

Kamei, M., Weinstein, B.M., 2005. Long-term time-lapse fluorescence imaging of developing zebrafish. *Zebrafish* 2, 113–123.

Kawamoto, S., Chikako Yoshida-Noro, Shin Tochinai, 2005. Bipolar head regeneration induced by artificial amputation in *Enchytraeus japonensis* (Annelida, Oligochaeta). *Journal of Experimental Zoology Part A: Comparative Experimental Biology* 303A, 615–627.

Keller, P.J., Schmidt, A.D., Wittbrodt, J., Stelzer, E.H.K., 2008. Reconstruction of Zebrafish Early Embryonic Development by Scanned Light Sheet Microscopy. *Science* 322, 1065–1069.

Keyl, F., 1913. Beiträge zur Kenntnis von *Branchiura sowerbyi* Beddard. *Z. Wiss Zool* 107:199-308.

Keys, D.N., Lewis, D.L., Selegue, J.E., Pearson, B.J., Goodrich, L.V., Johnson, R.L., Gates, J., Scott, M.P., Carroll, S.B., 1999. Recruitment of a *hedgehog* Regulatory Circuit in Butterfly Eyespot Evolution. *Science* 283, 532–534.

Klingenberg, C.P., Nijhout, H.F., 1998. Competition among growing organs and developmental control of morphological asymmetry. *Proceedings of the Royal Society B: Biological Sciences* 265, 1135–1139.

Korschelt, E., 1919. Über die natürliche und künstliche Teilung des *Ctenodrilus monostylos* Zeppelin. *Development Genes and Evolution* 45, 602–685.

Koziol, B., Markowicz, M., Kruk, J., Plytycz, B., 2006. Riboflavin as a Source of Autofluorescence in *Eisenia fetida* Coelomocytes. *Photochemistry and Photobiology* 82, 570–573.

Kragl, M., Knapp, D., Nacu, E., Khattak, S., Maden, M., Epperlein, H.H., Tanaka, E.M., 2009. Cells keep a memory of their tissue origin during axolotl limb regeneration. *Nature* 460, 60–65.

Krecker, F.H., 1910. Some phenomena of regeneration in *Limnodrilus* and related forms. *Zeitschrift fur Wissenschlaftliche Zoologie* 95, 383–450.

Krecker, F.H., 1923. Origin and activities of the neoblasts in the regeneration of microdrilous annelida. *Journal of Experimental Zoology* 37, 26–46.

L.C. Armendariz, 1999. Dinámica poblacional de *Allonais lairdi* (Oligochaeta, Naididae) en Los Talas, Provincia de Buenos Aires. *Ecologia Austral* 9, 20–27.

Lasserre, P., 1975. Clitellata. In Giese, A.C., Pearse, J.S., Pearse, V.B. (Eds.). *Reproduction of Marine Invertebrates.* Academic Press, New York, NY, pp. 215–275.

Lengfeld, T., Watanabe, H., Simakov, O., Lindgens, D., Gee, L., Law, L., Schmidt, H.A., Ozbek, S., Bode, H., Holstein, T.W., 2009. Multiple Wnts are involved in Hydra organizer formation and regeneration. *Developmental Biology* 330, 186–199.

Lesiuk, N.M., Drewes, C.D., 1999. Autotomy reflex in a freshwater oligochaete, *Lumbriculus variegatus* (Clitellata: Lumbriculidae). *Hydrobiologia* 406, 253–261.

Lindsay, S., Jackson, J., He, S., 2007. Anterior regeneration in the spionid polychaetes *Dipolydora quadrilobata* and *Pygospio elegans*. *Marine Biology* 150, 1161–1172.

Lindsay, S.M., 2010. Frequency of Injury and the Ecology of Regeneration in Marine Benthic Invertebrates. *Integrative and Comparative Biology* 50(4), 479-493.

Maginnis, T.L., 2006. The Costs of Autotomy and Regeneration in Animals: A Review and Framework for Future Research. *Behavioral Ecology* 17, 857–872.

Manylov, O.G., 2010. Regeneration in Gastrotricha—I. Light Microscopical Observations on the Regeneration in *Turbanella* sp. *Acta Zoologica* 76, 1–6.

Martinelli, C., Spring, J., 2004. Expression pattern of the homeobox gene *Not* in the basal metazoan *Trichoplax adhaerens*. *Gene Expression Patterns* 4, 443–447.

Martinez, V.G., Manson, J.M.B., Zoran, M.J., 2008. Effects of nerve injury and segmental regeneration on the cellular correlates of neural morphallaxis. *Journal of Experimental Zoology, Part B: Molecular and Developmental Evolution* 310B, 520–533.

Martinez, V.G., Menger Iii, G.J., Zoran, M.J., 2005. Regeneration and asexual reproduction share common molecular changes: upregulation of a neural glycoepitope during morphallaxis in *Lumbriculus*. *Mechanisms of Development* 122, 721–732.

McHugh, D., 2000. Molecular phylogeny of the Annelida. *Canadian Journal of Zoology* 78, 1873–1884.

Meulemans, D., Bronner-Fraser, M., 2005. Central role of gene cooption in neural crest evolution. *Journal of Experimental Zoology, Part B: Molecular and Developmental Evolution* 304B, 298–303.

Meyer, N.P., Seaver, E.C., 2009. Neurogenesis in an annelid: Characterization of brain neural precursors in the polychaete *Capitella* sp. I. *Developmental Biology* 335, 237–252.

Michel, A., 1898. Recherches sur les regenerations chez les annlides. *Bulletin Scientifique de la France* 13, 245–420.

Miller, M.W., Nowakowski, R.S., 1988. Use of bromodeoxyuridine-immunohistochemistry to examine the proliferation, migration and time of origin of cells in the central nervous system. *Brain Research* 457, 44–52.

Mladenov, P.V., Burke, R.D., 1994. Echinodermata: asexual propagation. In K.G. Adiyodi and R.G. Adiyodi (eds.). *Reproductive Biology of Invertebrates. Vol. VI Part B, Asexual propagation and reproductive strategies*. John Wiley & Sons, Chichester, UK, 339-383.

Moczek, A.P., 2005. The Evolution and Development of Novel Traits, or How Beetles Got Their Horns. *BioScience* 55, 937–951.

Moczek, A.P., 2008. On the origins of novelty in development and evolution. *BioEssays* 30, 432–447.

Moment, G.B., 1951. Simultaneous anterior and posterior regeneration and other growth phenomena in Maldanid polychaetes. *Journal of Experimental Zoology* 117, 1–13.

Morgan, T., 1897. Regeneration in *Allolobophora foetida*. *Development Genes and Evolution* 5, 570–586.

Morgan, T.H., 1901. *Regeneration*. Columbia University Biological Series. Macmillan, Norwood, MA.

Müller, M., 2004. Nerve development, growth and differentiation during regeneration in *Enchytraeus fragmentosus* and *Stylaria lacustris* (Oligochaeta). *Development, Growth and Differentiation* 46, 471–478.

Müller, M., Berenzen, A., Westheide, W., 2003. Experiments on anterior regeneration in *Eurythoe complanata* ("Polychaeta", Amphinomidae): reconfiguration of the nervous system and its function for regeneration. *Zoomorphology* 122, 95–103.

Myohara, M., 2004. Differential tissue development during embryogenesis and regeneration in an annelid. *Developmental Dynamics* 231, 349–358.

Myohara, M., Yoshida-Noro, C., Kobari, F., Tochinai, S., 1999. Fragmenting oligochaete *Enchytraeus japonensis*: a new material for regeneration study. *Development, growth & differentiation* 41, 549–55.

Naidu, K.V., Naidu, K.A., 1979. Occurrence of *Allonais pectinata* (Stephenson, 1910) (Oligochaeta: Naididae) in Andhra Pradesh, *India. Proc. Indian Acad. Sci.* 88B, 327–327.

Nemec, A.F.L., Brinkhurst, R.O., 1987. A comparison of methodological approaches to the subfamilial classification of the Naididae (Oligochaeta). *Canadian Journal of Zoology* 65, 691–707.

Neuhaus, B., Higgins, R.P., 2002. Ultrastructure, Biology, and Phylogenetic Relationships of Kinorhyncha. *Integrative and Comparative Biology* 42, 619 – 632.

Nielsen, C., 1994. Bryozoa entoprocta. In K.G. Adiyodi and R.G. Adiyodi (eds.). *Reproductive Biology of Invertebrates. Vol. VI Part B, Asexual propagation and reproductive strategies*. John Wiley & Sons, Chichester, UK, 309-314.

Nielsen, C., 2005. Trochophora larvae and adult body regions in annelids: some conclusions. *Hydrobiologia* 535/536, 23–24.

Nijhout, H.F., Emlen, D.J., 1998. Competition Among Body Parts in the Development and Evolution of Insect Morphology. *Proceedings of the National Academy of Sciences of the United States of America* 95, 3685–3689.

Nusbaum, J., 1908. Beitrag zur Frage über die Abhängigkeit der Regeneration vom Nervensystem bei *Nereis diversicolor* O. F. Müll. *Wilhelm Roux' Archiv fur Entwicklungsmechanik der Organismen* 25, 632–642.

O'Brien, J.P., 1946. Studies on the cellular basis of regeneration in *Nais paraguayensis*, and the effects of x-rays thereon. *Growth* 10, 25–44.

Okada, Y.K., 1929. Regeneration and fragmentation in the Syllidian Polychaetes. *Development Genes and Evolution* 115, 542–600.

Paps, J., Baguñà, J., Riutort, M., 2009. Bilaterian Phylogeny: A Broad Sampling of 13 Nuclear Genes Provides a New Lophotrochozoa Phylogeny and Supports a Paraphyletic Basal Acoelomorpha. *Mol Biol Evol* 26, 2397–2406.

Parzer, H.F., Moczek, A.P., 2008. Rapid antagonistic coevolution between primary and secondary sexual characters in horned beetles. *Evolution* 62, 2423–2428.

Petersen, J.A., 1994. Hemichordata. In K.G. Adiyodi and R.G. Adiyodi (eds.). *Reproductive Biology of Invertebrates. Vol. VI Part B, Asexual propagation and reproductive strategies*. John Wiley & Sons, Chichester, UK, 385-394.

Philippe, H., Brinkmann, H., Copley, R.R., Moroz, L.L., Nakano, H., Poustka, A.J., Wallberg, A., Peterson, K.J., Telford, M.J., 2011. Acoelomorph flatworms are deuterostomes related to *Xenoturbella*. *Nature* 470, 255–258.

Potswald, H.E., 1972. The relationship of early oocytes to putative neoblasts in the serpulid *Spirorbis borealis*. *Journal of Morphology* 137, 215–227.

R Development Core Team, 2011. *R: A Language and Environment for Statistical Computing*. Vienna, Austria.

Raff, R.A., 1996. *The shape of life: genes, development, and the evolution of animal shape.* The University of Chicago Press, Chicago.

Raff, R.A., 2000. Evo-devo: the evolution of a new discipline. *Nature Reviews Genetics* 1, 74–79.

Rajulu, G.S., Krishnan, N., 1969. Occurrence of Asexual Reproduction by Budding in Sipunculida. *Nature* 223, 186–187.

Randolph, H., 1891. The regeneration of the tail in *Lumbriculus*. *Zoologischer Anzeiger* 14, 154–156.

Randolph, H., 1892. The regeneration of the tail in *Lumbriculus*. *Journal of Morphology* 7, 317–344.

Read, V.M.S.J., 2008. The Onychophora of Trinidad, Tobago and the Lesser Antilles. *Zoological Journal of the Linnean Society* 93, 225–257.

Reitzel, A.M., Burton, P.M., Krone, C., Finnerty, J.R., 2007. Comparison of developmental trajectories in the starlet sea anemone *Nematostella vectensis*: embryogenesis, regeneration, and two forms of asexual fission. *Invertebrate Biology* 126, 99–112.

Reyners, H., 1969. Ultrastructure de la zone scissiparitaire d'un oligochaete naidide, *Nais pseudoobtusa* Piget. *Ann. Soc. R. Zool. Belg.* 99, 45–58.

Reznick, D., 1985. Costs of Reproduction: An Evaluation of the Empirical Evidence. *Oikos* 44, 257–267.

Rice, M.E., 1970. Asexual Reproduction in a Sipunculan Worm. *Science*, New Series 167, 1618–1620.

Rosa, R., Prud'homme, B., Balavoine, G., 2005. *caudal* and *even-skipped* in the annelid *Platynereis dumerilii* and the ancestry of posterior growth. *Evolution & Development* 7, 574–587.

Runham, N.W., 1993. Mollusca. In K.G. Adiyodi and R.G. Adiyodi (eds.). *Reproductive Biology of Invertebrates. Vol. VI Part A, Asexual propagation and reproductive strategies*. Oxford & IBH Publishing, New Delhi, 311-383.

Sánchez Alvarado, A., 2000. Regeneration in the metazoans: why does it happen? *Bioessays* 22, 578–590.

Sayles, L.P., 1927. Origin of the mesoderm and behaviour of the nucleolus in regeneration in *Lumbriculus*. *The Biological Bulletin* 52, 278–3121.

Sayles, L.P., 1936. Regeneration in the Polychæte *Clymenella torquata* III. Effect of Level of Cut on Type of New Structures in Anterior Regeneration. *Biological Bulletin* 70, 441–459.

Schlosser, G., Wagner, G.P., 2004. *Modularity in development and evolution*. The University of Chicago Press, Chicago, IL.

Schroeder, P.C., Hermans, C.O., 1975. Annelida: Polychaeta In Giese, A.C., Pearse, J.S., Pearse, V.B. (Eds.). *Reproduction of Marine Invertebrates.* Academic Press, New York, NY, pp. 1–213.

Seaver, E.C., Thamm, K., Hill, S.D., 2005. Growth patterns during segmentation in the two polychaete annelids, *Capitella* sp. I and *Hydroides elegans*:

comparisons at distinct life history stages. *Evolution & Development* 7, 312–326.

Semper, 1876. Die Verwandtschaftsbeziehungen der gegliederten Thiere. Chap.: Die Knospung der Naiden. *Arbeiten Zool. Insc. Wurzburg* 3.

Shostak, S., 1993. Cnidaria. In K.G. Adiyodi and R.G. Adiyodi (eds.). *Reproductive Biology of Invertebrates. Vol. VI Part A, Asexual propagation and reproductive strategies*. Oxford & IBH Publishing, New Delhi,45-105.

Shubin, N., Tabin, C., Carroll, S., 1997. Fossils, genes and the evolution of animal limbs. *Nature* 388, 639–648.

Shubin, N., Tabin, C., Carroll, S., 2009. Deep homology and the origins of evolutionary novelty. *Nature* 457, 818–823.

Sikes, J.M., Bely, A.E., 2010. Making heads from tails: Development of a reversed anterior-posterior axis during budding in an acoel. *Developmental Biology* 338, 86–97.

Simmons, L.W., Emlen, D.J., 2006. Evolutionary trade-off between weapons and testes. *Proceedings of the National Academy of Sciences* 103, 16346–16351.

Sjolin, E., Erseus, C., Kallersjo, M., 2005. Phylogeny of Tubificidae (Annelida, Clitellata) based on mitochondrial and nuclear sequence data. *Molecular Phylogenetics and Evolution* 35, 431–441.

Sköld, H.N., Obst, M., Sköld, M., Åkesson, B., 2009. Stem cells in asexual reproduction of marine invertebrates, in: Rinkevich, B., Matranga, V. (Eds.), *Stem Cells in Marine Organisms*. Springer, New York, NY, pp. 105–137.

Sperber, C., 1948. A taxonomical study of the Naididae.*Zool. Bidr. Uppsala* 28: 1-296.

Srivastava, M., Begovic, E., Chapman, J., Putnam, N.H., Hellsten, U., Kawashima, T., Kuo, A., Mitros, T., Salamov, A., Carpenter, M.L., Signorovitch, A.Y., Moreno, M.A., Kamm, K., Grimwood, J., Schmutz, J., Shapiro, H., Grigoriev, I.V., Buss, L.W., Schierwater, B., Dellaporta, S.L., Rokhsar, D.S., 2008. The *Trichoplax* genome and the nature of placozoans. *Nature* 454, 955–960.

Stearns, S.C., 1989. Trade-Offs in Life-History Evolution. *Functional Ecology* 3, 259–268.

Stewart, S., Stankunas, K., 2012. Limited dedifferentiation provides replacement tissue during zebrafish fin regeneration. *Developmental Biology* 365, 339–349.

Stone, J.R., Hall, B.K., 2004. Latent homologues for the neural crest as an evolutionary novelty. *Evolution & Development* 6, 123–129.

Stone, R.G., 1932. The effects of x-rays on regeneration in *Tubifex tubifex*. *Journal of Morphology* 53, 389–431.

Stone, R.G., 1933. The effects of X-rays on anterior regeneration in *Tubifex tubifex*. *Journal of Morphology* 54, 303–320.

Stout, J.D., 1958. Aquatic Oligochaetes Occurring in Forest Litter.—I. *Transactions and Proceedings of the Royal Society of New Zealand* 84, 97–102.

Streit, A., 2008. Reproduction in *Strongyloides* (Nematoda): a life between sex and parthenogenesis. *Parasitology* 135, 285–294.

Struck, T.H., Paul, C., Hill, N., Hartmann, S., Hosel, C., Kube, M., Lieb, B., Meyer, A., Tiedemann, R., Purschke, G., Bleidorn, C., 2011. Phylogenomic analyses unravel annelid evolution. *Nature* 471, 95–98.

Sugio, M., Yoshida-Noro, C., Ozawa, K., Tochinai, S., 2012. Stem cells in asexual reproduction of *Enchytraeus japonensis* (Oligochaeta, Annelid): Proliferation and migration of neoblasts. *Development, Growth & Differentiation* 54(4). 439-450.

Sugiura, T., Taniguchi, Y., Tazaki, A., Ueno, N., Watanabe, K., Mochii, M., 2004. Differential gene expression between the embryonic tail bud and regenerating larval tail in *Xenopus laevis*. *Development, Growth & Differentiation* 46, 97–105.

Sweet, H., Amemiya, S., Ransick, A., Minokawa, T., McClay, D.R., Wikramanayake, A., Kuraishi, R., Kiyomoto, M., Nishida, H., Henry. 2004. Blastomere Isolation and Transplantation. *Methods in Cell Biology* 74, 243–271.

Tadokoro, R., Sugio, M., Kutsuna, J., Tochinai, S., Takahashi, Y., 2006. Early segregation of germ and somatic lineages during gonadal regeneration in the annelid *Enchytraeus japonensis*. *Current Biology* 16, 1012–1017.

Takeo, M., Yoshida-Noro, C., Tochinai, S., 2008. Morphallactic regeneration as revealed by region-specific gene expression in the digestive tract of *Enchytraeus japonensis* (Oligochaeta, Annelida). *Developmental Dynamics* 237, 1284–1294.

Tanaka, E.M., Reddien, P.W., 2011. The Cellular Basis for Animal Regeneration. *Developmental Cell* 21, 172–185.

Technau, U., Bode, H.R., 1999. *HyBra1*, a *Brachyury* Homologue, Acts During Head Formation in Hydra. *Development* 126, 999–1010.

Thiemann, M., Ruthmann, A., 1991. Alternative modes of asexual reproduction in *Trichoplax adhaerens* (Placozoa). *Zoomorphology* 110, 165–174.

Timm, T., 1984. Potential age of aquatic Oligochaeta. *Hydrobiologia* 115, 101–104.

Tomkins, J.L., Kotiaho, J.S., LeBas, N.R., 2005. Phenotypic Plasticity in the Developmental Integration of Morphological Trade-Offs and Secondary Sexual Trait Compensation. *Proceedings of the Royal Society B: Biological Sciences* 272, 543–551.

Troedsson, C., Bouquet, J., Aksnes, D.L., Thompson, E.M., 2002. Resource allocation between somatic growth and reproductive output in the pelagic chordate *Oikopleura dioica* allows opportunistic response to nutritional variation. *Mar Ecol Prog Ser* 243, 83–91.

Tuomi, J., Hakala, T., Haukioja, E., 1983. Alternative Concepts of Reproductive Effort, Costs of Reproduction, and Selection in Life-History Evolution. *American Zoologist* 23, 25 –34.

Turner, C.D., 1934. The effects of x-rays on posterior regeneration in *Lumbriculus inconstans*. *Journal of Experimental Zoology* 68, 95–119.

Turner, C.D., 1935. The effects of x-rays on anterior regeneration in *Lumbriculus inconstans*. *Journal of Experimental Zoology* 71, 53–81.

van Cleave, C.D., 1929. An Experimental Study of Fission and Reconstitution in *Stenostomum*. *Physiological Zoology* 2, 18–58.

Van Cleave, C.D., 1937. A study of the process of fission in the naid *Pristina longiseta*. *Physiological Zoology* 10, 299–314.

van Noordwijk, A.J., de Jong, G., 1986. Acquisition and Allocation of Resources: Their Influence on Variation in Life History Tactics. *The American Naturalist* 128, 137.

von Wagner, F., 1900. Beitrage zur Kenntnis der Regenerationsprozesse bei *Lumbriculus variegatus*. I. *Teil. Zool. Jb. Abt. Anat. u. Ontog*. 13, 198–205.

von Wagner, F., 1906. Beitrage zur Kenntnis der Regenerationsprozesse bei *Lumbriculus variegatus*. II. *Teil. Zool. Jb. Abt. Anat. u. Ontog.* 136, 255–318.

Vorontsova, M.A., Liosner, L.D., 1960. *Asexual propagation and regeneration*. Pergamon Press, London.

Wallace, R.L., Ricci, C., Melone, G., 1996. A Cladistic Analysis of Pseudocoelomate (Aschelminth) Morphology. *Invertebrate Biology* 115, 104–112.

Watson, A.T., 1906. A Case of Regeneration in Polychoete Worms. *Proceedings of the Royal Society of London. Series B, Containing Papers of a Biological Character* 77, 332–336.

Whitehead, G.G., Makino, S., Lien, C.-L., Keating, M.T., 2005. *Fgf20* Is Essential for Initiating Zebrafish Fin Regeneration. *Science* 310, 1957–1960.

Whitfield, P.J., Evans, N.A., 1983. Parthenogenesis and asexual multiplication among parasitic platyhelminths. *Parasitology* 86, 121–160.

Williams, J.D., 2004. Reproduction and morphology of *Polydorella* (Polychaeta: Spionidae), including the description of a new species from the Philippines. *Journal of Natural History* 38, 1339–1358.

Yoshida-Noro, C., Myohara, M., Kobari, F., Tochinai, S., 2000. Nervous system dynamics during fragmentation and regeneration in *Enchytraeus japonensis* (Oligochaeta, Annelida). *Development Genes and Evolution* 210, 311–319.

Zattara, E.E., Bely, A.E., 2011. Evolution of a novel developmental trajectory: fission is distinct from regeneration in the annelid *Pristina leidyi*. *Evolution & Development* 13, 80–95.

Zera, A.J., Harshman, L.G., 2001. The Physiology of Life History Trade-Offs in Animals. *Annual Review of Ecology and Systematics* 32, 95–126.

Zhou, Q., Wang, W., 2008. On the origin and evolution of new genes--a genomic and experimental perspective. *J Genet Genomics* 35, 639–648.

Zrzavy, J., Riha, P., Pialek, L., Janouskovec, J., 2009. Phylogeny of Annelida (Lophotrochozoa): total-evidence analysis of morphology and six genes. *BMC Evolutionary Biology* 9, 189.